Winter 1981

Numerical Model Simulation of Offshore Flow During the Winter Season

Maria Cintia Piccolo
Old Dominion University

NUMERICAL MODEL SIMULATION OF OFFSHORE FLOW DURING THE WINTER SEASON

by

Maria Cintia Piccolo
Maestra Normal Nacional, 1968
Colegio Nino Jesus de Praga, Argentina
Licenciada en Ciencias Meteorologicas, 1975
Universidad de Buenos Aires, Argentina

A Dissertation Submitted to the Faculty of
Old Dominion University in Partial Fulfillment of the
Requirements for the Degree of

DOCTOR OF PHILOSOPHY

OCEANOGRAPHY

OLD DOMINION UNIVERSITY
December, 1981

Approved by:

Earl C. Kindle (Director)

ABSTRACT

NUMERICAL MODEL SIMULATION OF OFFSHORE FLOW
DURING THE WINTER SEASON

Maria Cintia Piccolo
Old Dominion University, 1981
Director: Dr. Earl C. Kindle

Because of the step function variability of heat and moisture flux in coastal zones, adequate descriptive models of mesoscale coastal circulation and weather patterns demand high spatial resolution in the analysis of wind, temperature and moisture patterns. To obtain realistic concepts of offshore flow the sparse offshore data networks need to be supplemented by mesoscale numerical models. The problems associated with the modeling of offshore flow across the east coast of the United States during the winter season have been investigated with a simple two dimensional numerical model of the planetary boundary layer.

The model has two predictive equations for the potential temperature and humidity fields. A diagnostic equation based upon observed data is used to determine wind velocities. At each horizontal step the wind was integrated with height, and the equations for the temperature and humidity were solved for each level. A second

order model using the Dufort-Frankel finite difference scheme with two vertical grid spacing and eddy coefficient formulations was applied to actual cases of offshore winter flow. The results of the model were compared with measurements at anemometer level at offshore stations. Different flux formulations were tested. Key problems related to the use of the Dufort-Frankel scheme were indicated.

Problems associated with the use of a K-theory profile for the turbulent fluxes in the marine planetary boundary layer were isolated. The initial air-sea temperature difference and the K-theory formulations were crucial to the computational stability of the model as well as the resolution of the model, even after the stability problems were solved. A bulk aerodynamic formulation produced better results in the marine surface layer, however when merged with K-theory for the rest of the planetary boundary layer disastrous results can occur. A first order model with a similar resolution was applied to the same situation and showed superior results.

LA PREGUNTA

"Y qué quieres ser tú? -dijo el Destino.
Respondí: Yo, ser santo;
y repuso el Destino:
"Habrá que contentarse
con menos..."

Pesaroso,
aguarde en mi rincón una pregunta
nueva:
"Qué quieres ser? - dijo el Destino
otra vez: - Yo, ser genio, respondíle;
y él irónico: "Habrá que contentarse
con menos..."

Mudo y triste
en mi rincón de sombra, ya no espero
la pregunta postrer, a la que sólo
responderá mi trágico silencio...

Amado Nervo

ACKNOWLEDGEMENTS

I would like to express my deep gratitude and appreciation to all the people who provided both guidance and assistance throughout the course of this study. I wish to thank Dr. Earl C. Kindle, my dissertation director, for his unselfish contribution of time and advice. I will always remember the long afternoons of work and coffee. He made every meeting a learning experience.

I would like to thank with all my heart Dr. Chester E. Grosch, not only for his continued direct support, but also for the warm and instructive conversations about science and everything that is related to life. Thanks also goes to Dr. Ronald E. Johnson who provided assistance, friendship and encouragement during the years that I stayed at Old Dominion University. I am also indebted to Dr. Thomas B. Gatski for many valuable criticisms and suggestions during the progress of this study.

Appreciation is expressed to the Graduate Program Director, Dr. Carvel H. Blair, and to my advisor, Dr. George H. Hecker, for their valuable help and assistance on administrative procedures.

Financial support was provided by CONICET (Consejo Nacional de Investigaciones Cientificas y Tecnicas). In particular, I wish to express my gratitude to Mr. Benjamin Fernandez Vinez for promptly solving any problem that I had. Part of the financial support was also provided by ONR Grant N00014-77-C-0377.

I also wish to thank Mr. Herman Wobus for his help and kindly assistance with the data reading and computer programming. I would like to thank Mr. James E. Smith his patient answers to every question that I had about the meteorological data.

I feel obligated to Mrs. Roberta K. Johnson, because she was there when I felt homesick and because she made me feel that I have a second home in this wonderful country.

I would like to thank the graduate students of the Department of Oceanography, in particular, those in room 120 (Mike J. Jugan, David Timpy, Gregory V. Kopansky and Joe J. Bleicher) for their comradeship and moral support. My special thanks goes to my fellow graduate student, Im Sang Oh (now Ph.D.), because he always lent a sympathetic ear to my problems; to Joung Won Kim and his wife, for their help with the figures of this study. Special thanks to Beth S. Hester for her sincere friendship and her assistance in the review of drafts of this work.

Quiero tambien expresar las gracias a mi madre, Sra. Maria A. B. de Piccolo. Gracias por su ejemplo como ser humano, sus oraciones y su carino. Gracias por tener fe en mi como persona. Tambien quiero agradecer a los padres de mi esposo, Sr. Romulo Perillo Y Sra. Catalina L. de Perillo, porque con su continua ayuda moral han demonstrado ser mis segundos padres. Quiero agradecer al resto de mi familia por haber esperado nuestro regreso pacientemente y nos han brindado su carino y amor.

I am especially indebted to my husband (and fellow graduate student) Gerardo M. E. Perillo, for his love, camaraderie and encouragement. I do not have words to express my gratitude.

Above all, my thanks go to the bearer of all my burdens and the answerer of all my prayers.

Finally, I wish to thank Becky Alden for typing this dissertation.

TABLE OF CONTENTS

LIST OF TABLES

LIST OF FIGURES

LIST OF SYMBOLS

Cd	Drag coefficient
Cp	Specific heat at constant pressure
Dx	Horizontal step size
E	Ratio between Reynolds and Rossby numbers
f	Coriolis parameter
g	Gravity force
H	Heigth of the model
He	Moisture flux
Hs	Sensible heat flux
k	Von Karman constant
Kh	Eddy conductivity
Km	Eddy viscosity
Ke	Eddy diffusivity
L	Monin-Obukhov length
P	Atmospheric pressure
q_o	Specific humidity corresponding to the sea surface temperature
q	Air specific humidity
Ri	Richardson number
S	Smoothing factor
T	Air temperature
Ts	Sea surface temperature

u_*	Friction velocity
U, V	Components of the wind speed
Ug, Vg	Components of the geostrophic wind
X	Horizontal axis
z	Vertical axis
z_i	Height of the inversion
z_o	Surface roughness parameter
ρ	Density
θ	Air potential temperature
θ_v	Virtual air potential temperature
θ_o	Potential temperature corresponding to the sea surface temperature

Chapter 1

INTRODUCTION

1.1 Previous Work

The passage of a cold, strong flow of air over the water in late fall and winter can result in extensive modification of the air by the underlying surface. The primary interaction is the exchange of momentum, sensible, and latent heat across the interface between the atmosphere and the ocean. Over the past forty years several studies related to the modification of an air mass traveling over the ocean have been published. Most of them described the transformation based on observational data or developed empirical formulas to compute such modification.

Lenschow (1973) took measurements of sensible and latent heat fluxes, surface and air temperatures, mean wind and humidity from an aircraft. He examined the boundary layer structure over the Great Lakes for two cases in the late fall, when the water was warmer than the air above. He found that, in response to variation in the lake surface temperature, the sensible and latent heat fluxes at 147 m varied by as much as a factor or two along the flight path across Lake Michigan.

McBean (1975) described the turbulent fluxes of momentum, sensible, and latent heat associated with a cold frontal passage over Lake Ontario. He found that the periods of frontal passage followed by strong northwesterly winds were responsible for over 60% of the lake's temperature decrease, but occupied less than 15% of the time. He noted the tremendous amount of energy involved in the lake-to-atmosphere latent and sensible heat transfers during October (approximately 7 10^{25} ergs).

Other studies on the modification of a cold air mass by the sea were presented by Burke (1945), Burbidge (1951), Manabe (1957), Bunker (1960), Lenschow (1965, 1972), Manogo et al. (1974), Bean (1975), and Wessels (1979).

In the last ten years, some studies have used numerical simulations to describe the planetary boundary layer (PBL) over water surfaces. Most of these were related to stable conditions. Pandolfo (1971) described some preliminary comparative tests of alternative modelling formulas in a numerical model of the coupled tropical air-sea PBL. He found that the eddy coefficients formulation worked reasonably well for the tropical ocean.

Lavoie (1972) used a single-layer numerical model and predictive equations for the horizontal components of velocity, potential temperature and humidity to describe the PBL over the Great Lakes during Arctic Air outbreaks.

The equation set was solved numerically for a 2000-point grid mesh centered on Lake Erie. He concluded that a single layer can be used to represent many of the significant aspects of lake-effect storms. Maddukuri et al. (1978) applied a two dimensional atmospheric boundary layer model to the northern shore of Lake Erie to simulate the observed wind and temperature profiles. They concluded that the profiles predicted by the model agreed reasonably well with the observed profiles.

There has been extensive research on the effects of abrupt changes in surface conditions on turbulent boundary layers, most of them related to internal boundary layers. Taylor (1971) described the modification of the airflow in the lowest 50-100 m of the atmosphere that resulted from changes in surface roughness and surface temperature. He predicted an increase in the shear stress at the outer edge of the internal boundary layer under these conditions: a step change in heat flux and no change in roughness.

The problem of air flow over a sudden change in surface temperature and humidity has been investigated using mixing-length theory by Weisman (1975). Using a two dimensional model, he described the turbulent fluxes in the internal boundary layer that develops downwind of a change in surface conditions. He concluded that a mixing-length model for the leading edge problem is a

useful tool for the calculation of evaporation and sensible heat from a water surface.

Estoque and Bhumralkar (1970), Clarke (1970), Deardorff (1972, 1974), and Mahrt and Lenschow (1976) have also studied the dynamics of the unstable PBL.

1.2 Purpose of Study

Contemporary numerical weather prediction models work poorly in regions of strong surface temperature contrasts. This is particularly true during the winter along the coasts of continents and at the northern boundary of the subtropical ocean waters. In recent experiments (Yasuda, 1979), results on a synoptic scale show apparent improvement by applying similarity theory to single surfaces varying from 500 to 1500 m in depth. However, the approach does not lend itself to the study of the intense offshore mesoscale features that are associated with strong flow during the winter season.

The step function variability in temperature, humidity and momentum under these conditions induces unstable PBL. The inherent scarcity of data in the offshore domain has prevented the development of physical and descriptive models. By supplementing existing data sources with representative numerical simulations, one could hopefully

arrive at the requisite description of these intense mesoscale features.

Initially, the author considered the development of an hydrodynamical model that would provide a quantitative understanding of this intense mesoscale feature that commonly occurs in coastal regions during the winter season. Due to the inherent variability of the forcing functions (momentum, heat and moisture flux) the model would have to include a high resolution representation of the meteorological parameters. Further, the model would have to treat a highly unstable boundary layer with extremely strong vertical wind shear.

It is clear, from examination of previous work (Kindle et al. 1976), that successful modeling of this feature would require improved treatment of the vertical moisture and heat fluxes in the offshore domain. To date, extensive research in the literature has produced a very limited number of sources on high resolution modeling of the unstable boundary layer. Many comprehensive studies showed that application of bulk aerodynamic formulation to the marine surface layer gives excellent results. However, successful treatment of the unstable PBL (typically using K-theory or a K-theory equivalent) was highly suspected and not well reported. Furthermore, a clear understanding of the strengths and weaknesses of contemporary numerical and physical formulations is

critically needed to insure progress in this important area of modelling.

Accordingly, the research described herein is concerned with the development of several numerical simulations that incorporate different contemporary numerical integration techniques into the prediction of heat and moisture flux in a high resolution unstable coastal domain. Therefore, the purposes of this study are:

1. Application of different simulations to selected actual cases of offshore winter air flow to permit comparison of results between the various numerical and physical techniques, as well as comparison with observed data; and

2. Diagnosis of the physical and computational reliability and weaknesses of each of the numerical techniques in portraying an unstable high resolution PBL.

Chapter 2

THE PHYSICAL MODEL

2.1 Physical Description of the Problem

The changes in the physical properties of a given air flow depend on the surface over which it passes. The transformation processes start at the surface and affect the temperature, humidity, and flow characteristics of the air above. As cold air moves out over warmer water, its content of heat and water vapor are increased by the flux of sensible and latent heat from the sea. The energy thus gained by the air is rather quickly distributed over substantial portions of the atmosphere. The heat released to the overlying air column is largely a function of the air-sea temperatures, vapor pressure differences, and wind velocity.

The region under investigation, part of the Eastern coast of North America, is characterized by a strong offshore air flow during the winter season. This phenomenon is rare in that it produces an unstable PBL with strong wind over mesoscale to medium synoptic regions. A characteristic of the wind profile is the almost constant direction with height which indicates regions of strong

vertical exchange. Other places of known occurrence of this particular condition are off the South coast of France, in the South China Sea and at the north wall of the Gulf Stream current (Kindle et al., 1976). In these areas the most intense flux of heat and moisture into the atmosphere are associated with the intense surface heating and strong winds.

In modeling the PBL over the ocean, three distinct vertical regions were considered (Figure 1). The first is the surface Boundary Layer (SBL) which represents the lowest few tens of meters and is characterized by strong gradients in moisture and temperature. This is essentially a constant flux layer; that is, at heights small compared with the boundary layer depth, the turbulent fluxes are approximately equal to the surface flux values. Above this near-ground layer, and extending nearly to the inversion base at z_i, is the Ekman or mixed layer. In this layer vertical mixing flattens out the vertical profiles of mean temperature and humidity, and the gradients are usually smaller. The mixing in this layer is induced both mechanically through strong winds and thermally as a result of the surface heating. Above this layer an inversion is found where the turbulence is extinguished by the stable stratification. Therefore, the profiles approach the conditions of the free atmosphere.

2.2 Governing Equations

In this section the general equations and theories to be applied are discussed. The x-axis is taken in the direction of the mean wind and represents the horizontal distance from the shore (where $x = 0$). z is considered vertically upward from the sea surface (where $z = 0$) (Figure 2).

The model is a steady state one with an assumed negligible mean vertical motion. Due to the strong winds, the rates of turbulent transfer were considered to dominate the radiation effects. This is a common assumption for this type of problem. In his study of the transformation of Polar Continental Air to Polar Maritime Air, Burke (1945) used this hypothesis, following a discussion presented by H. V. Sverdrup in three courses of Maritime Meterorology at the Scripps Institute of Oceanography. From measurements, Craddock (1951) computed the amount of sensible heat and water vapor released to the air by the ocean and the amount of heat lost by radiation. He concluded that the correction for radiation effects is small compared to the heat flux which the air is receiving from other processes.

If radiation processes are neglected, the transformation of the air mass can be considered as a problem of turbulent heat and moisture exchange. In a steady

state two dimensional systems the governing equations are

$$U\ \partial\theta/\partial x = -\ (1/\rho\ Cp)\ \partial Hs/\partial z \qquad (2.1)$$

$$U\ \partial q/\partial x = -\ (1/\rho)\ \partial He/\partial z \qquad (2.2)$$

$$\theta = T\ (1000/P)^{\kappa} \qquad \kappa = 0.286 \qquad (2.3)$$

$$f\ (V - Vg) = -\ \frac{\partial(Km\ \partial U/\partial z)}{\partial z} \qquad (2.4)$$

$$f\ (U - Ug) = -\ \frac{\partial(Km\ \partial V/\partial z)}{\partial z} \qquad (2.5)$$

where ρ is the mean density of the air, Cp is the specific heat at constant pressure, θ is the potential temperature of the air, U and V are the components of the wind speed in the x and y direction, q is the specific humidity, Hs is the sensible heat flux, He is the moisture flux, Ug and Vg are the x and y components of the geostrophic wind, P is the atmospheric pressure, T is the temperature of the air, and Km is the eddy viscosity.

2.2.1 Turbulent Flux Formulations

One of the main subjects of this research is the description, modelling, and comparison of the mean vertical profiles of temperature and humidity with different

formulations of the characteristic turbulence parameters such as eddy viscosity and turbulent heat fluxes.

In this investigation the resulting heat distribution are calculated by a type of gradient-transport model, that is the K formulations involved the assumption that the turbulent transports are proportional to the gradient of the transported quantities. In using these types of models it is assumed that the length and time scales of the mean motion are slightly larger than the length and time scales of the turbulence. This, of course, is not always the case and constitutes one disadvantage of these models. According to Lumley (1969) the gradient-transport models break down in situations which have several length or time scales. These models tend to fail in situations where there is a rapid change in the streamwise direction of the flow and also in convective situations where both buoyancy and wind shear are important.

Other models for this turbulence problem exist, such as the higher order closure schemes. According to Bodin (1980) the schemes which model the third order terms in the equation of turbulent motion require several ad hoc assumptions. This implies a considerable complication of the turbulence closure problem and leads to additional equations in order to simulate the PBL. Blackadar (1969) also concludes that even though researchers are trying to

develop non-K-type theories, the present state of the art has not progressed much beyond K-type theories.

Heat flux formulations for the mixed layer. Two distinct formulas for the computation of sensible heat were compared by modifications to equation (2.1). The basic differences between them lies in the form that the release of sensible heat, associated with evaporation of water in the air, takes in the equations. In general, the sensible heat is given by

$$Hs = - \rho \; Kh \; Cp \; \partial\theta/\partial z \qquad (2.6)$$

Although over dry land the contribution of moisture to the heat flux is negligible, this is not true over the ocean. This effect can be taken into account in an approximate way, as suggested by Lumley and Panofsky (1964), by replacing the potential temperature with the virtual potential temperature which is defined as,

$$\theta v = (1.0 + 0.61 \; q)\,\theta \qquad (2.7)$$

where θv represents the temperature that dry air would have if its pressure and specific volume were equal to those of a given sample of moist air. The equation for the sensible heat flux becomes,

$$Hs = - \rho \; Cp \; Kh \; \partial v/\partial z \qquad (2.8)$$

where Kh is the eddy conductivity coefficient.

The second formulation of sensible heat flux that was evaluated is that given by Brook (1978). He has shown that the influence of water vapor fluctuations in the vertical turbulent flux of sensible heat in the air is predominantly due to the dependence of the specific heat of the air on specific humidity, rather than the effects of water vapor on air density and buoyancy. In this formulation

$$Hs = - \rho \, Cp \, Kh \, (\partial\theta/\partial z + 0.84 \, T \, \partial q/\partial z) \qquad (2.9)$$

Equation (2.9) is a simplified form of the flux gradient equation derived by Brook, as presented by Reinking (1980). The moisture flux equation is

$$He = - \rho \, Ke \, \partial q/\partial z \qquad (2.10)$$

where Ke is the eddy diffusivity coefficient. Equations (2.8) or (2.9) and (2.10) have been employed to model the profiles in the Ekman Layer.

Heat flux formulations for the SBL. In the last decade considerable effort has been expended in attempts to measure the exchange of momentum, sensible heat and moisture between the atmosphere and the ocean in the SBL. Therefore, there are many bulk aerodynamic formulations that, from a practical point of view, are useful because they relate these exchanges to more standard observations

such as mean wind speed and air-sea temperature differences. The bulk formulation has been used in the present model in the SBL calculations, while the flux gradient formulae have been adopted in the mixed layer.

In order to compare different bulk formulations, the following set of equations (Reinking, 1980) was used:

$$\frac{Hs}{\rho\, Cp} = Ch\ U\ ((\theta_z - \theta_o) + 0.84\ T\ (q_z - q_o)) \qquad (2.11)$$

$$\frac{He}{\rho} = -\ Ce\ U\ (q_z - q_o) \qquad (2.12)$$

where q_z and θ_z are the specific humidity and the potential temperature at a given height z, U is the wind speed at z, q_o and θ_o are the specific humidity and potential temperature corresponding to the sea surface temperature. $Ch = Ce = 1.6 \times 10^{-3}$ was set when the SBL was 10 m thick, otherwise, Ch was calculated as a function of z (Section 2.2.3). The other expressions given by Smith (1980) are

$$\frac{Hs}{\rho\, Cp} = \begin{cases} (3.2 + 1.0\ (T_s - T_a)\ U)\ 10^{-3} & \text{unstable cases} \\ (-0.1 + 0.83\ (T_s - T_a)\ U)\ 10^{-3} & \text{stable cases} \end{cases} \qquad (2.13)$$

where Ts is the sea surface temperature and T_a is the air temperature at height z. Equations (2.12) and (2.13) are the second set of equations that were used.

These two methods for the computation of the sensible heat were selected because they are based on different principles. Reinking's technique incorporated the moisture effect, that is the dependence of the specific heat at constant pressure on specific humidity. His method did not take into account a dependence of the drag coefficient on the stability. Nevertheless, one was able to change the values of the drag coefficient according to the type of stability that each situation presented. Smith's formulation was based on measurements taken on an offshore stable platform with wind speeds over the ocean varying from 6 to 22 m/sec. This latter method may be more appropriate in this numerical simulation because almost all of the cases that were studied fall into this range of wind speeds.

2.2.2 Eddy Coefficient Formulation

The expressions for the eddy coefficient differed according to the region of the PBL where they were employed (i.e. SBL and mixed layer). Two kinds of K profiles were tested in the mixed layer in this research. The first one, given by Estoque and Bhumralkar (1970), was an implicit K model where K is assumed to be determined by the configuration of wind shear, statis stability, and height. By introducing this relationship, the K distribution is generated in the model, step by step, in accordance with

the evolving wind and temperature patterns. In this method a mixing length l, is assumed that characterizes the turbulence scales containing the energy. The formulation of the eddy viscosity given by Estoque and Bhumralkar (1970) is,

$$Km = \begin{cases} l^2 \, S \, (1 + \alpha \, Ri) & Ri < 0 \\ \\ l^2 \, S \, (1 - \alpha \, Ri)^{-1} & Ri > 0 \end{cases} \qquad (2.14)$$

$$l = \frac{k(z + z_o)}{1 + k(z + z_o)/\lambda}$$

$$\lambda = 0.00027 \, Ug \, f^{-1}$$

$$S = ((\partial u/\partial x)^2 + (\partial V/\partial z)^2)^{1/2}$$

$$\alpha = -3$$

$$Ri = \frac{g(\partial\theta/\partial z)}{\theta \, S^2}$$

where z_o is the surface roughness, and Ri is the Richardson number.

The second formulation is an explicit K profile in which the form of the vertical distribution is specified with a scale to be determined by the surface and free atmosphere conditions. O'Brien (1970) proposed a functional form of the eddy coefficient. The values of K and their derivatives with respect to z_a (height of top of

surface layer) and z_b (height of PBL) were used to derive a third order Hermite-interpolating polynomial given by

$$K(z) = Ka + ((z - za) / (dz)) [Kb - Ka + (z - zb) (Kb' + 2.0 (Kb - Ka) / dz)] \quad (2.15)$$

where $Ka' = 0$ and $dz = za - zb$.

Given Km, Kh was computed from the ratio Kh/Km suggested by Deardorff (1968), where

$$\frac{Kh}{Km} = 1.0 - \frac{a\ Ri}{Ri + a} \quad (2.16)$$

$$a = 2/3 \quad \text{for} \quad Ri > 0$$
$$a = -2 \quad \text{for} \quad Ri < 0$$

Figure 3 is a plot of the ratios of (Kh/Km) implied by the profile theories according the equation (2.16). Ke was always assumed to be equal to Kh.

Two different approaches were applied in the constant flux layer in order to match the formulations in the mixed layer. The first is given by the following expression (Estoque, 1963):

$$Km = \begin{cases} l^2\ S\ (1.0 + \alpha\ Ri)^2 & Ri < 0 \\ l^2\ S\ (1.0 - \alpha\ Ri)^{-2} & Ri > 0 \end{cases} \quad (2.17)$$

where all the variables are defined as in equation (2.14). Kh was estimated by the ratio Kh/Km given by equation (2.16).

The second expression for Kh for the surface boundary layer was obtained directly from Hs as computed from the bulk aerodynamical equations ((2.11) and (2.13)):

$$Kh = \frac{Hs(bulk)}{\rho\ Cp\ \partial\theta/\partial z} \tag{2.18}$$

2.2.3 The Drag Coefficient

When the bulk aerodynamic formulation was applied to the marine surface boundary layer (equations (2.11) and (2.13)), the drag coefficient was calculated for each level of the model within the assumed SBL. The drag coefficient is defined as

$$Cd = (u_*/U)^2 \tag{2.19}$$

During unstable conditions near the ground the wind speed is given by the formula,

$$U = (u_*/k)\ (\ln\ (z/z_o) - \psi(z/L)) \tag{2.20}$$

where $\psi(z/L)$ is a universal function. Hanna (1969) found that this function could be approximated by the relation

$$\psi(z/L) = 0.05\ |z/L|^{1/3} \tag{2.21}$$

With the following assumption (Krauss, 1972),

$$|z/L| \cong Ri$$

equation (2.21) becomes

$$\psi(z/L) = 0.95 \ |Ri|^{1/3} \tag{2.22}$$

On the basis of dimensional considerations, Charnock (1955) suggested that the surface roughness parameter should be given by

$$z_0 = m \ u_*^2/g \tag{2.23}$$

Incorporating (2.22) and (2.23) into (2.20) one obtaines

$$u_* = \frac{U \ k}{\ln \ ((z \ g)/(m \ u_*^2)) - (0.95 \ |Ri|^{1/3})} \tag{2.24}$$

Equation (2.24) was solved for u_* by the Fix Point algorithm. After u_* was calculated as a function of z, the drag coefficient was computed. From (Krauss, 1972) it was assumed that Cd = Ch = Ce.

2.3 Boundary Conditions

The complete set of equations were solved numerically, subject to the boundary conditions:

i) At z = H

$\theta(x,H) = \theta_1$

$q(x,H) = q_1$ $\quad 0 < x < d_1$

$U(x,H) = Ug$

$V(x,H) = Vg$

ii) At $z = 0$

$\theta(x,0) = \theta sea$

$q(x,0) = qsea$

$U(x,0) = 0$ $\quad 0 < x < d_1$

$V(x,0) = 0$

iii) At $x = 0$

$\theta(0,z) = \theta(z)$

$q(0,z) = q(z)$

$U(0,z) = U9z)$ $\quad 0 < z < H$

$V(0,z) = V(z)$

where d_1 represents the distance of the station offshore, and H, the height of the top of the inversion (Figure 1). The value θ_1 and q_1 corresponded to the ones given by the initial profiles at that height.

Chapter 3

THE NUMERICAL SIMULATIONS

Five simulations were carried out in this study. In each the governing equations ((2.1) to (2.5)) described in Chapter 2 were solved. However, different heat formulations, eddy coefficient distributions and finite difference schemes were applied in each.

3.1 Simulation I

This simulation used a nonuniform vertically spaced grid (Figure 4). The thickness of the marine surface layer was assumed to be 10 m. The eddy coefficient for that layer was inferred from the bulk aerodynamic formulation given by Reinking (1980) as follows:

$$Kh = \frac{\rho\ Cp\ U((\theta_z - \theta_o) + 0.84\ \bar{T}\ (q_z - q_o))}{\rho\ Cp\ \frac{\partial \theta}{\partial z}}$$

The eddy viscosity for the mixed layer was computed from the form given by Estoque and Bhumralkar (1970) (equation (2.14)), with Kh calculated from the ratio suggested by Deardorff (1968) (equation (2.16)). The heat

flux parameterization given by Lumley and Panofsky (1964),

$$Hs = - \rho \, Cp \, Kh \, \partial\theta v/\partial z$$

$$He = - \rho \, Ke \, \partial q/\partial z$$

was utilized for the planetary boundary layer calculations. In all simulations Ke was considered equal to Kh. The Dufort-Frankel scheme was used in the second order formulations (I to III and V-A). The finite difference equations are described in Appendix A.

3.2 Simulation II

The main difference between this simulation and the previous one is that bulk aerodynamic formulation was not used for the marine surface layer. Instead the eddy viscosity was computed directly from the formulation given by Estoque (1963):

$$Km = \begin{cases} l^2 \, S \, (1.0 + \alpha \, Ri)^2 & Ri < 0 \\ l^2 \, S \, (1.0 - \alpha \, Ri)^{-2} & Ri > 0 \end{cases}$$

where all the variables were defined in Chapter 2. Therefore, all fluxes in PBL were obtained using a K-theory formulation. All the other calculations and the grid system were the same as those described for Simulation I.

3.3 Simulation III

This simulation was similar to Simulation I. The same formulas were employed for computing the turbulent fluxes. However, two grid systems were used, as a weighted average of the eddy coefficients was introduced. Simulation III was divided into two sections. Simulation III-A considered an SBL of 10 m and a buffer zone of 40 m above, where the average between bulk aerodynamic and K-theory formulations was computed to merge both distributions from the SBL to the mixed layer. Figure 5 shows how the weighted average of the eddy coefficients was obtained. Simulation III-B used an evenly spaced vertical grid in the PBL. Two different vertical spaced intervals were tested (i.e. Dz = 50 m and Dz = 15 m).

3.4 Simulation IV

This simulation differed from Simulation I only, in that the second order Dufort-Frankel scheme was replaced by a first order approximation. In this simulation the heat fluxes (Hs and He) were calculated for each layer. The heat flux gradient was obtained from a parabolic interpolation since an uneven grid was utilized, and incorporated into the governing equations (2.1) and (2.2). Simulation IV-A employed the same distribution of heat flux and eddy coefficients that Simulation I used.

In order to compare different heat flux formulations, Simulation IV-B was conceived. Rather than using Lumley and Panofsky's heat flux formulation, Reinking's (1980) distribution was tested

$$Hs = - \rho\ Cp\ Kh\ (\partial\theta/\partial z + 0.84\ T\ \partial q/\partial z)$$

$$He = - \rho\ Ke\ \partial q/\partial z$$

The other parameters were computed as in Simulation IV-A.

3.5 Simulation V

In previous simulations (I, II and III), the eddy coefficient profile suggested by Estoque and Bhumralkar (1970) was used to compute the sensible heat and moisture flux. Simulation V was developed to compare differences in K-theory formulations. This simulation was similar to Simulation III-B, but the O'Brien's formulation was used to compute the eddy coefficients in the mixed layer. An evenly spaced vertical grid (Dz = 50 m) was utilized. The remaining computations were similar to those in Simulation III-B.

The eddy coefficients derived from bulk aerodynamic formulation were applied in the SBL and constituted the lower boundary for the O'Brien's profile, K'b and Kb in equation (2.15). Another significant change was the modification of the eddy coefficient at the top of the

boundary layer (ka) while it was assumed to be .1 cm^2/sec (Pielke, 1974). Simulation V-B was similar to V-A, but the first order finite difference scheme was applied. A nonuniform vertical grid was used (Figure 4). In order to clarify the different techniques used in the numerical simulations, Appendix E presents a summary of each simulation.

3.6 The Finite Difference Equations

Each meteorologic situation represented different PBL heights and inversion thicknesses. Therefore, when a nonuniformly spaced grid was applied, the first six levels were held constant for all the cases. The remaining height between level six and the top of the inversion was divided into levels of thickness of about 200 m. The inversion was divided into two levels regardless of its thickness. Each case had a different number of levels. All initial variables were interpolated linearly at each level.

a) The Second Order Model

The differential equations that described the transformation of offshore flow are

$$u(\partial\theta/\partial x) = (\partial K/\partial z)\ (\partial\theta/\partial z) + K\ (\partial^2\theta/\partial z^2)$$
$$u(\partial q/\partial x) = (\partial K/\partial z)\ (\partial q/\partial z) + K\ (\partial^2 q/\partial z^2) \qquad (3.1)$$

These are second order differential equations. The procedure followed to obtain the first and second vertical derivatives for a nonuniform grid is found in Appendix A. A Dufort-Frankel scheme was applied. The finite difference forms of the governing equations for the potential temperature and specific humidity are also shown in Appendix A. A forward Dufort-Frankel scheme was used for the first space step.

b) The First Order Model

The finite difference scheme for the first order model is very simple. To solve equations (2.1) and (2.2), $\partial H/\partial z$ was calculated for each level (Appendix A). Therefore, the finite difference equation became

$$\theta_{\ell}^{n+1} = \theta_{\ell}^{n-1} + (2\ Dx/U_{\ell}^{n})\ \partial Hs/\partial z)_{\ell}^{n}$$

$$q_{\ell}^{n+1} = q_{\ell}^{n-1} + (2\ Dx/U_{\ell}^{n})\ \partial He/\partial z)_{\ell}^{n} \qquad (3.2)$$

Both heat fluxes were calculated per unit mass. The method of solution is described in Appendix B.

3.7 The Initial Conditions

3.7.1 The Sea Surface Temperature

The sea surface temperature was interpolated at each grid point using the parabolic profile

$$Tsea\,(x) = T_2 + a\,(X - X_2) + b\,(X - X_2)^2 \qquad (3.3)$$

Knowing the sea surface temperature at three locations one can apply equation (3.3) to obtain a set of two equations with two unknowns:

$$\begin{aligned} T_1 - T_2 &= a\,(X_1 - X_2) + b\,(X_1 - X_2)^2 \\ T_3 - T_2 &= a\,(X_3 - X_2) + b\,(X_3 - X_2)^2 \end{aligned} \qquad (3.4)$$

where T_1 is the sea temperature at the coast, T_2 at the middle of the trajectory and T_3 at its end, and X is the respective distance from the coast. Solving the system (3.4) for a and b, one obtains

$$a = \frac{(T_1 - T_2)(X_3 - X_2)^2 - (T_3 - T_2)(X_1 - X_2)^2}{(X_1 - X_2)(X_3 - X_2)^2 - (X_3 - X_2)(X_1 - X_2)^2}$$

and

$$b = \frac{(X_1 - X_2)(T_3 - T_2) - (X_3 - X_2)(T_1 - T_2)}{(X_1 - X_2)(X_3 - X_2)^2 - (X_3 - X_2)(X_1 - X_2)^2} \,.$$

Equation (3.3) was used to calculate the sea surface temperature at each grid point. The potential temperature, the virtual potential temperature, and the specific humidity at each grid point were also calculated.

3.7.2 The Geostrophic Wind

The geostrophic wind at the surface (Ug_o, Vg_o) was calculated by analyzing the pressure distribution around the Wallops Island station. To find the pressure field, data from four stations were utilized: Atlantic City, Richmond, Hatteras and Chesapeake Light Tower. Figure 6 shows the station distributions used to calculate the horizontal pressure and temperature gradients.

Finally, the geostrophic wind equations are

$$Vg_o = (1/f\rho)\ \partial P/\partial x \qquad (3.5)$$

$$Ug_o = -(1/f\rho)\ \partial P/\partial y \qquad (3.6)$$

To calculate the pressure gradients in the area the pressure at any given station was assumed to be

$$P(x,y) = P_o + (\partial P/\partial y)\ Y + (\partial P/\partial x)\ X$$

A system of two equations with two unknowns was obtained for the four stations considered. They were

$$P_4 - P_3 = (\partial P/\partial y)\ (Y_4 - Y_3) + (\partial P/\partial x)\ (X_4 - X_3) \qquad (3.7)$$

$$P_2 - P_1 = (\partial P/\partial y)\ (Y_2 - Y_1) + (\partial P/\partial x)\ (X_2 - X_1). \quad (3.8)$$

Solving for $(\partial P/\partial y)$ and $(\partial P/\partial x)$, one was able to calculate Vg_0 and Ug_0. Assuming that the real wind at the top of the model was equal to the geostrophic wind, one could calculate the variation in the wind with height $((\partial Ug/\partial z)_1, (\partial Vg/\partial z)_1)$.

Vertical shear of the geostrophic wind with height is also related to the horizontal temperature gradient by

$$(\partial Ug/\partial z)_2 = - (g/f\ T)\ \partial T/\partial y \quad (3.9)$$

$$(\partial Vg/\partial z)_2 = (g/f\ T)\ \partial T/\partial x \quad (3.10)$$

With a procedure similar to that described above for the pressure, the temperature gradients and the geostrophic shear were calculated. An average value for the wind shear due to the pressure and temperature distributions was computed to compensate for discrepancies between both formulations. The geostrophic wind varied with height and was computed for each level. These winds were assumed to be constant along the trajectory, because relatively short travel distances were considered.

3.8 Integration of the Wind with Height

The wind was integrated with height by two methods. The equations

$$\frac{\partial^2 u}{\partial z^2} = -\frac{f}{K} v + \frac{f}{K} vg - \frac{1}{K}\frac{\partial K}{\partial z}\frac{\partial u}{\partial z} \qquad (3.11)$$

$$\frac{\partial^2 v}{\partial z^2} = \frac{f}{K} u + \frac{f}{K} ug - \frac{1}{K}\frac{\partial K}{\partial z}\frac{\partial v}{\partial z} \qquad (3.12)$$

that describe vertical variation of the wind field were integrated with height. The results of a Runge-Kutta method (Ralston, 1962) and a Shoting method (Burden et al., 1978) were compared. The formulation of K by equation (2.14) was introduced into equations (3.11) and (3.12) to apply the Runge-Kutta method. The equations were solved for u and v with assumed values of the vertical gradients of the wind components. The equations were solved by Newton's method for two dimensional functions of two variables until the parameters E_1 and E_2, defined as

$$E_1 = Utop - \tilde{U}top$$

$$E_2 = Vtop - \tilde{V}top$$

were minimized. $\tilde{U}top$ and $\tilde{V}top$ were the calculated values; Utop and Vtop, the observed ones at the top of the PBL.

With the Shoting method a different procedure was used. The eddy coefficients (equation (2.14) were calculated first, and with these values equations (3.11) and (3.12) were solved for u and v. The method was

repeated until E_1 and E_2 had a minimum value. Both methods gave the same results, but the latter used less CPU time. Consequently, the Shooting method was selected for the calculations. Due to the almost constant direction with height, the V component of the wind was small, and, therefore, neglected. A characteristic wind profile obtained from the Shoting method, corresponding to December 17, 1972 is shown below.

Height (m)	U (m/s)	V (m/s)
10	13.1	2.3
25	15.7	0.7
50	17.9	-0.7
100	20.4	-2.2
200	22.8	-3.0
350	24.7	-5.0
559	26.3	-5.5
769	27.4	-5.5
979	28.2	-6.1
1189	28.9	-6.3
1316	29.9	-6.8

Chapter 4

CASE DESCRIPTIONS

Six individual cases of offshore air flow were selected for the test. Each represented different characteristics in the sea surface temperature distribution and in the air mass temperature. The meteorological data were provided by the National Weather Service of the National Oceanic and Atmospheric Administration. The sea surface temperatures were obtained from charts provided by the Department of Transportation of the U.S. Coast Guard Oceanic Unit. The charted surface isotherms were prepared from data collected by a remote sensing infrared thermometer on board a Coast Guard aircraft.

Wallops Island to Chesapeake Light Tower was selected to test the model for relatively short distances (102 km). The sea surface temperature between these stations did not show great changes. The path between Wallops Island and a buoy located at 36.5°N, 73.5°W was chosen for long distance (222 km) tests. The sea surface temperatures between these locations had a large gradient due to the presence of the Gulf Stream. Figure 6 shows the location of the two pairs of stations between which air mass

transformation was studied. At the offshore stations all the variables at anemometer level were measured, and those values were compared with those forecasted by the model. There were no measurements of temperature and dew point temperature with height; therefore, comparison of real data with the profiles given by the model was impossible. The following cases were considered:

Case 1

November 16, 1972. Wallops Island - Chesapeake Light Tower

Figure 7 shows the profiles at 2400Z for the initial conditions. The air mass temperatures were cold. The surface temperature was 275°K, while the sea surface temperature at the coast was 283.16°K. This initial state represented an appreciable jump in the lower boundary conditions. "Jump" is defined as the rapid increase in the temperature at the coastline. This case was considered unstable.

The air mass was relatively dry; therefore, there was also a jump in the humidity conditions. The PBL was 1106 m thick, and a thick inversion was present (496 m). The wind was almost constant in direction with height and had an average of 350°. The wind speed varied between 5 and 15 m/sec. The sea surface conditions along the trajectory were almost homogeneous with a gradient of 0.01°K/km.

This case showed the reaction of the model when a jump in the initial conditions of the lower boundary was present.

Case 2

December 18, 1972. Wallops Island - Buoy

This case represented relatively cold conditions with surface temperatures below condensation point (271.16°K). The air mass was very dry with a dew point at the surface of 266.16°K.

The wind speed varied between 7 and 21 m/sec, and the mean direction was 310°. The height of the PBL was 1374 m, and the inversion thickness was 151 m. The increase in the sea surface temperature from the coast to the buoy was 10°K. This was viewed as one of the most unstable cases. Figure 8 shows the initial characteristics of this cool air mass at 2400Z.

Case 3

December 7, 1972. Wallops Island - Buoy

This case was quite unstable, because the onshore air temperature of the surface was 274.85°K, and the sea surface temperature at the coast was 281.66°K. The water temperature increased 8.5 degrees along the trajectory.

The height of the PBL was 931 m, and a thin, dry inversion of 155 m was present.

The north winds were almost constant in direction, and the magnitude was between 6 to 14 m/sec. The onshore dew point temperature at the surface was 269.16°K. Figure 9 shows the initial profile of the variables at 1200Z.

Case 4

November 6, 1972. Wallops Island - Chesapeake Light Tower

Figure 10 shows the initial profiles of the temperature and dew point temperature of the air mass at 2400Z, plotted on a Stuve diagram at the Wallops Island station. The temperature at the surface was 284.8°K, and the dew point was 280.0°K. The height of the mixed layer was considered to be the height of the top of the inversion (zi), which was 1499 m in this case. A thin inversion of 219 m was present. The wind in this layer varied between 5 and 11 m/sec in magnitude. The direction was almost constant, with a ten degree variation from top to bottom of the PBL.

The sea surface temperature at the coast was 285.0°K. Therefore, the air mass found a 4.3°K increase in the water temperature as it travelled to the Light Tower. The air temperature at anemometer level was approximately equal

to the water temperature. This was considered to be a relatively stable case, since the initial conditions did not produce a drastic change in the lower boundary.

Case 5

December 26, 1972. Wallops Island - Chesapeake Light Tower

This case was considered stable, because the air temperature at anemometer level was the same as the sea surface temperature at the coast. The air temperature at the surface was 280.8°K, and the dew point temperature was 279°K. The mixed layer was thin (487 m), and the inversion was 103 m. This case depicted saturation conditions at the base of the inversion. Figure 11 shows the initial profiles of the variables. The sea surface temperature gradient was 0.01°K/km, consequently the water temperature conditions were almost homogeneous along the trajectory. The wind blew from the North, and the speed varied little in magnitude (6 m/sec). This case was selected specifically to test the model in relatively stable conditions.

Case 6

November 29, 1972. Wallops Island - Chesapeake Light Tower

Almost all the previous cases were at 2400Z; this case was at 1200Z. The sea surface temperature at the coast was 282.66°K, and the gradient along the trajectory

was small (0.01°K/km). The surface air temperature was 277.76°K, and the dew point was 271.0°K.

There was a larger difference in the initial air-sea temperature at the lower boundary than in the previous case, and the air mass was significantly drier than in Case 3. Figure 12 shows the initial profiles of temperature and dew point. The wind speed varied between 5 and 13 m/sec and was almost constant in direction with height. This case represented a PBL of 818 m.

To clarify the concept of "jump" and stability of each case, Figure 13 provides a schematic representation of the temperature changes at the lower boundary for each of the cases.

Chapter 5

RESULTS AND DISCUSSION

The simulations which were described in Chapter 3 were then applied to the actual cases described in Chapter 4. To clarify the results, the application of these numerical simulations to one case is discussed in detail in this chapter.

5.1 Numerical Simulations Applied to Case 1

This meteorological situation featured an initial large step change in temperature in the lower boundary (Figure 13). There was an 8°K difference between the air mass and the sea surface temperature (DT = Tsea - Tair) at the coastline. This very unstable condition caused strong heat flux into the air. There was only a 1°K change in the sea surface temperature along the trajectory.

5.1.1 Simulation I

Simulation I was considered first. Here a Kh value for the SBL (10 m) was inferred from a bulk aerodynamic formula, and a K for the mixed layer was obtained from

Estoque and Bhumralkar's (1970) formulation of the eddy coefficient. The nonuniformly spaced vertical grid described in Figure 4 was used.

When Simulation I with step size of 1000 m (Dt = 1000 m/U) was applied to this case, computational instability grew rapidly. The Dufort-Frankel scheme applied to a linear problem is normally stable for any value of γ, where γ is defined by

$$\gamma = \frac{2\ K\ Dx}{UDZ^2} = \frac{2\ K\ Dt}{DZ^2}$$

Due to the great variation in eddy flux in these unstable domains, variable eddy coefficients are needed for realistic simulations. Therefore, the model admitted a "nonlinear" effect in the term $(\partial K/\partial z)(\partial \theta/\partial z)$ because the K distribution depended on $\partial \theta/\partial z$. Furthermore, since the original purpose in using the model was to portray the high resolution features of offshore flow, a variable length grid spacing was used to provide high resolution in the boundary layer. Apparently one or both of these features contributed to the instability of the Dufort-Frankel scheme.

The simulation was rerun with a step size decreased to 250 m which reduced γ four fold, but the model ran a few more steps before becoming unstable again. Unstable high frequency waves propagated horizontally as well

as vertically. To dampen these unstable waves vertical and horizontal smoothing was introduced.

Systematic explicit smoothing included in numerical models will dampen computational high frequency wave number components, which are generally a focal point of the instability. In this model the following simple three point operator (Shapiro, 1970) was applied to the vertical and horizontal computed values:

$$\phi_i = (1 - S)\ \phi_i + (S/2)\ (\phi_{i+1} + \phi_{i-1}), \qquad (5.1)$$

ϕ represents any forecasted variable and S is a constant that varies between 0 and 1 (i.e. $S = 0$ means no smoothing).

If the operator is applied to the harmonic form

$$\phi_i = A\ e^{ikx}$$

where the wave number is given by $2\pi/L$ and A is a constant which may be complex, the result (Haltiner and Williams, 1980) is

$$\phi_i^* = R\ \phi_i$$

R is referred as the response function as given by

$$R(L) = 1 - 2\ S\ \sin^2\ (\pi Dx/L)$$

It is evident that this particular smoothing operator does not affect the wave number nor the phase (provided $R > 0$) of the original wave, but only its magnitude. If S equals 0.5, for a wavelength equal to $2Dx$, $R = 0$, hence two gridlength waves will be removed by the smoother. Moreover, wavelengths larger than $2Dx$ will be dampened by the smoother. For example, with L equal to $10\ Dx$, R equals 0.905, which is less than ten percent reduction in amplitude.

The inclusion of smoothing produces two important effects in numerical simulations of the diffusion equation. First, it dampens or removes the short wave length components, and secondly increases the order of the diffusion in the model. The latter might be explained in the following way: if a layer i is considered in the system and heat flux is occurring, part of the heat is advected downward from layer i and part is advected upward and replaced by heat coming from layers $i+1$ and $i-1$, respectively. If the smoothing is applied twice, the heat from layer $i-1$ entering layer i must also advect heat from layer $i-2$, and perhaps $i-3$. Similarly, the diffused heat from $i+1$ must contain heat from the layer above.

Smoothing factors from 0.1 to 0.5 were applied to Simulation I with little improvement. Inspection of the results showed that the major instability occurred at the grid level above the sea surface. This was the region

where very large eddy diffusion coefficients, small vertical grid intervals, and very large gradients in $K(z)$ occur. Clearly, two grid waves formed and oscillated with successive 180 degree phase shifts and increasing amplitude. Figures 14 and 15 show this behavior for Case 2. This clearly was some form of computational instability.

One suspected that the inclusion of the term $(\partial K/\partial z \cdot \partial\theta/\partial z)$ would falsely exaggerate the negative contribution if values of $\partial K/\partial z$ are overestimated. Simulation I became stable only after a heavy smoother ($S = 0.8$) was applied to a horizontal grid interval of 250 m. While the application of a smoother damped those unstable computational waves, excess smoothing compromises the purposes of the high resolution system.

In summary, the attainment of computational stability required the reduction of the grid interval to 250 m and the double application of a very heavy smoother which masked the high resolution features of the model and warmed the entire layer unrealistically. The results (Table 1) fit the observed data poorly.

From these results two major problems were apparent and will be addressed separately: (a) computational instability in the surface layer, and (b) excessive warming at the top of the model which totally destroyed the

inversion in an unrealisticly short time. Initially, attention was concentrated on (a).

5.1.2 Simulation II

The Dufort-Frankel approach is inherently stable in classical application. The nonuniform grid interval and the strong variability in K (one or both) had to be contributing factors to the instability. The model was systematically modified to isolate the effects of these two major factors. Since the primary instability was located in a region with a step function K variability, this problem was addressed first.

To test this hypothesis, Simulation II was applied, in which K-theory formulation was used for the eddy coefficient in the surface layer rather than a K derived from the bulk aerodynamical formula. While this form would increase the SBL K value by an order of magnitude, it would reduce the value of $\partial K/\partial z$ in the area of maximum instability and hopefully minimize the effect of the gradient of K.

With a $Dx = 1000$ m and $S = 0.1$ the model became very unstable. When S was increased to 0.4 and the step size reduced to 250 m the model became stable. This was very significant. That is, in spite of the fact that the actual K at the major level of instability was

dramatically increased, computational stability was attained with only a modest smoother ($S = 0.4$) compared with that required ($S = 0.8$) in Simulation I. The results confirmed the hypothesis that the large values of $(\partial K/\partial z \cdot \partial\theta/\partial z)$ contributed (directly or indirectly) to the instability. The instability properties of this term will be further confirmed by an analytic analysis in this chapter.

The above statement is also illustrated by comparison of the magnitude of the term $(\partial K/\partial z \cdot \partial\theta/\partial z)$ in the basic equation that described the transformation of the grid level above the sea surface. The values are

$$\partial K/\partial z \cdot \partial\theta/\partial z \sim -0.64\,^{\circ}K/sec \qquad \text{Simulation I}$$

$$\partial K/\partial z \cdot \partial\theta/\partial z \sim -0.25\,^{\circ}K/sec \qquad \text{Simulation II}$$

It is clear that in Simulation II the term that presented the gradient at K was less than half the value in Simulation I, after the first step.

Simulation II strongly over-predicted the anemometer level temperatures at the offshore site (Table 1), but with the large magnitude of K in the SBL this was to be expected. While Simulation II was more successful from a computational viewpoint, one should not expect realistic results with K-theory applied to the flux in the SBL. Again, heat flux into the top of the model was excessive

and cuased the rapid destruction of the inversion leaving a well mixed layer below 1700 m (Figures 16 and 17).

The analysis of the results showed that the initial temperature at 10 m was 274.63°K, in the first step (250 m) the temperature at that level increased dramatically to 282.16°K. After the first step, a "back and forth" oscillation of two degrees developed. Figure 18 shows this behavior for case 3. After 35 steps, this behavior disappeared, and a constant temperature increase occurred with distance. The same behavior was found with the specific humidity profile. In a few meters the variables at the first level reached the conditions that the air mass should have found at the end of the trajectory.

From the foregoing, the almost arbitrary decrease of the magnitude of $\partial K/\partial z$ was achieved, by increasing the value of K in the SBL, which did reduce the instability. However, K-theory applied to the SBL in unstable domains results in much higher heat flux into the SBL than the more realistic bulk theory. It would seem to be preferable to reduce $\partial K/\partial z$ by reducing K in the PBL just above the SBL. However, the variable K in the unstable PBL is a significant factor and is needed for realism in the computations. Accordingly, better results should be expected if any modification of the K profile were based on physical principles if possible, or physical intuition if necessary.

5.1.3 Simulation III

To diagnose the physical implications of this step function in K, an analytical solution for Case 1 was developed by simplifying the physical model in which mild physical constraints were imposed on the lowest two layers of the model. The modified physical system consisted of a cold air mass flowing offshore over a warmer but uniform temperature water surface. Bulk theory flux was applied in the first layer (between levels 1 and 2) and K-theory heat flux in the second layer (Figure 19). Supported by observed results $K \cdot \partial\theta/\partial z$ in layer 2 was assumed to be the same as layer 3, i.e. the temperature at level 3 would remain constant.

Furthermore, K and $(\partial K/\partial z)$ at level 2 were taken to be constant in time. Thereby, the diffusion equation was reduced to an ordinary differential equation that permitted an analytic solution for the behavior of the temperature at level 2 (the upper boundary of the SBL). The differential equation becomes (Appendix C)

$$\frac{\partial\theta_2}{\partial t} + \gamma_2\,\theta_2 = \frac{\gamma_2\,K'}{2\,K_2} + \gamma_2\,\bar{\theta} = M \qquad (5.2)$$

where

$$\gamma_2 = (2\,K/Dz^2)$$

$$K' = K_{2.5} - K_{1.5}$$

$$\bar{\theta} = (\theta_3 + \theta_1)/2$$

$$\theta' = (\theta_3 - \theta_1)/2$$

Therefore,

$$\Delta\theta = \theta(t) - \theta_2(o) = (\bar{\theta} - \theta_2^o)(1 - e^{-\gamma_2 t}) + \frac{K'\theta'}{2K_2}(1 - e^{-\gamma_2 t})$$

Because $\gamma_2 > 0$,

$$\Delta\theta \longrightarrow (\bar{\theta}_o - \theta_2^o) + \frac{K'}{2K}\theta' \qquad (5.3)$$

$$t \longrightarrow \infty$$

This equation was applied to characteristic temperature distributions of the unstable offshore boundary layer (case 1). K values were inferred from bulk theory for the layer between levels 1 and 2 (Figure 19), and pure K-theory for the layer above, that is,

$$\theta_3 = 269°K$$

$$\theta_2 = 270°K$$

$$\theta_1 = 280°K$$

$$K_{1.5} = 1.0\ m^2/sec$$

$$K_2 = 5.0 \text{ m}^2/\text{sec}$$

$$K_{2.5} = 20.0 \text{ m}^2/\text{sec}$$

Solving equation (5.3) with these values gave a change in temperature at level 2 of -5.95°K. This negative value is admittedly larger than would be expected in the real world because in reality it would be damped by the changing values of the eddy coefficient in the adjustment process. In any event, this indicates that with this step function in K, a marked low level inversion base at the top of the SBL would develop. Since observational evidence does not support such an inversion and therefore it must conclude that part of the problem resides in the physical constraints.

Bulk aerodynamic formulation has been tested extensively by measurements over the ocean. The author suggests that the step function variation of flux arising from abutting K-theory and bulk theory at the top of the SBL is not realistic, particularly in unstable domains. Merging K-theory and bulk theory through a "buffer zone" above the SBL would seem to be a more reasonable exploratory approach.

Simulation III was a duplicate of the ill-fated Simulation I, but K-values above the SBL were "faired in" as shown in Figure 5. The "buffer zone" had a thickness

of 40 m. For the same Dx (250 m), this simulation required much less smoothing (S = 0.2) to make the model run, demonstrating much less computational instability. This method reduced the instability by a factor of two. After the first step size, the temperature at 10 m did not increase as rapidly as it did in Simulation II. From the results, the bulk aerodynamic formulation appeared to parameterize the heat flux from the ocean into the air more accurately.

A variation of Simulation III-A which increased the "buffer zone" from 40 to 90 m was next applied. However, no improvement was obtained in the resulting profiles of temperature and humidity. This suggested that the selection of 40 m as the "buffer zone" was appropriate and that there was no need to increase the "buffer zone" thickness to improve calculations or reduce instability, in this particular case. Perhaps with stronger winds and greater instability this might be necessary.

5.1.4 Effect of the Use of a Nonuniform Grid

In the foregoing, large variations of K in the vertical obviously contributed to computational instability when using the normally stable Dufort-Frankel scheme. Brown and Pandolfo (1979) studied the advection-diffusion equation with finite difference schemes that are

unconditionally stable when the grid interval is uniform. They found that when such schemes were generalized to account for nonuniform grid spacing, instability could result. The effect of the nonuniform grid interval was not as intuitively evident and was more difficult to isolate.

To ascertain whether or not a nonuniform vertical grid was a factor in these unstable cases, Simulation III-B was developed. This simulation was identical to III-A except that a uniform grid interval was used which was equal to the smallest grid interval in the variable grid system. A uniform Dz = 15 m was considered in the vertical.

The increased number of levels increased the computational cost drastically so the total computational distance was restricted to 25 km (instead of 102km). Simulations III-A and III-B were run and compared for the same potential temperature distributions for these simulations for a travel distance of 25 km.

Two conclusions were reached as a consequence of the comparisons of the results between III-A and III-B:

a) There was no improvement in the computational stability with the uniform grid system. Hence, the nonuniform grid was probably not a factor in the earlier computational instability.

b) The decrease in heat introduced into the system from the top of the model by III-B compared to III-A was striking. These very small grid intervals on either side of the inversion would drastically reduce the effect of the smoothing process and this clearly points out a major problem in the use of smoother.

Figures 22 and 23 show the results of Simulation III-B for this case when Dz = 50 m, Dx = 250 m, S = 0.1, and the travel distance was 102km. Figure 24 shows the eddy coefficient profiles. The shape of the temperature distribution was similar to Figure 21. But due to the increase in Dx at the inversion levels, there was an increase in the warming of these layers. This effect is discussed in the next sections. This case ran with half of the smoother that was used in Simulation III-A as a result of the increase in vertical thickness at the lower boundary.

The nonuniform grid seems to present no general problems in the investigation. However, it is suggested here that if a nonuniform grid is required, the following approach might be preferable to the nonuniform scheme used in these simulations. One solution to the problem is to apply a coordinate transformation

$$\xi = F(z); \qquad z = F^{-1}(\xi)$$

and then use equal spacing in the new variable ξ.

This technique was suggested by Taylor and Delage (1972) and Grosch and Orszag (1977). If higher resolution in the layers near the inversion is desired, the transformation must be carefully selected.

5.1.5 Simulation IV

The ill-fated Simulation I required the integration of a second order equation, i.e.

$$u \frac{\partial \theta}{\partial x} = \frac{\partial K}{\partial z} \cdot \frac{\partial \theta}{\partial z} + K \frac{\partial^2 \theta}{\partial z^2}$$

$$u \frac{\partial q}{\partial x} = \frac{\partial K}{\partial z} \cdot \frac{\partial q}{\partial z} + K \frac{\partial^2 q}{\partial z^2}$$

The identical problem can be addressed through a first order equation (Simulation IV-A):

$$u \frac{\partial \theta}{\partial x} = - \left(\frac{1}{\rho Cp}\right) \frac{\partial Hs}{\partial z}$$

$$u \frac{\partial q}{\partial x} = \left(- \frac{1}{\rho}\right) \frac{He}{\partial z}$$

where H at the SBL is still computed from bulk theory but $H(z)$ in the mixed layer is deduced from K-theory, i.e.

$$Hs = - \rho Cp \, Kh \, \partial\theta/\partial z$$

$$He = - \rho Ke \, \partial q/\partial z$$

and K is computed from the Estoque and Bhumralkar's (1970)

profile exactly as in Simulation I. The only difference between this simulation and Simulation I was the mathematical scheme (i.e. first order equation). The finite difference equations were described in Chapter 3. The nonuniformly spaced vertical grid from Simulation I (Figure 4) was used. In this simulation the heat fluxes (Hs and He) were calculated for each later. The heat flux gradient was obtained from a parabolic interporlation, to accommodate the uneven grid.

Figures 25 and 26 show the results of case 1 for this simulation for a step size of 250 m and a smoother of 0.1. The first 200 m were unstable, though the rest of the layer was stable. These profiles showed the steep temperature graduents in the layers near the sea surface. The high resolution that was maintained in the lower layers elucidated these results. The first order simulation produced results similar to those of the earlier simulations, but required less computing time.

Comparison between Simulation IV-A and III-A showed similar results of anemometer level at the offshore station. However, the smoothing factor was half the value needed for Simulation III-A. Again the heat flux coming through the top of the model was excessive. In Simulation IV-A the heat flux formulations did not merge the K-theory and bulk theory in a "buffer zone"; however, the characteristic instability at the lower boundary was not present.

Probably, the fit of a parabolic curve to $\partial H/\partial z$ reduced the problem. That is, for the flux value at level 2, data at the three lowest grid points were used. This constituted an implicit smoother that merged the heat flux formulations itself.

5.1.6 Simulation V

The second major problem found in these simulations was the large downward heat flux from the inversion layer. This spurious feature dominated the model and unrealistically destroyed the upper inversion. While direct comparison with observed data was not possible at the upper boundary, the excessive heat flux descending from the top was evident in all the simulations. The diffusion process would be expected to weaken and lower the inversion, but the rate at which this process occurs in the model was not observed in nature.

This ficticious heat flux down through the inversion was attributed to two distinct model features:

a) The effects of smoothing applied to maintain computational stability were amplified by the increase in frequency of application associated with the reduction of the space step (Dx decreased to 250 m). These effects were further intensified in the top layers of the model by the large values of Dz in these regions.

a) The large values of the diffusion coefficients that were a product of the technique used to compute them. A physical analysis of both of these features and potential approaches for reducing their effects are discussed in the following paragraphs.

5.1.7 Effect of Excess Smoothing

Figures 20 and 21 show the resulting profiles for the potential temperature for a nonuniform grid (Simulation III-A) and an evenly spaced vertical grid of 15 m thickness (Simulation III-B), respectively. When the inversion layer was divided into many levels the effects of the downward flux was greatly reduced, even though the same smoother (S = 0.2) was applied in both simulations. The effect of smoothing for a given smoother increases dramatically with the increase of the size interval.

There are two sources of changes in the model variables, one due to the diffusion equation in its simplified form

$$\theta^{x+\delta x} - \theta^{\delta x} = \frac{K\ Dx}{U\ Dz^2} \left(\theta^{\delta x}_{i+1} + \theta^{\delta x}_{i-1} - 2\ \theta^{\delta x}_{i}\right)$$

or

$$\Delta\theta^{*n} = 2\ \gamma\ (\bar{\theta} - \theta^{n}_{i})$$

where

$$\bar{\theta} = \frac{1}{2} \left(\theta_{i+1}^{\delta x} + \theta_{i-1}^{\delta x}\right)$$

and the second is due to the smoothing process:

$$\Delta\theta^n = S \left(\bar{\theta} - \theta_i^n\right) .$$

The ratio between these two effects is given by:

$$\frac{\Delta\theta^n}{\Delta\theta^{*n}} = \frac{S}{2\gamma}$$

In the case of the evenly spaced vertical grid (15 m), γ was approximately 1.4 and S was 0.2, therefore

$$\Delta\theta^n = 0.07 \ \Delta\theta^{*n}$$

This meant that the resulting change in temperature due to the smoother was only 7% of the one given the diffusion scheme. When a nonuniform grid was used, γ was equal to 0.005 and S was the same as before, therefore

$$\Delta\theta^n = 20 \ \Delta\theta^{*n}$$

This showed that the effect of the smoother (S) was exaggerated by the large vertical thickness in III-A in the vicinity of the inversion. The smoothing with large grid intervals (Figure 20) destroyed the resolution needed to maintain the temperature jump characteristic of

the inversion. The fixing of the constant temperature at the upper boundary provided an unlimited heat sources.

In general, the excess smoothing presents an enigma. That is, the reduction of the grid interval does dampen the "diffusion augmentation" of smoothing, but it also requires a shorter spacial step, which increases the frequency of application of the smoother. Clearly, an optimum approach would be to minimize the computational stability requirement and reduce (or hopefully remove) the need for smoothers.

5.1.8 Effect of Overestimation of the Diffusion Coefficient in the Upper Levels of the Model

It is suggested that the eddy coefficient values obtained from Estoque and Bhumralkar's (1970) distribution are much too large for K values in the vicinity of the inversion. Initially, Estoque and Bhumralkar's (1970) profile was selected to determine the vertical distribution of the eddy viscosity, primarily because this coefficient was explicitly dependent upon the wind shear, the static stability and height. This distribution was expected to produce more meaningful values for the eddy flux coefficients. As a result of this study, it can be seen that this seemingly more precise approach generally overestimates the eddy coefficient in unstable areas.

Deardorff (1972) found the same problem when he used the nonlinear eddy viscosity formulation of Smagorinsky (1973). He found that the eddy coefficient was too large in the vicinity of the interface at the top of the PBL. This smeared the temperature jump, which tends to form in this region in nature. A few attempts to correct this problem, such as modifying the mixing length were mentioned by Bodin (1980), but all of them were rather arbitrary.

The poor behavior of the eddy coefficients at the top of the model might be explained by the characteristic length scales that were present in the model. In reality, heights above the base of the inversion are related to geostrophic flow. The ratio between the Rossby and Reynolds numbers ($E = K/f\ L$) should approach zero, because friction is negligible, and the vertical scale L is large. As a result of the large K's generated at the top of the inversion, E was different from zero. Within the PBL the parameter E approximated one so that Ekman equations could be applied. It does not seem likely that a parameterization for diffusion coefficients applicable to the lower part of the unstable PBL would provide realistic values in the inversion and in the free atmosphere. Further, while it is reasonable that the scale of the eddies would increase with distance from the very "hard" earth surface, it would be reasonable to expect a decrease

in the eddy scale as the "soft" boundary of the inversion base is approached.

For these reasons it is felt that the K-theory values of the diffusion coefficients were unrealistically high in the inversion and in the free atmosphere above. If the Ekman layer is thicker than the constant flux layer, the level of maximum K lies just above the SBL (O'Brien, 1970) or higher in the unstable regions. This type of profile was not generated by the K-theory computations.

As an alternative, a simpler technique was suggested which is not based upon layer by layer properties, but upon a characteristic profile grounded in physical principles and explicitly determined by boundary conditions at the top and bottom of the model, such as an O'Brien's (1970) profile (Figure 27). The eddy coefficients derived from bulk aerodynamical formulation were applied in the SBL and constituted the lower boundary for the O'Brien's (1970) distribution. The value of the eddy coefficient at the top of the boundary layer was assumed to be 1 cm^2/sec (Pielke, 1974).

Using this approach to obtain the diffusion coefficient, Simulations V-A and V-B were developed. Simulation V-A was run with a second order scheme and an evenly spaced vertical grid (Dz = 50 m), and Simulation V-B with a first order scheme and a nonuniform vertical grid as

used in Simulation I. The use of K values generated by an O'Brien's profile (1970) eliminated most of the problems mentioned earlier. The O'Brien formulation also does not have the extreme step function in $\partial K/\partial z$ in the SBL found in previous simulations. This removed the computational instability and permitted a larger step size and a smaller smoothing factor was applied less frequently.

The results were much more realistic with this approach. With a greater Dx (1000 m) and a smoothing factor of 0.1, Simulation V-A gave reasonable results for the layer at anemometer level. The amount of heat incorporated into the system was greatly reduced. Only a 1°K increase in the mean potential temperature occurred.

Figures 28 and 29 show the results for Simulation V-A. These figures show that the inversion was preserved along the trajectory over the water. Because little heat came from the inversion (i.e. low values of K), the profiles above 500 m were not greatly modified. This was expected and confirmed by measurements over the Great Lakes (Lenschow, 1965).

5.1.9 Simulation V-B

The first order scheme with O'Brien's distribution to the eddy coefficient applied to an unevenly spaced vertical grid (Simulation V-B) was run with one of the most unstable

cases (Case 2). The simulation gave again very reasonable results (Table 2). Figures 30 and 31 show the resulting profiles. From the results of Simulation V one may conclude that the simple formulations and schemes should be preferred in the unstable domains, until more research is done to improve parameterization techniques in unstable zones.

From these results, the use of the O'Brien's eddy coefficient profile eliminated both sources of the spurious heat flux through the top of the model. That is,

a) The minimizing of the computational instability problems permitted much larger spacial steps and smaller smoothing coefficients thereby reducing the smoothing effect in the upper level without reducing the grid interval size.

b) The reduced K values in the vicinity of the inversion controlled the previous overestimation of the diffusion through the inversion. Further, the gentle K profiles in the vicinity of the SBL removed the need for arbitrary adjustment in the eddy coefficient distribution which in turn seems to favor more realistic temperature changes in the SBL.

5.2 Results of Linear Computational Stability Analysis Applied to the Numerical Simulations

The basic prediction equation used in the simulations is given by

$$u \frac{\partial \theta}{\partial x} = \frac{\partial}{\partial z} \left(K \frac{\partial \theta}{\partial z} \right) = K \frac{\partial^2 \theta}{\partial z^2} + \frac{\partial K}{\partial z} \cdot \frac{\partial \theta}{\partial z} \qquad (5.4)$$

where K and θ are functions of z and t. The variable K which is determined through a diagnostic equation makes equation (5.4) nonlinear. The Dufort-Frankel finite difference formulation is given by

$$\theta_m^{n+2} = \frac{1-\gamma}{1+\gamma} \theta_m^n + \frac{2\gamma}{1+\gamma} \theta_m^{n+1} + \frac{\gamma'}{1+\gamma} \theta'^{n+1}_m \qquad (5.5)$$

where

$$\gamma = (2K\ Dt)/Dz^2$$

$$\gamma' = (2\ K'\ Dt)/Dz^2$$

$$K' = K_{m+\frac{1}{2}} - K_{m-\frac{1}{2}}$$

$$\bar{\theta}^{n+1}_m = (\theta^{n+1}_{m+1} + \theta^{n+1}_{m-1})/2$$

$$\theta'^{n+1}_m = (\theta^{n+1}_{m+1} - \theta^{n+1}_{m-1})/2$$

Equation (5.5) can be reformulated as

$$\Delta\theta = \theta_m^{n+2} - \theta_m^n = \Delta\theta_2 + \Delta\theta_1 = \frac{2\gamma}{1+\gamma}\left(\bar{\theta}_m^{n+1} - \theta_m^n\right) + \frac{\gamma'}{1+\gamma}\,\theta'^{n+1}_m \tag{5.6}$$

If K and K' are held constant in time, equation (5.6) can be linearized; however, since $\partial K/\partial z$ does not equal zero, the second term on the right-hand side admits a nonlinear effect to the solution hence this term was alluded to as the "nonlinear" term. If either $\Delta\theta_1$ or $\Delta\theta_2$ become unstable it would unquestionably amplify the computation of the other. However, if both are stable the system should remain stable.

$$\Delta\theta_1 = \frac{2\gamma}{1+\gamma}\left(\bar{\theta}_m^{n+1} - \theta_m^n\right) \tag{5.7}$$

This is the traditional form of the Dufort-Frankel system applied to the linear diffusion equation and is shown to be inherently stable (Appendix D). The contribution from the "variable K" term is given by equation (5.8)

$$\Delta\theta_2 = \frac{\gamma'}{2(1+\gamma)}\left(\theta_{m+1}^{n+1} - \theta_{m-1}^{n+1}\right) = \frac{C^*Dt}{Dz} \tag{5.8}$$

where

$$C^* = \frac{K'}{(1+\gamma)\ Dz}$$

It is identical in form to the advection equation ($\partial U/\partial t = C^*\ \partial U/\partial x$) which is shown to be unstable for

$C^* \Delta t/Dx > 1$ in the three time level "leapfrog" scheme. Equation (5.8) will become unstable (Appendix D) if

$$\frac{\gamma'}{1+\gamma} > 2$$

or

$$K' > 2K$$

Clearly, the instability criterion ($K' > 2K$) is rarely satisfied in the atmosphere. However, in the very unstable boundary layer in which the effective diffusion coefficients for the SBL are inferred from bulk theory and K in the layer just above is derived from classical K-theory, K' is frequently many times greater than K. According to the above, computational instability could be unavoidable in this domain without special precautions. This type of instability was manifested at the top of the SBL in several of the simulations.

In running Simulation I, computational stability at the top of the SBL was impossible without using a double smoother of $S = 0.3$ and reducing the time step to $250/u$. This smoothing practically eliminates high frequency waves (the focal point of computational instability in the advection equation) and hence also removed much of the high resolution significance of the model. Further, the extensive smoothing grossly over-exaggerated the diffusion effects in the more stable portion of the domain and

further exaggerated the flux of heat into the system from the upper and lower boundaries. The requisite smoothing was undoubtedly also the major factor in the excessive heating of the PBL in all the simulations, and was particularly noted by the excessive heat flux through the upper boundary. Further, the amplifying "two grid" waves propagated upwards through the model which is an anticipated quality of the advection equation.

In Simulation II the surface layer eddy coefficient was determined from K-theory and although it increased the value of K itself by an order of magnitude or so, the resulting decrease of $\partial K/\partial z$ let the model become stable with the smoothing factor of only $S = 0.4$. This strongly supports the hypothesis that the above form of the term that presented the gradient of K was the primary source of computational instability in the SBL. The reduction of the coefficient in the nonlinear term was realized even by increasing K with the resulting decreased $\partial K/\partial z$.

In Simulation III-A the value of $K'/2K$ was reduced by "fairing in" K of the surface layer (determined from bulk theory) with the K's above the surface layer determined from K-theory (Figure 5). This modification drastically reduced the values of $K'/2K$ and again permitted the model to become stable with a smoothing coefficient as low as $S = 0.2$. The same effect of

reducing K was introduced by the O'Brien's formulation of the eddy coefficient distribution and hence the instability at the SBL did not occur.

From the analysis of the simulations runs it was clear that the instability in the SBL was primarily caused by the nonlinear term and might be eliminated in the Dufort-Frankel system by normalizing the third term of equation (5.5) by dividing by $1 + \gamma'/2$, i.e.

$$\theta_m^{n+2} = \frac{1-\gamma}{1+\gamma}\ \theta_m^n + \frac{2\gamma}{1+\gamma}\ \bar{\theta}_m^{n+1} + \frac{\gamma'}{1+\gamma'/2}\ \theta'^{n+1}_m$$

The use of the normalizing factor $(1 + \gamma'/2)$ in the "variable K" term of the prediction equation would have eliminated many of the problems encountered in Simulations I, II and III. The reduction of the computational instability would have permitted more realistic predictions of the heat and moisture changes in the lower levels of the model. While there would still be noise level in wavelengths less than four grid units, this noise level would be considerably reduced. The most important improvement would be realized by the permitted increase in the spatial step and removal of the smoothing operations. This would greatly reduce the spurious heat flux in the system from the upper and lower boundaries.

5.3 Comparison of Different Heat Flux Formulations

There is currently some disagreement about the most effective formulation of the heat flux in the SBL and PBL. Because we are dealing with a problem which is quite sensitive to the technique for computing heat flux, different heat flux formulations were tested.

In Simulation III-A two different bulk formulations discussed in Chapter 2 were used. Brook (1978) has shown that the influence of water vapor in the vertical turbulent flux of sensible heat in the air is predominantly due to the specific heat of the air on specific himidity, rather than the effects of water vapor on air density and buoyancy. A simplified form of the equation derived by Brook (1978) was presented by Reinking (1980):

$$\frac{Hs}{\rho Cp} = Ch\ U\ ((\theta_z - \theta_o + 0.84\ T\ (q_z - q_o)$$

The second formulation was given by Smith (1980):

$$\frac{Hs}{\rho Cp} = \begin{cases} (3.2 + 1.0\ (Ts - Ta)\ U)\ 10^{-3} & \text{unstable cases} \\ (-0.1 + 0.83\ (Ts - Ta)\ U)\ 10^{-3} & \text{stable cases} \end{cases}$$

This equation was obtained from a fit to measurements over the ocean under strong wind conditions. From the results and for the precision required in this type of model, any

type of bulk aerodynamic formula can be utilized. The discrepancy in the calculations due to the different bulk formulations was minimal.

In order to compare two different flux formulations for the PBL, Simulation IV-B was applied. In all the previous simulations the distribution given by Lumley and Panofsky (1964) for the sensible heat flux was used:

$$Hs = - \rho \, Cp \, Kh \, \partial\theta v/\partial z$$

Simulation IV-B was identical to IV-A (first order scheme) but incorporated the formulation given by Reinking (1980) for the sensible heat flux:

$$Hs = - \rho \, CP \, Kh \, (\partial\theta/\partial z + 0.84 \, T \, \partial q/\partial z)$$

This significant difference in a comparison of both simulations was that Simulation IV-B needed a higher smoother to maintain stability; this form was more unstable than the previous simulation (IV-A). Due to the increase in the smoothing factor, the formulation from Reinking (1980) incorporated more heat flux into the mixed layer than did that from Lumley and Panofsky (1964). For the same conditions, the mean potential temperature at the off-shore station was 2 or 3 degrees greater in all cases. Therefore, Lumley and Panofsky's parameterization for the PBL is recommended for these unstable domains. In general, more snesible heat flux than moisture flux was incorporated

into the atmosphere. The latter represented a small fraction, two to four orders of magnitude less.

5.4 Graphic Analysis of Case 3

All the simulations were applied to the rest of the cases, and all showed the same type of results. The greater the step function temperature variability at the coastline and the steeper the sea surface temperature gradient, the shorter the horizontal step and the heavier the smoother that had to be applied to make the model run. The results of all the cases are shown in Tables 1 to 6. Whenever O'Brien's profile for the distribution of the eddy coefficient was employed, a large step and a light smoothing factor were needed.

A graphic summary of the behavior of the various simulations is shown in Figure 32. For this analysis the difference between the air potential temperature computed at anemometer level and the sea surface temperature was calculated for this case using various simulations. The differences as a function of distance are shown in Figure 32. The simulations were not run with identical conditions, primarily because of instability in the second and third simulations. Only those conditions for which each simulation gave the best agreement with the observed values are presented. These were the following:

Curve 1 (Simulation II): Dx = 250 m, S = 0.4

Curve 2 (Simulation III-A): Dx = 500 m, S = 0.3

Curve 3 (Simulation III-B): Dx = 500 m, S = 0.2

Curve 4 (Simulation V-A): Dx = 500 m, S = 0.05

Curve 5 (Simulation V-B): Dx = 1000 m, S = 0.15

Curve 5 most closely approximated reality, followed by curve 3. The former curve (5) was produced by the first order model, using O'Brien's profile for the PBL, bulk aerodynamic formulation for the SBL, and a nonuniform vertical grid. The values at the offshore station agreed with the observed. These results exhibited a rapid increase in the first 25 km followed by an equilibrium in the temperature difference, even though there was a continuous increase of 8.5°K in the sea surface temperature conditions.

Curve 3 produced by a second order model, using profiles suggested by Estoque and Bhumralkar (1970) for the PBL and bulk formulation for the marine surface layer with an evenly spaced vertical grid (Dz = 50 m). The curve showed characteristics similar to curve 5.

Curve 4 produced temperatures cooler than the observed. This curve was obtained from O'Brien's profile, a uniform grid interval (Dz = 50 m) and a second order scheme. The cooling occurred because little smoothing (S = 0.05) was applied and because the K values obtained

from this distribution were small. However, with a slight increase of S to 0.1 gave results identical to curve 5.

The poor behavior of Simulation II (using K-theory distribution along all the PBL) is evident from examining curve 1 in Figure 32. The temperature of the air was greater than that of the water at distances less than 50 km from the coast; therefore, there was a negative surface flux; this fact is extremely unrealistic. At distances greater than 150 km, the flux again became positive. Less extreme, but similar behavior is represented by curve 2. That curve was generated with a weighted average between bulk aerodynamical and K-theory formulations at the 50 m SBL, using a nonuniformly spaced grid and a second order scheme.

Figure 33 gives the computed differences between the specific humidity at the sea surface temperature and that of the air at anemometer level. Curve 4 gave the best results, followed by curves 3 and 5, although the latter overestimated the humidity of the air. In general, the behavior of the specific humidity difference was similar to that of the temperature. The simulations that worked better for one parameter did so for the other.

Curve 2 showed a wave form at the middle of the trajectory. This may have been caused by the reaction of the finite difference scheme to the distribution of the

sea surface temperature. Curve 1 which represents data calculated using K-theory at the surface produced unrealistic results: high values for the air specific humidity. This curve showed the rapid increase in the humidity at the first layer of the model in the first kilometers of travel. This was produced in response to the large K values employed to calculate the heat flux from the ocean.

These figures suggest that a simple first order model can represent the distinctive conditions of the winter season along the east coast of the United States. Bulk aerodynamic formulation gives results that are superior to those of K-theory for the marine surface layer. The result of the different simulations for this case are shown in Table 3.

Chapter 6

SUMMARY AND CONCLUSION

The model applied in this study was simple, but its use allowed the identification of some of the problems that heat flux techniques generate in regions of strong cold offshore air flow. Many problems were found that were due to the finite difference scheme employed, the grid system selected, and the flux techniques utilized. With the present techniques the modelling of strong offshore air flow during the winter season is a very difficult task.

A model using a Dufort-Frankel scheme with variable diffusion coefficients was applied to the highly unstable marine PBL. In the SBL (the lowest 10 meters) bulk aerodynamic theory was used to infer the K values, while in the remainder of the PBL classical K theory was applied. In order to accommodate a desired high resolution in the lowest layers, a nonuniform grid system was applied.

Computational instability in this model was severe and even with smoothing and reduced time steps, instability was not feasible without some modification of the physical concepts embodied in the model. Analysis of the results

showed the instability to be concentrated at the top of the SBL (10 m) where a step function increase in K occurred which was a product of the change in formulations for diffusion coefficient computation above and below that point. Accordingly, it was conjectured that the variable K term in the finite difference formulation was the primary source of the instability.

To test this hypothesis, classical K-theory was substituted for bulk theory in the computation of the coefficients in the SBL even though this resulted in much larger K values in the layer. With this adaptation a fourfold reduction in the time step and some smoothing, computation stability was achieved. However, as expected, the large eddy coefficient values from the classical K-theory over-estimated the flux of heat from the surface into the atmosphere. In an analysis of the physical role of the term that present the nonlinear effect it was shown that the magnitude of this increase of K at the top of the SBL was not physically realistic.

More realism could be expected in the model if bulk theory K's were restored to the SBL while the classical eddy coefficients in the three layers above the SBL would be "faired in" with the SBL value. This modification was made and ran with the same data. With the same reduction in time step and a small amount of smoothing, computational

instability was again achieved but with a decrease of this fictitious heat flux from the surface boundary.

The use of smoothing, combined with the reduction of time step, introduced another kind of undesirable effect, spurious introduction of heat into the system from the boundaries, particularly across the upper boundary. In both of the revised models described above the characteristic inversion at the top of the PBL was destroyed with unrealistic rapidity.

To test the potential difficulties associated with the nonuniform grid, the simulation with the "faired in" K values in the lowest four layers was rerun using a uniform grid in which the grid interval was comparable to the smallest grid interval in the nonuniform system. Apparently the nonuniform grid did not contribute to the instability since there was no reduction in computational problems by using the uniform grid in the simulation. There was, however, a reduction of heat flux from the upper boundary which would be expected from smoothing terms applied over smaller grid intervals.

A linear analysis of the computation scheme was performed to diagnose the specific computational instability problems of the term $(\partial K/\partial z \cdot \partial\theta/\partial z)$. This clearly demonstrated the nonlinear term as a primary offender, but that might be controlled by modifying the Dufort-Frankel

scheme normalizing by a denominator in that term. It is also reasoned that this modification would permit such larger time steps and require little or no smoothing, which in turn would reduce the spurious heat flux into the system from the upper and lower boundaries.

By using a different mathematical formulation, a first order equation was developed that replaced a second order Dufort-Frankel integration. This first order finite difference system using this mathematical formulation was applied to the identical system of the most unstable of the models mentioned above and was surprisingly trouble free. Computational stability was possible with much larger time steps and less smoothing, and the results were comparable. Those conditions reduced the spurious influx of heat from the boundaries.

Even with this last simulation there was still an excessive heat flux from the upper boundary which still destroyed the inversion but not quite as rapidly. On re-examination of the results it became clear that even without smoothing the very large values of the diffusion, coefficients computed from the classical K-theory would still result in excessive heat across the upper boundary and ficticiously destroy the inversion.

Upon examination of the eddy coefficient profiles, it becomes clear that K-theory does not provide realistic

values below, through and above the inversion. K-theory determines the diffusion coefficients on a layer by layer basis with eddy coefficients uniquely dependent upon the physical properties of the layer. In the unstable domains it does not seem likely that the magnitude of the eddies in a given layer are independent of the magnitude of the eddies in the layers above and below. In fact, in the highly unstable planetary boundary layer it is quite likely that the effect of surface drag coefficient are a significant influence throughout the PBL. Clearly, the scale of the eddies should increase with distance from the "hard" surface boundary. But similarly, one would expect some damping of the eddies on approaching the "soft" boundary created by the inversion.

Magnitudes of turbulent stress, pressure and inertial forces in the PBL should be quite different from those in the inversion and in the free atmosphere above, and it is quite unlikely that a parameterization that is applicable in the PBL would be suitable in and above the inversion. From the results obtained in this study and in line with the above reasoning, classical K-theory will not provide realistic results in heat, moisture, and momentum flux in the unstable marine boundary layer.

O'Brien proposed a technique for computing eddy coefficients which was based upon a characteristic profile deduced from physical reasoning and fixed by K values

(or derivatives) at key levels where these values could be known with reasonable accuracy. Several of the most troublesome simulations described in the foregoing were rerun using O'Brien's (1970) profile for diffusion coefficient values. These results showed remarkable improvement with respect to (a) removal of computational instability, (b) realistic model results when compared with offshore station data, and most important (c) a reduction of heat flux from the upper boundary which maintained the inversions throughout the computations.

For the marine surface layer, bulk aerodynamical formulation provided reasonable magnitude of heat flux from the ocean. The discrepancy in the calculations due to the two different bulk formulations (Reinking, 1980; and Smith, 1980) was minimal. Reinking's (1980) heat formulations for the PBL produced forecasted values greater than those predicted by Lumley and Panofsky's (1964) technique. Therefore, the latter is recommended in these unstable cases.

TABLES

Table 1. Results of selected numerical simulations for case 1, November 16, 1972.

SIMULATION	I	II	III-A	III-B		IV-A	V-A		V-B	
Smoothing Factor	0.80	0.40	0.20	0.10	0.10	0.10	0.10	0.10	0.15	0.10
Step Size (m)	250.00	250.00	250.00	500.00	250.00	250.00	1000.00	500.00	1000.00	500.00
Initial Mean Potential Temperature (°K)	276.83	276.83	276.83	276.83	276.83	276.83	276.83	276.83	276.83	276.83
Final Mean Potential Temperature (°K)	284.34	284.31	283.86	279.22	280.02	282.16	278.64	279.06	279.60	280.07
Initial Mean Specific Humidity (g/kg)	2.47	2.47	2.47	2.47	2.47	2.47	2.47	2.47	2.47	2.47
Final Mean Specific Humidity (g/kg)	4.67	4.75	3.66	2.29	2.75	3.94	2.98	3.27	3.66	3.83
Observed Potential Temperature (°K)	279.02	279.02	279.02	279.02	279.02	279.02	279.02	279.02	279.02	279.02
Forecasted Potential Temperature (°K)	283.84	283.85	283.51	275.80	278.44	281.61	278.80	280.21	280.12	280.69
Observed Specific Humidity (g/kg)	3.82	3.82	3.82	3.82	3.82	3.82	3.82	3.82	3.82	3.82
Forecasted Specific Humidity (g/kg)	7.41	7.44	5.60	1.93	3.83	6.05	4.79	5.84	5.64	5.91

Table 2. Results of selected numerical simulations for case 2, December 18, 1972.

SIMULATION	II	III-A	III-B	IV-A	V-A		V-B	
Smoothing Factor	0.50	0.50	0.30	0.10	0.10	0.10	0.20	0.10
Step Size (m)	250.00	500.00	500.00	250.00	1000.00	500.00	2000.00	1000.00
Initial Mean Potential Temperature (°K)	269.63	269.63	269.63	269.63	269.63	269.63	269.63	269.63
Final Mean Potential Temperature (°K)	280.40	276.90	276.78	281.91	272.68	275.79	274.54	274.52
Initial Mean Specific Humidity (g/kg)	0.96	0.96	0.96	0.96	0.96	0.96	0.96	0.96
Final Mean Specific Humidity (g/kg)	5.42	2.18	1.89	1.75	2.27	4.38	2.80	2.79
Observed Potential Temperature (°K)	277.00	277.00	277.00	277.00	277.00	277.00	277.00	277.00
Forecasted Potential Temperature (°K)	286.62	280.63	280.91	283.71	278.32	287.03	279.72	279.41
Observed Specific Humidity (g/kg)	4.40	4.40	4.40	4.40	4.40	4.40	4.40	4.40
Forecasted Specific Humidity (g/kg)	10.41	4.89	4.69	10.29	5.97	14.20	6.68	6.51

Table 3. Results of selected numerical simulations for case 3, December 7, 1972.

SIMULATION	II	III-A	III-B		IV-A	V-A		V-B	
Smoothing Factor	0.40	0.40	0.20	0.10	0.10	0.10	0.05	0.20	0.15
Step Size (m)	250.00	250.00	500.00	500.00	250.00	1000.00	500.00	2000.00	1000.00
Initial Mean Potential Temperature (°K)	273.67	273.67	273.67	273.67	273.67	273.67	273.67	273.67	273.67
Final Mean Potential Temperature (°K)	284.06	283.77	282.52	279.45	283.45	278.63	278.20	280.43	281.40
Initial Mean Specific Humidity (g/kg)	2.14	2.14	2.14	2.14	2.14	2.14	2.14	2.14	2.14
Final Mean Specific Humidity (g/kg)	4.46	3.94	2.36	0.96	5.20	3.53	3.28	3.78	3.96
Observed Potential Temperature (°K)	283.57	283.57	283.57	283.57	283.57	283.57	283.57	283.57	283.57
Forecasted Potential Temperature (°K)	286.56	286.33	284.07	276.13	285.19	280.83	280.01	282.49	283.65
Observed Specific Humidity (g/kg)	6.00	6.00	6.00	6.00	6.00	6.00	6.00	6.00	6.00
Forecasted Specific Humidity (g/kg)	8.98	8.55	5.25	-1.01	7.90	6.60	6.02	7.16	7.57

Table 4. Results of selected numerical simulations for case 4, November 6, 1972.

SIMULATION	II		III-A		IV-A	V-A		V-B	
Smoothing Factor	0.20	0.10	0.10	0.10	0.10	0.10	0.10	0.20	0.10
Step Size (m)	1000.00	500.00	1000.00	500.00	250.00	1000.00	500.00	2000.00	500.00
Initial Mean Potential Temperature (°K)	283.30	283.30	283.30	283.30	283.30	283.30	283.30	382.30	283.30
Final Mean Potential Temperature (°K)	286.90	286.80	286.05	286.55	286.79	284.79	285.03	284.87	283.82
Initial Mean Specific Humidity (g/kg)	3.99	3.99	3.99	3.99	3.99	3.99	3.99	3.99	3.99
Final Mean Specific Humidity (g/kg)	4.93	4.82	3.89	3.86	4.72	3.90	4.41	4.59	4.29
Observed Potential Temperature (°K)	286.10	286.10	286.10	286.10	286.10	286.10	286.10	286.10	286.10
Forecasted Potential Temperature (°K)	286.60	286.40	285.20	285.80	286.38	284.83	285.45	284.70	282.72
Observed Specific Humidity (g/kg)	6.16	6.16	6.16	6.16	6.16	6.16	6.16	6.16	6.16
Forecasted Specific Humidity (g/kg)	8.52	8.22	6.22	6.43	7.80	6.92	8.01	7.46	6.41

Table 5. Results of selected numerical simulations for case 5, December 6, 1972.

SIMULATION	II		III-A		IV-B	V-A	
Smoothing Factor	0.20	0.10	0.20	0.10	0.10	0.20	0.10
Step Size (m)	1000.00	500.00	1000.00	1000.00	250.00	2000.00	500.00
Initial Mean Potential Temperature (°K)	278.72	278.72	278.72	278.72	278.72	278.72	278.72
Final Mean Potential Temperature (°K)	280.30	280.20	280.24	277.86	281.00	280.28	280.81
Initial Mean Specific Humidity (g/kg)	4.79	4.79	4.79	4.79	4.79	4.79	4.79
Final Mean Specific Humidity (g/kg)	5.54	5.64	5.28	5.98	4.96	4.80	4.71
Observed Potential Temperature (°K)	280.10	280.10	280.10	280.10	280.10	280.10	280.10
Forecasted Potential Temperature (°K)	279.79	279.74	279.73	278.42	280.30	279.47	280.02
Observed Specific Humidity (g/kg)	5.30	5.30	5.30	5.30	5.30	5.30	5.30
Forecasted Specific Humidity (g/kg)	6.43	6.44	6.23	6.39	5.86	5.72	5.71

Table 6. Results of selected numerical simulations for case 6, November 29, 1972.

SIMULATION	II	III-A	III-B	IV-A	V-A		V-B	
Smoothing Factor	0.30	0.20	0.10	0.10	0.10	0.10	0.15	0.10
Step Size (m)	250.00	250.00	500.00	250.00	1000.00	500.00	1000.00	500.00
Initial Mean Potential Temperature (°K)	277.07	277.07	277.07	277.07	277.07	277.07	277.07	277.07
Final Mean Potential Temperature (°K)	282.96	282.79	279.11	282.21	278.53	279.18	279.84	280.32
Initial Mean Specific Humidity (g/kg)	1.95	1.95	1.95	1.95	1.95	1.95	1.95	1.95
Final Mean Specific Humidity (g/kg)	3.55	3.45	2.08	3.01	2.27	2.60	2.67	2.71
Observed Potential Temperature (°K)	279.88	279.88	279.88	279.88	279.88	279.88	279.88	279.88
Forecasted Potential Temperature (°K)	282.23	281.93	279.04	281.89	278.15	279.52	279.56	280.14
Observed Specific Humidity (g/kg)	3.54	3.54	3.54	3.54	3.54	3.54	3.54	3.54
Forecasted Specific Humidity (g/kg)	6.55	6.74	3.79	5.42	4.10	5.09	4.83	4.95

FIGURES

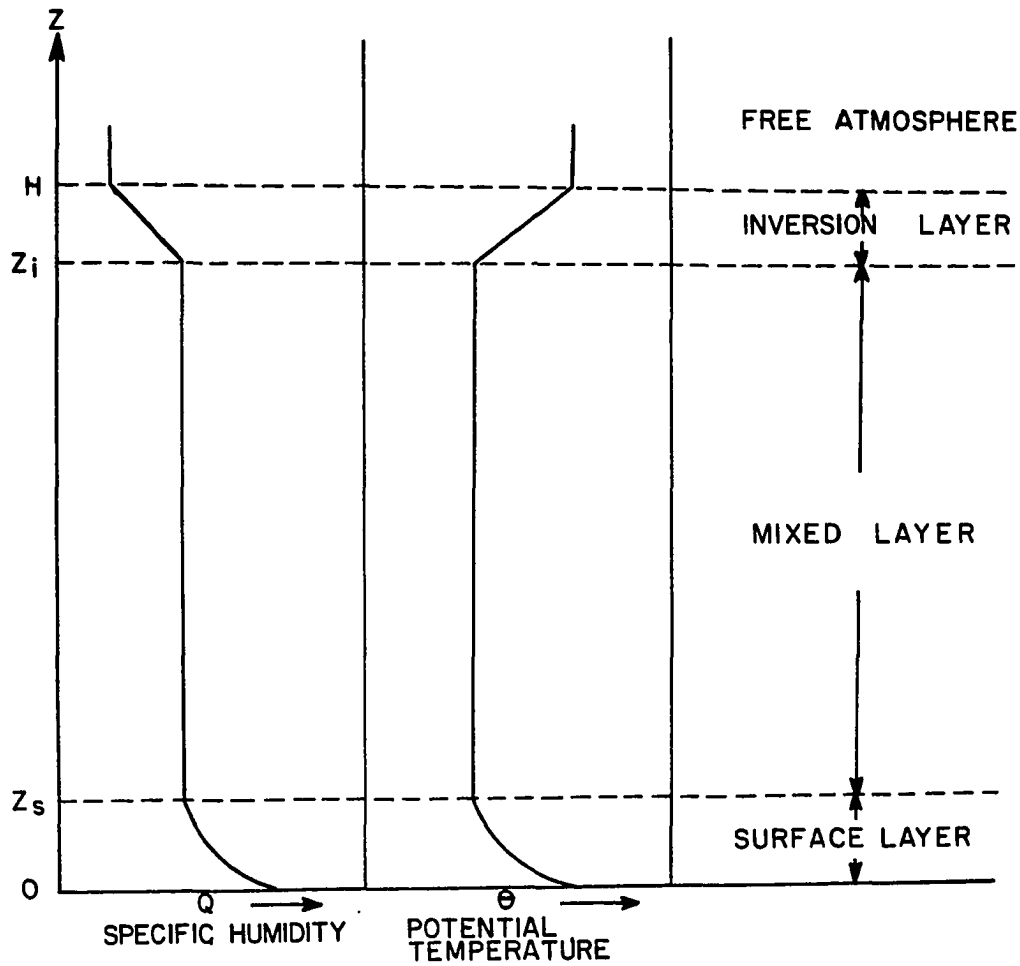

Figure 1. Schematic representation of the vertical regions considered.

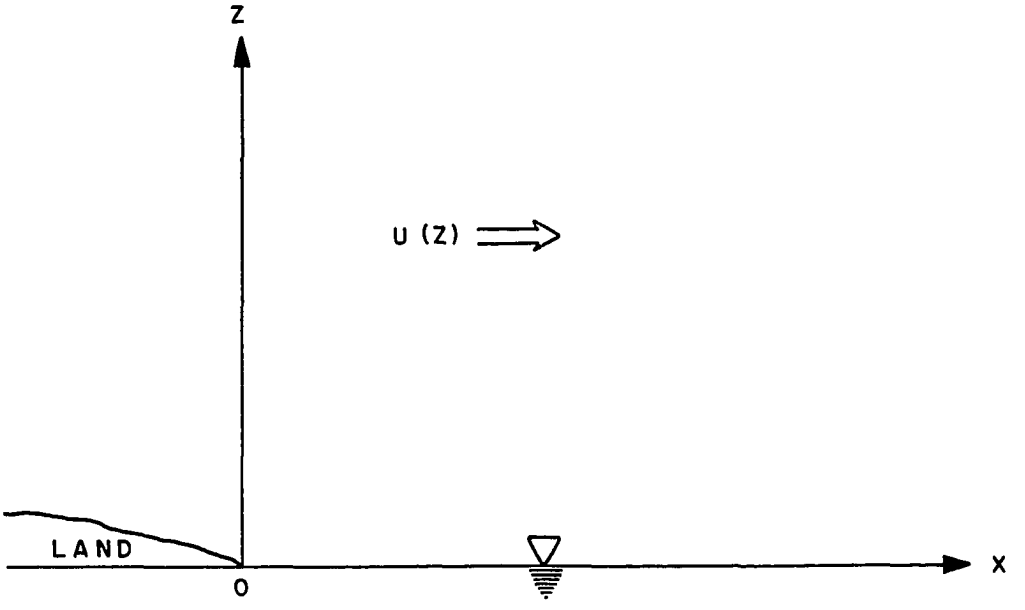

Figure 2. Coordinate system used.

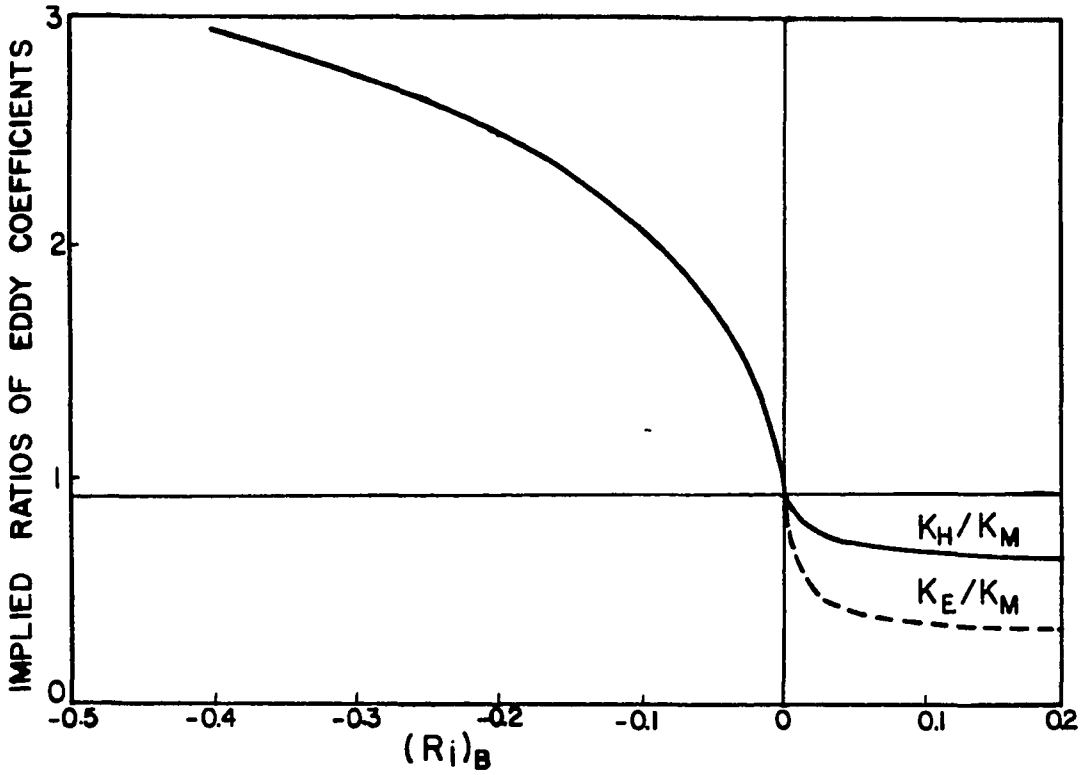

Figure 3. Ratio of K_h/K_m according to Deardorff (1968).

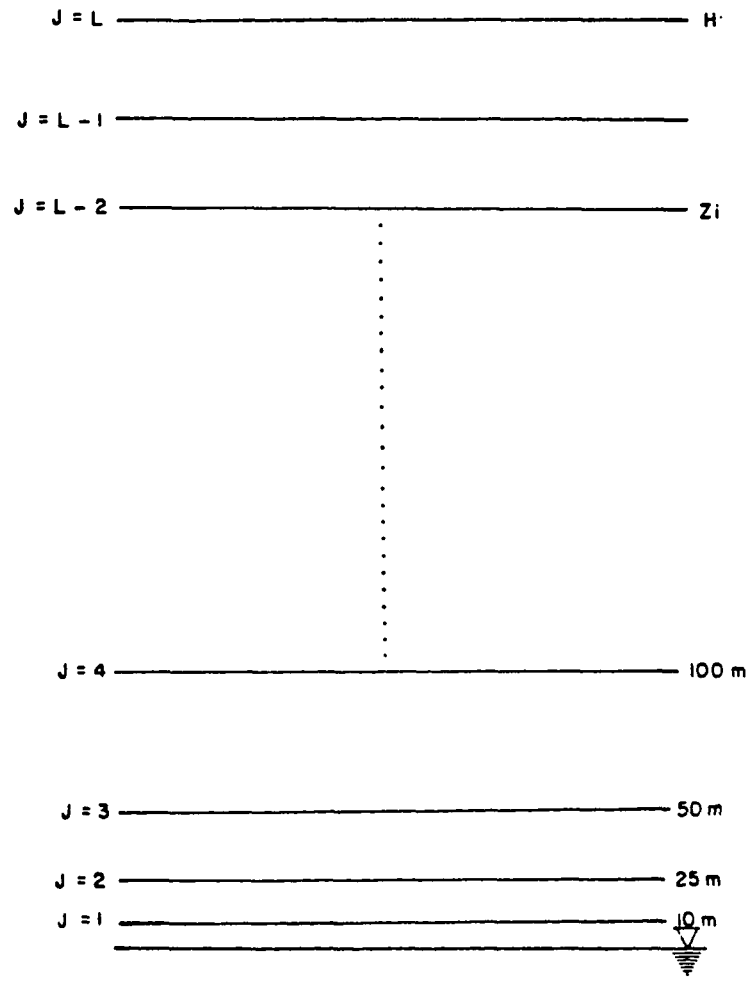

Figure 4. Nonuniform finite difference grid used in some simulations.

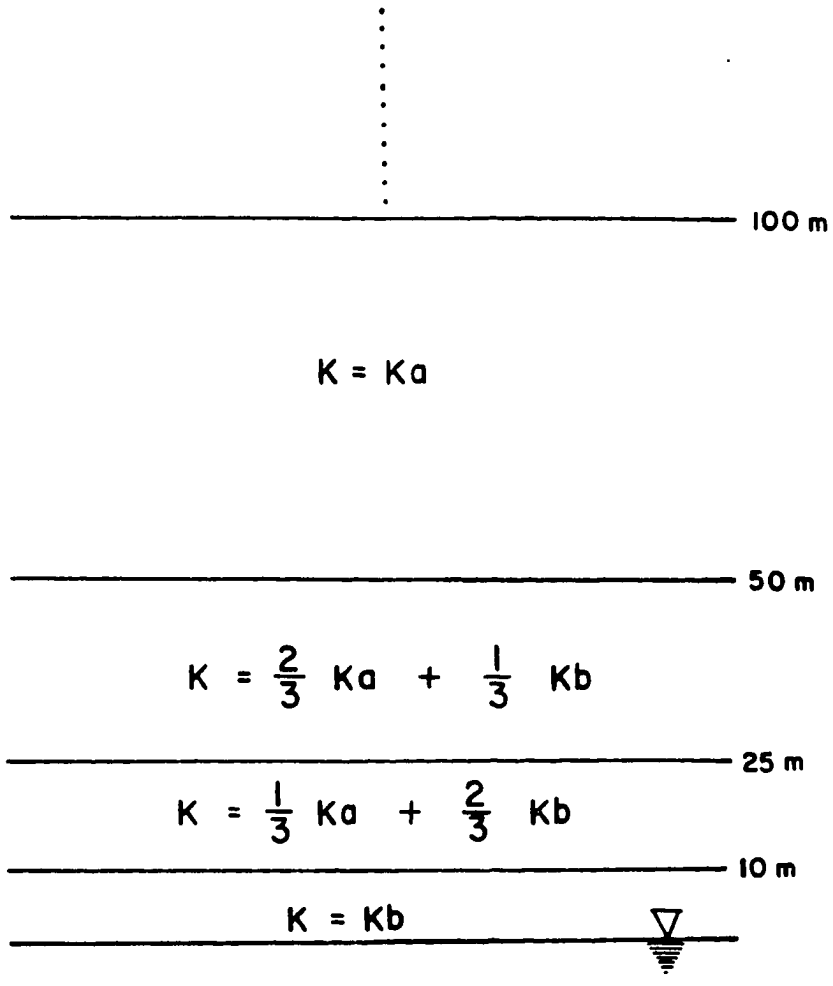

Figure 5. Weighted average between K-theory and bulk aerodynamic formulation.

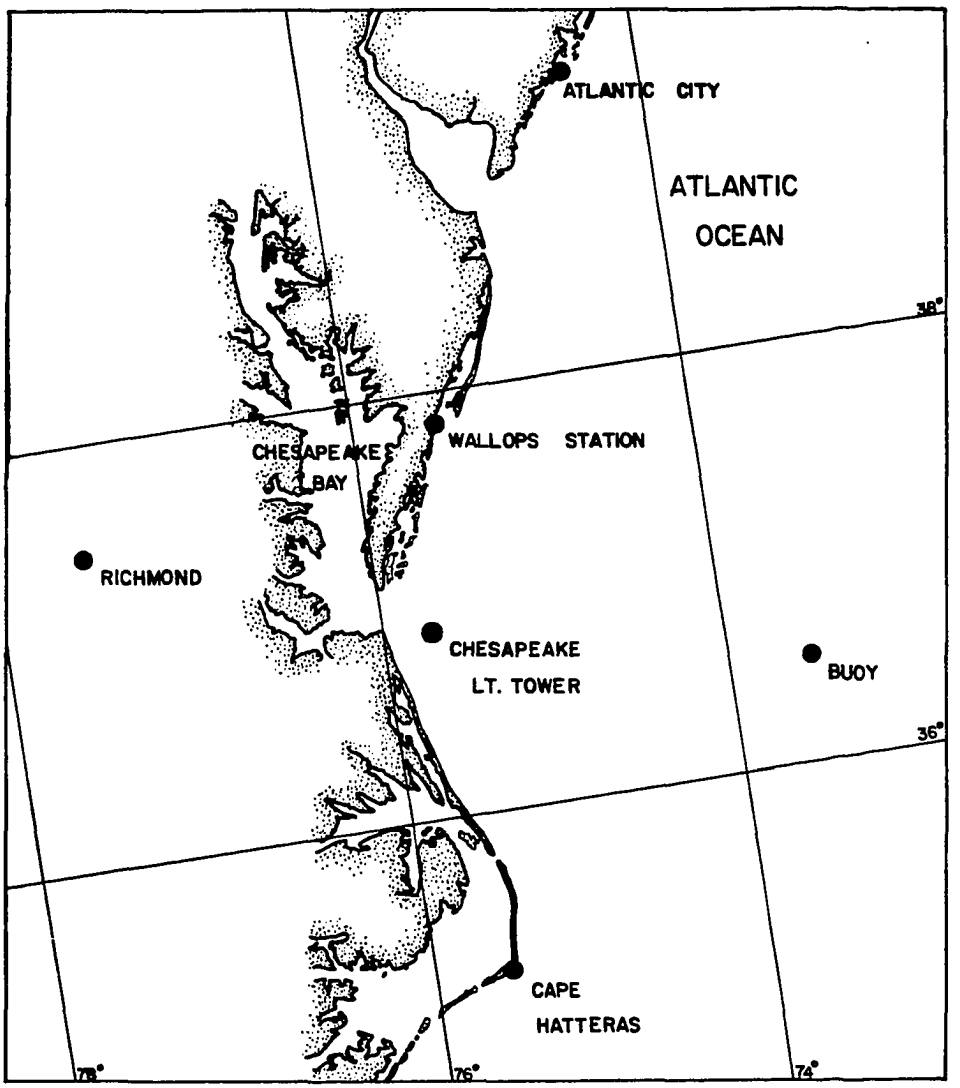

Figure 6. Station distribution used in computing the geostrophic wind and the pressure distribution.

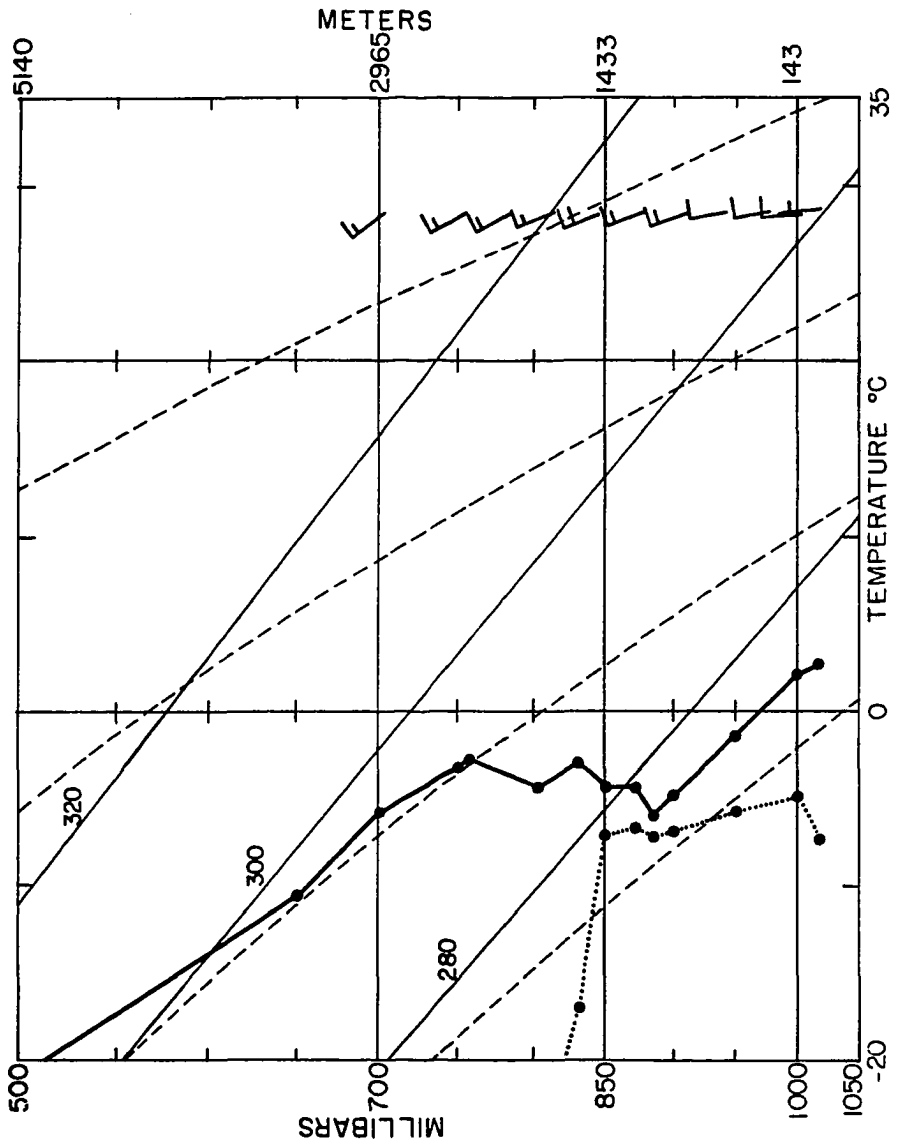

Figure 7. Stuve diagram for November 16, 1972.

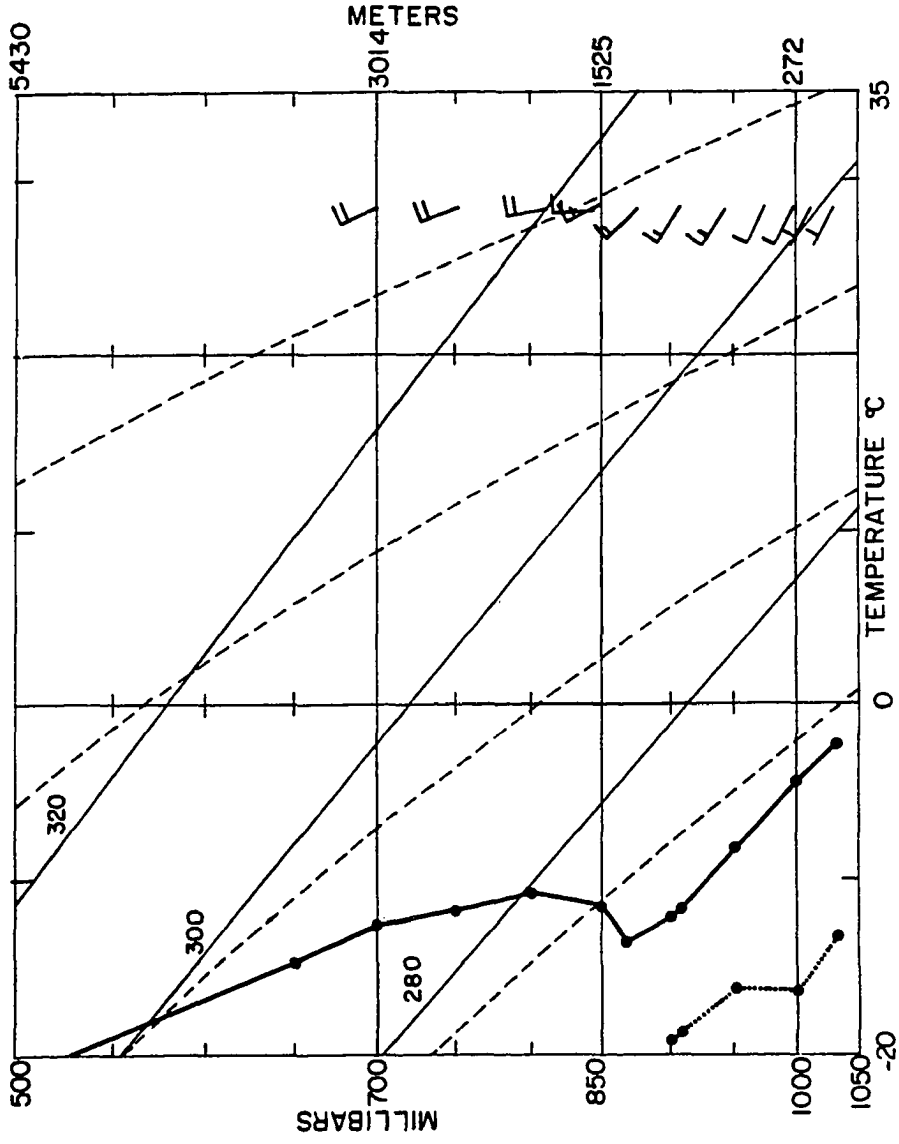

Figure 8. Stuve diagram for December 18, 1972.

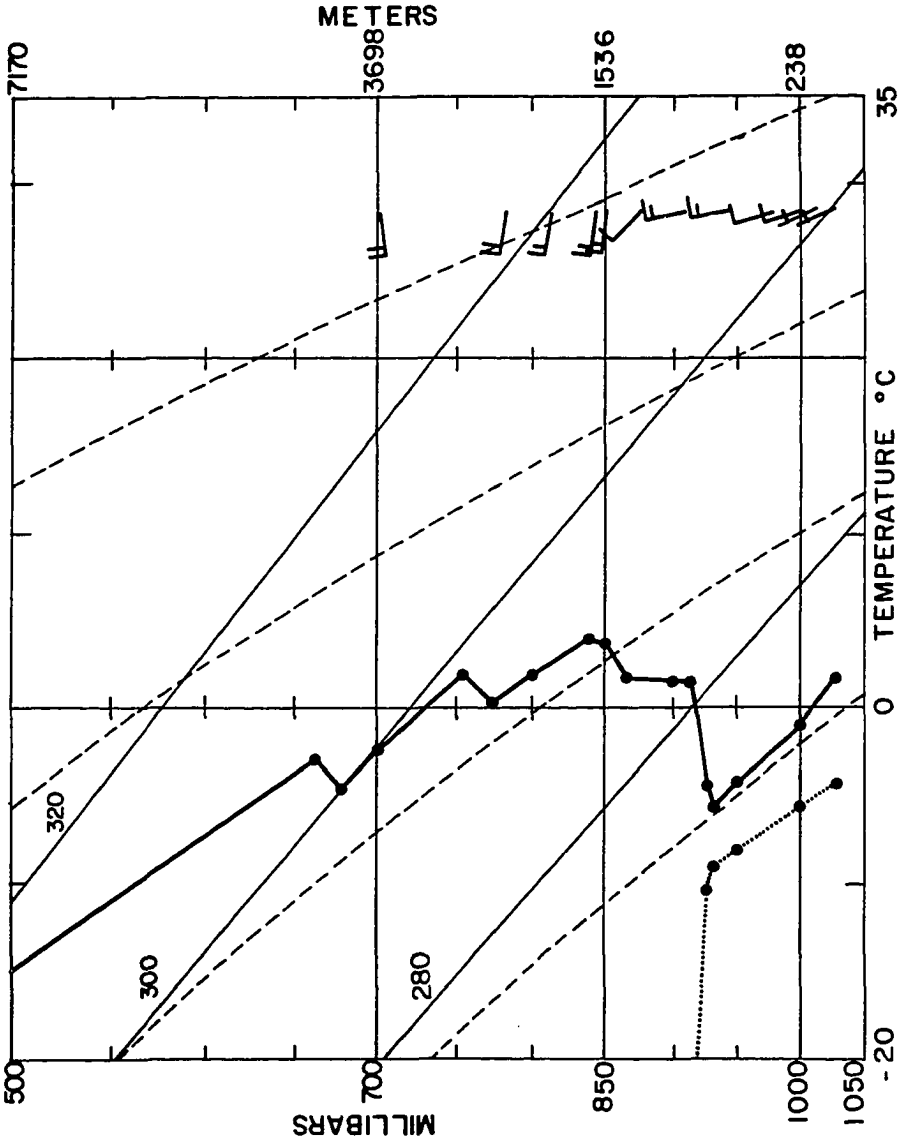

Figure 9. Stuve diagram for December 7, 1972.

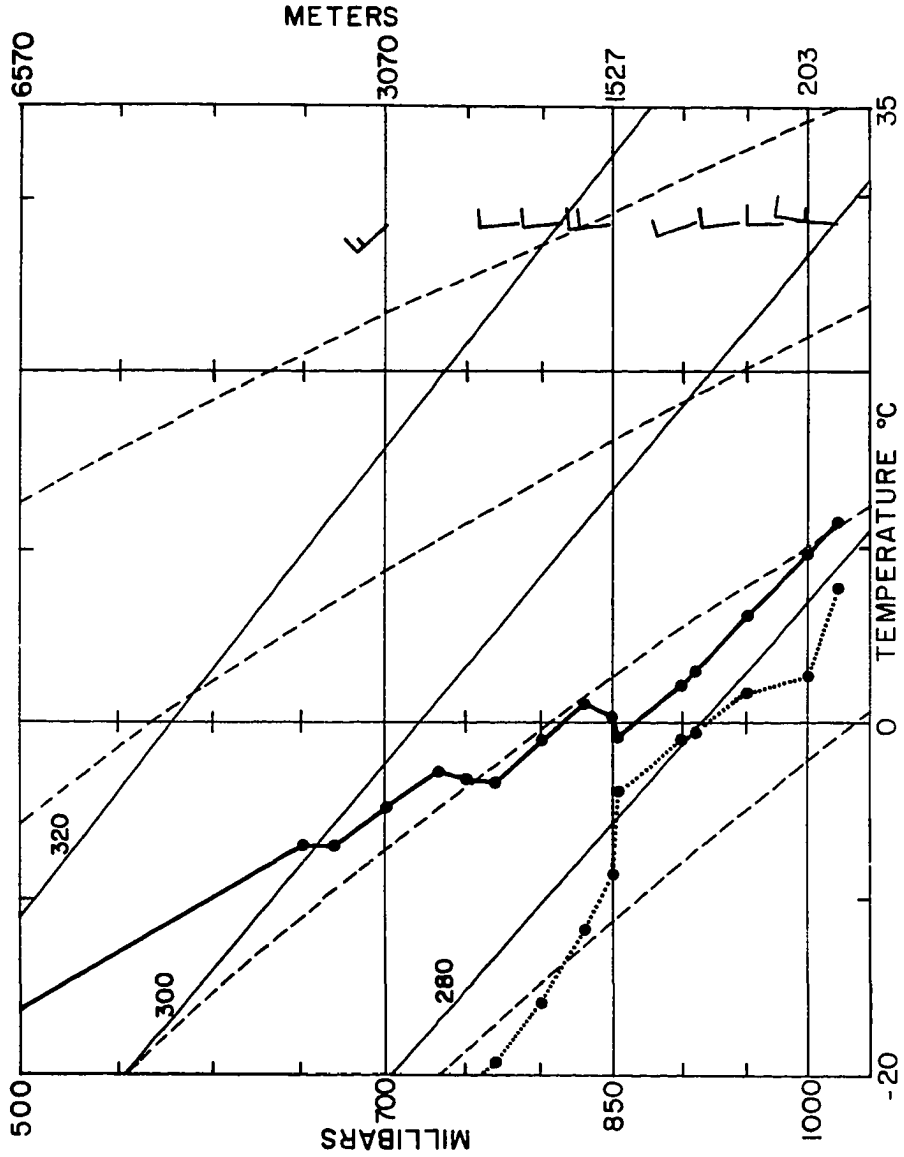

Figure 10. Stuve diagram for November 6, 1972.

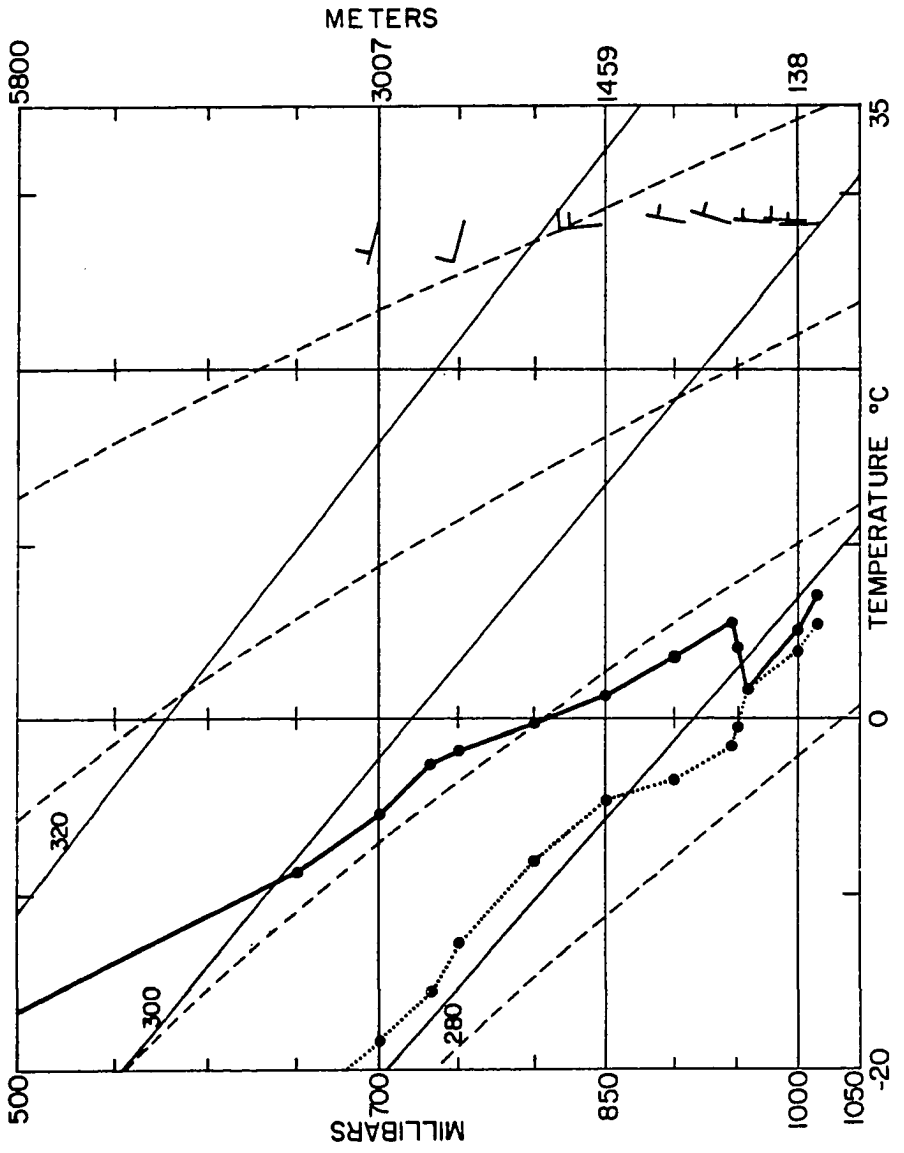

Figure 11. Stuve diagram for December 26, 1972.

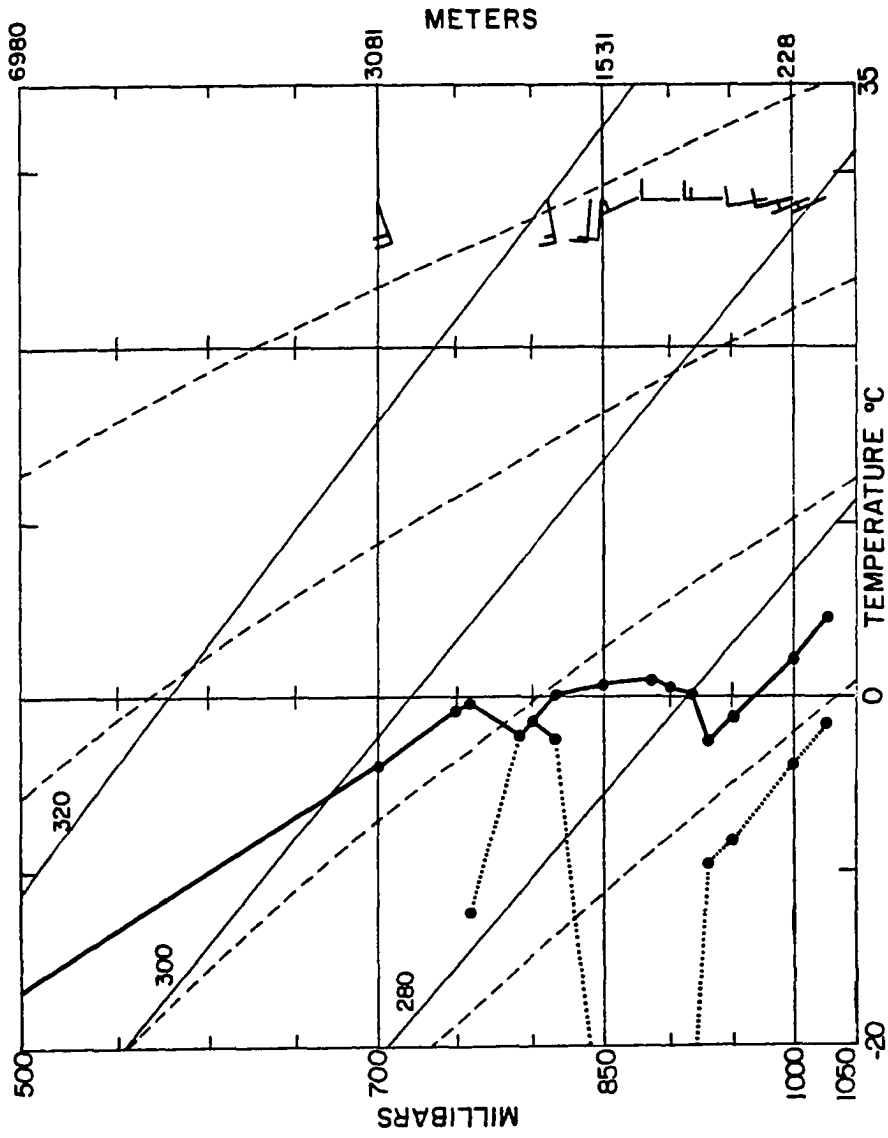

Figure 12. Stuve diagram for November 29, 1972.

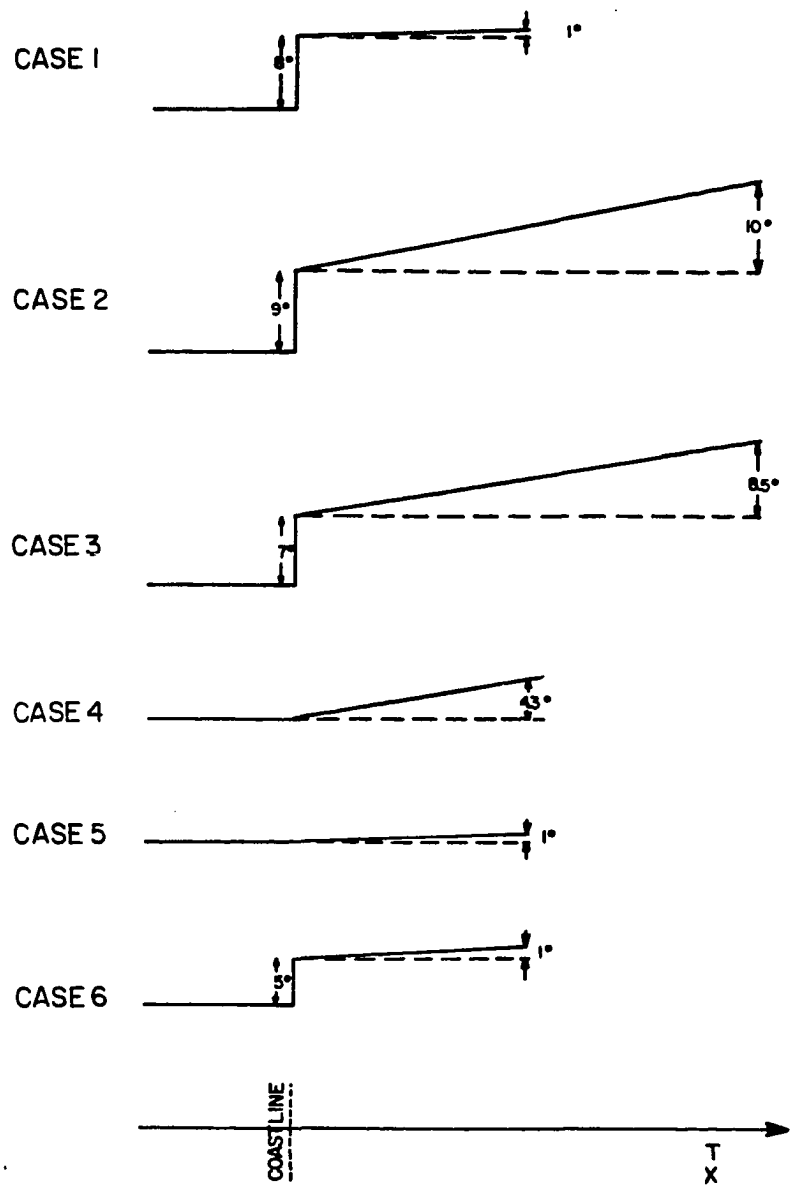

Figure 13. Schematic representation of the temperature conditions at the lower boundary for the different cases.

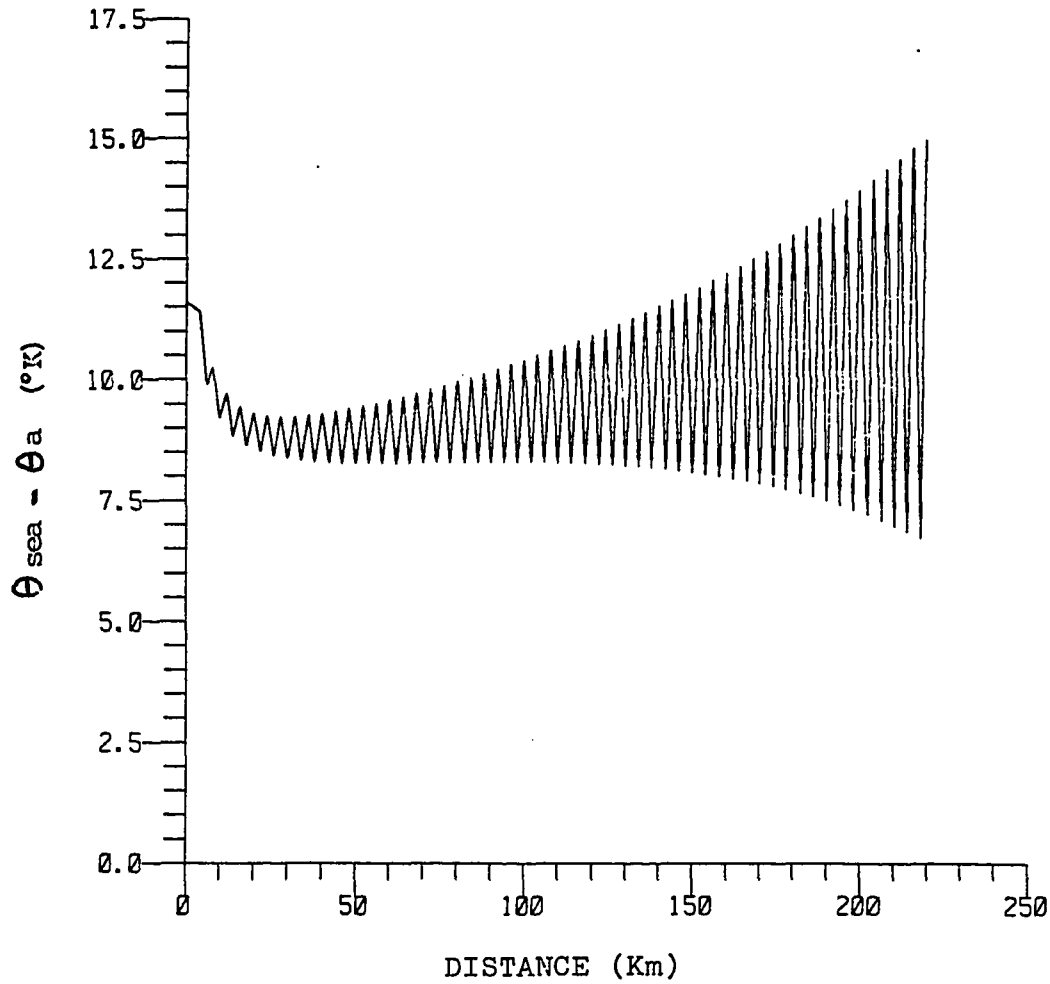

Figure 14. Growth of the two grid oscillation for the sea surface and air potential temperature difference for case 2.

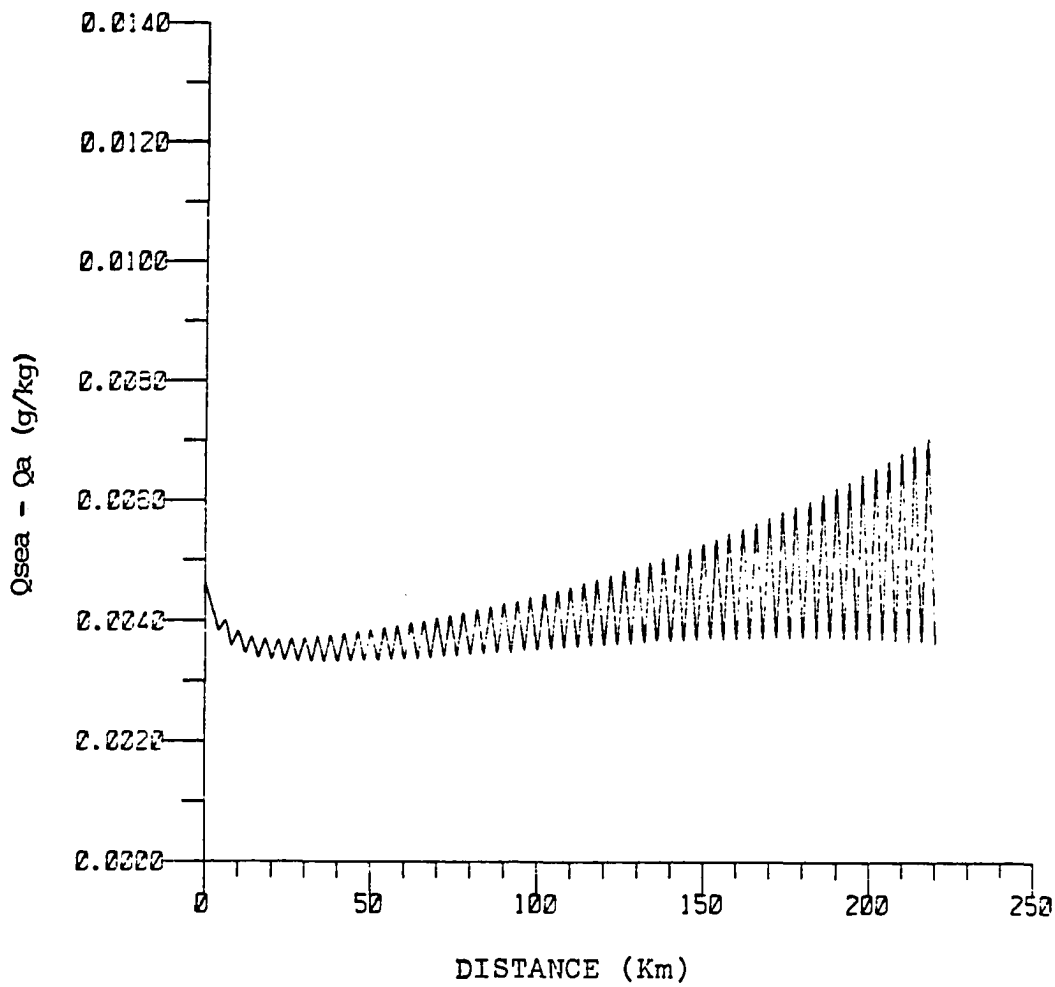

Figure 15. Growth of the two grid oscillation for the sea surface and air specific humidity difference for case 2.

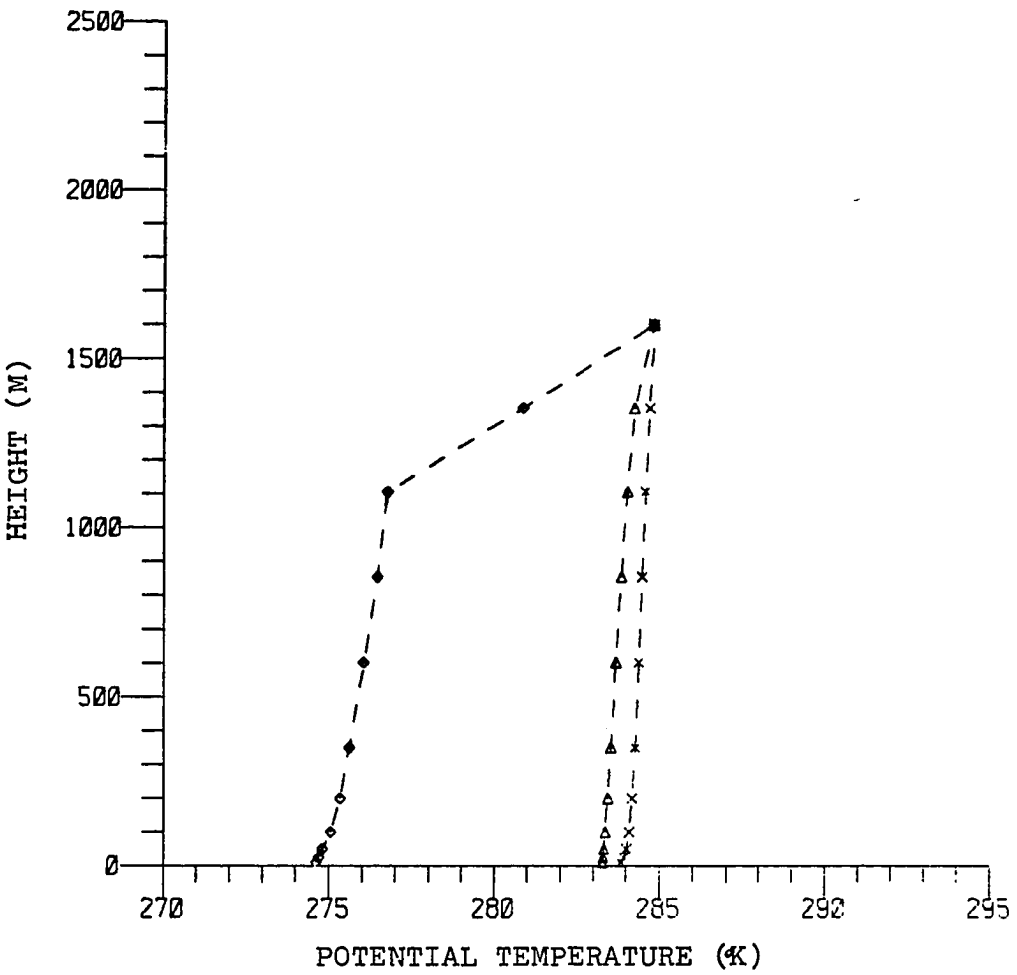

Figure 16. Potential temperature profiles of Simulation II for November 16, 1972. Dx = 250 m, S = 0.4, ◆ = initial profile, ▲ = mid-distance profile, X = offshore station profile.

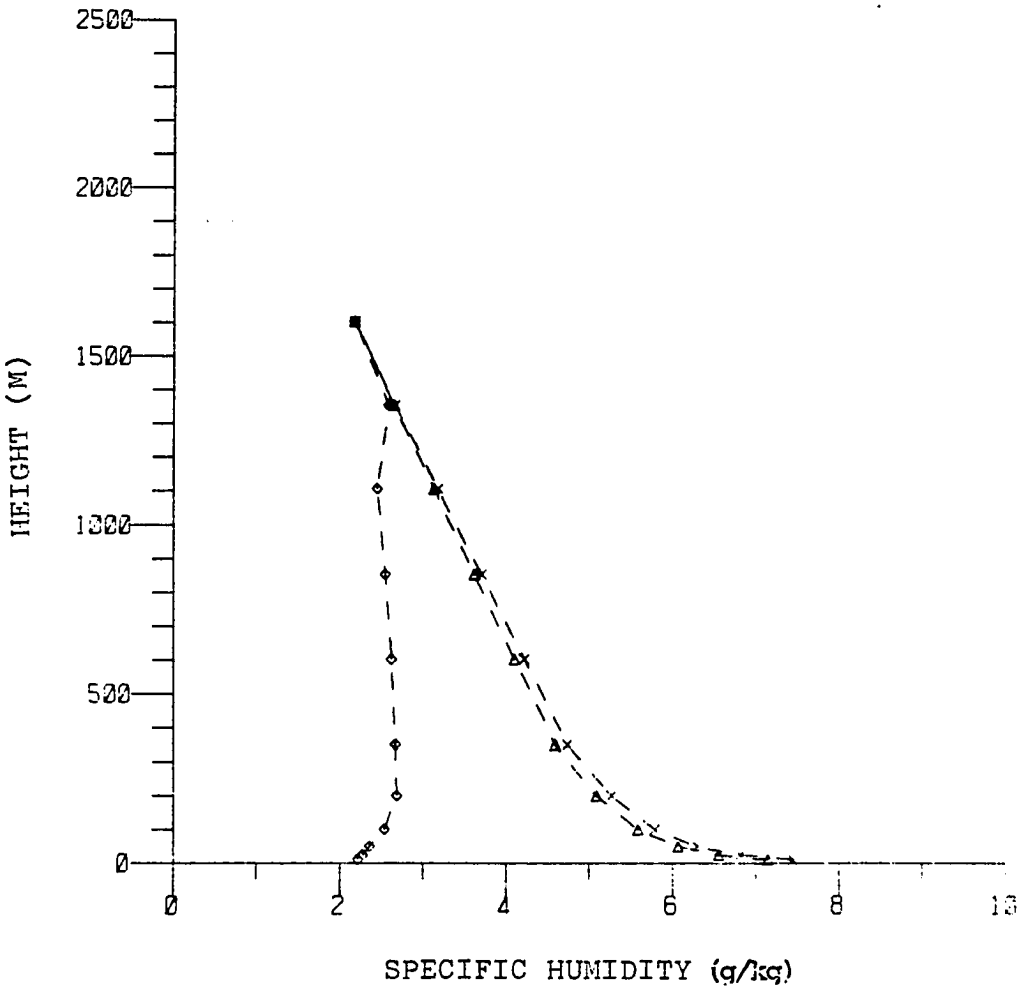

Figure 17. Specific humidity profiles of Simulation II for November 16, 1972. Dx = 250 m, S = 0.4, ◇ = initial profile, △ = mid-distance profile, X = offshore station profile.

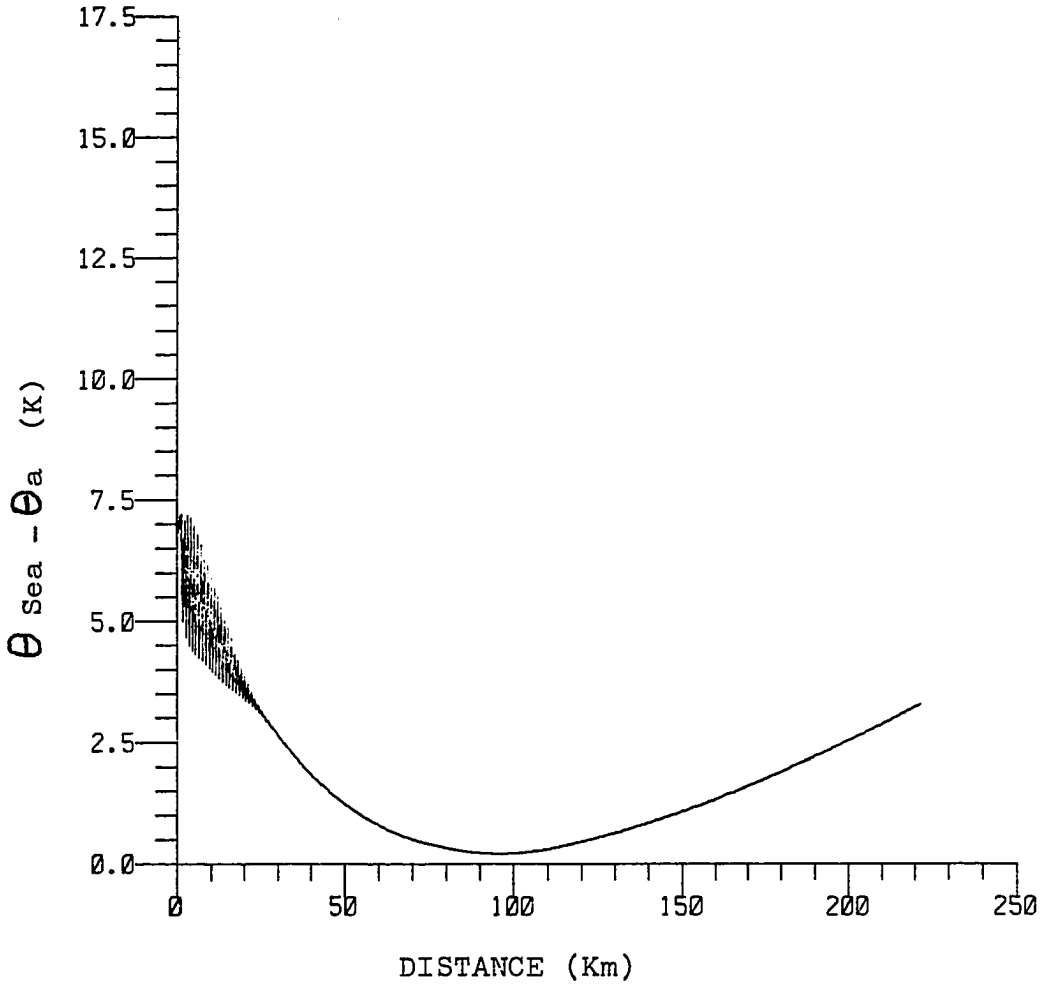

Figure 18. Distance evolution of the sea surface-air potential temperature difference for Simulation II for case 3.

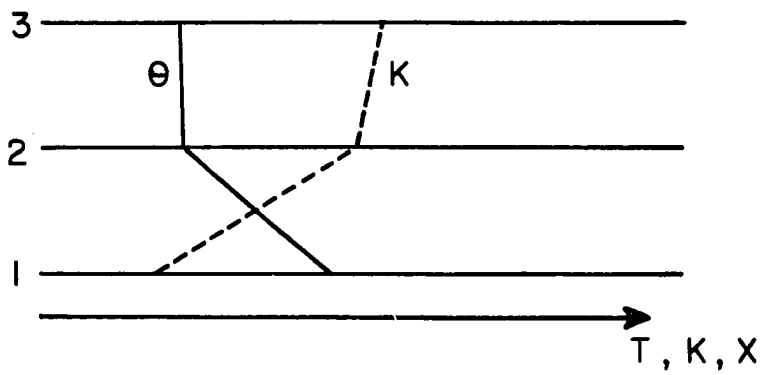

Figure 19. Two layer system considered to analyze the partial differential equation.

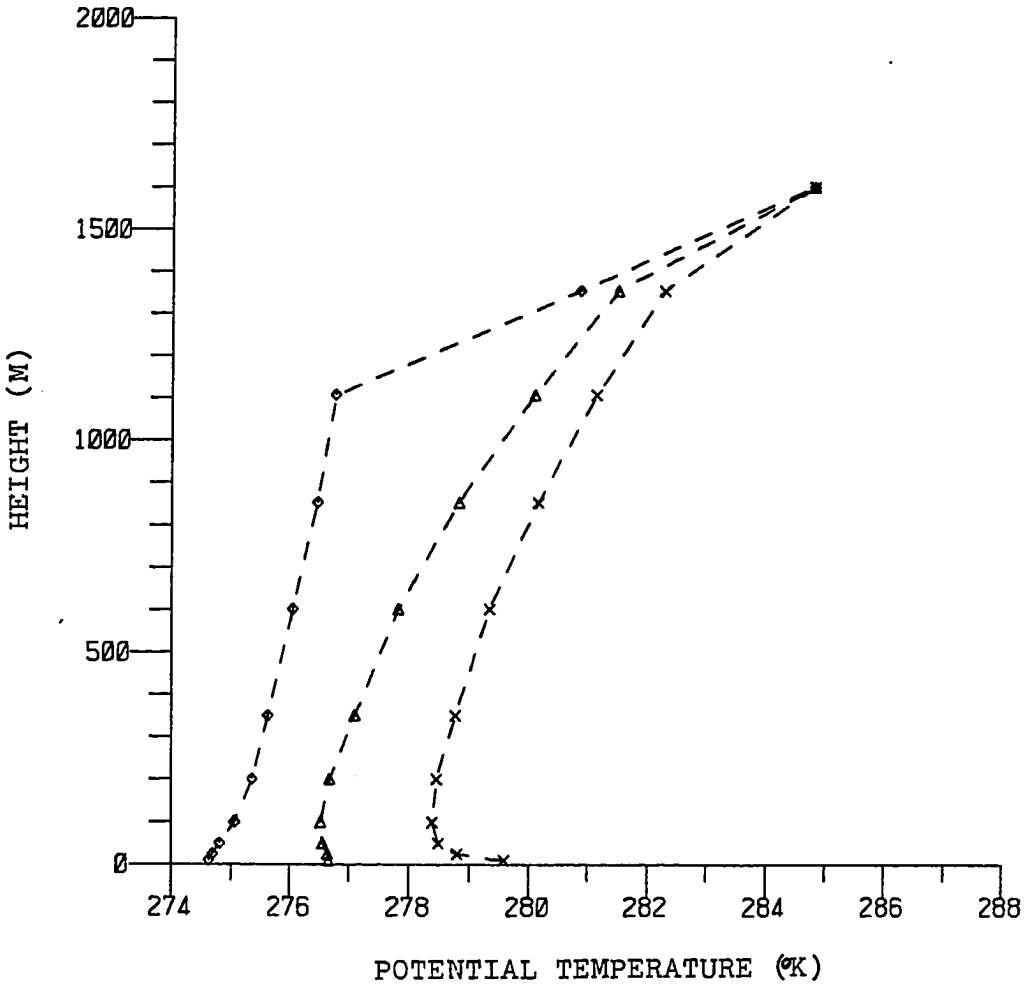

Figure 20. Potential temperature profiles of Simulation III-A for November 16, 1972. Dx = 250 m, S = 0.2, travel distance = 25 km, ◇ = initial profile, △ = mid-distance profile, × = offshore station profile.

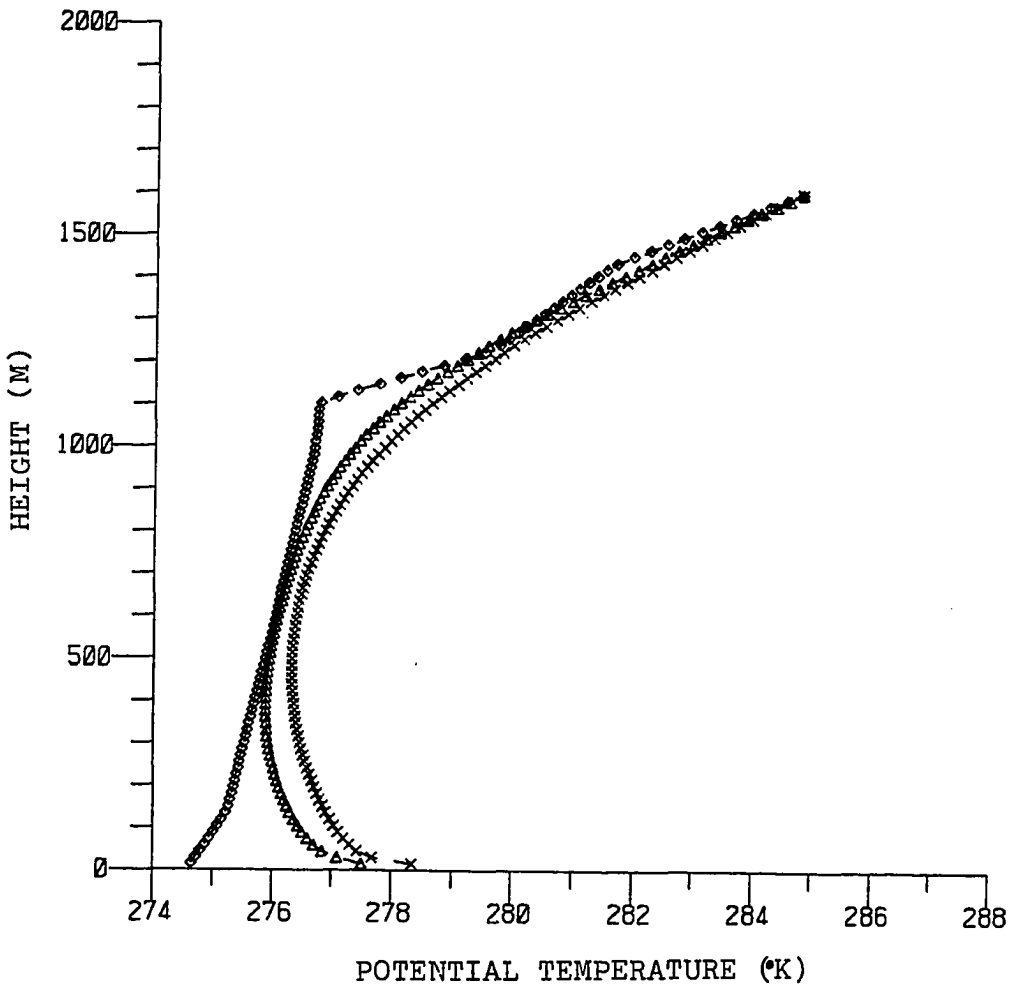

Figure 21. Potential temperature profiles of Simulation III-B for November 16, 1972. Dx = 250 m, S = 0.2, travel distance = 25 km, ◇ = initial profile, △ = mid-distance profile, × = offshore station profile.

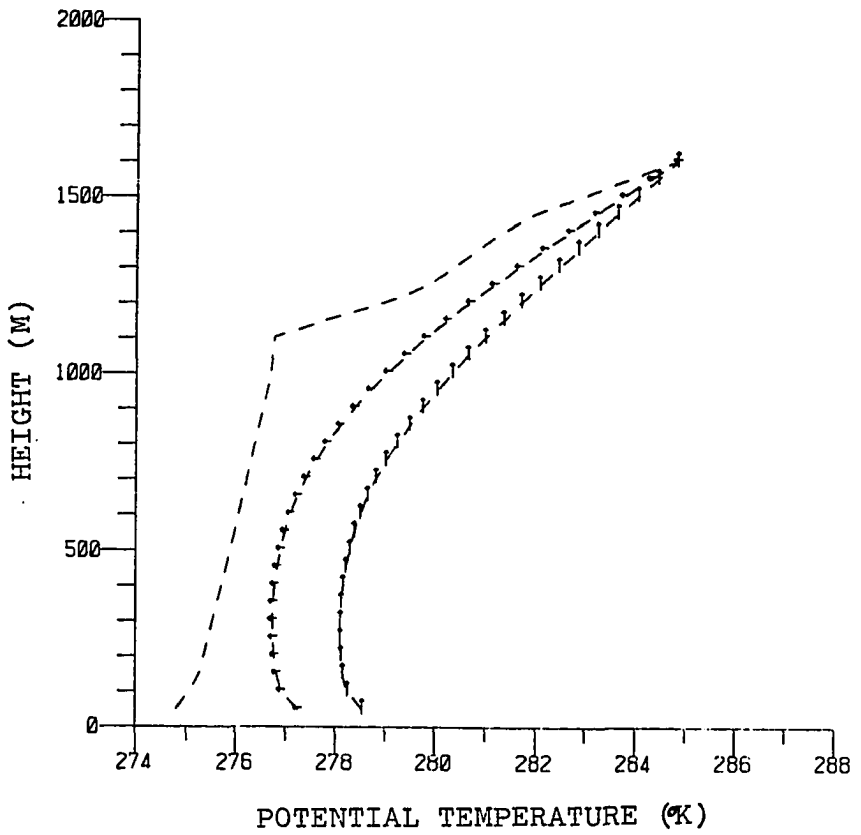

Figure 22. Potential temperature profiles of Simulation III-B for November 16, 1972. Dx = 250 m, S = 0.1, - = initial profile, ← = mid-distance profile, ↑ = offshore station profile.

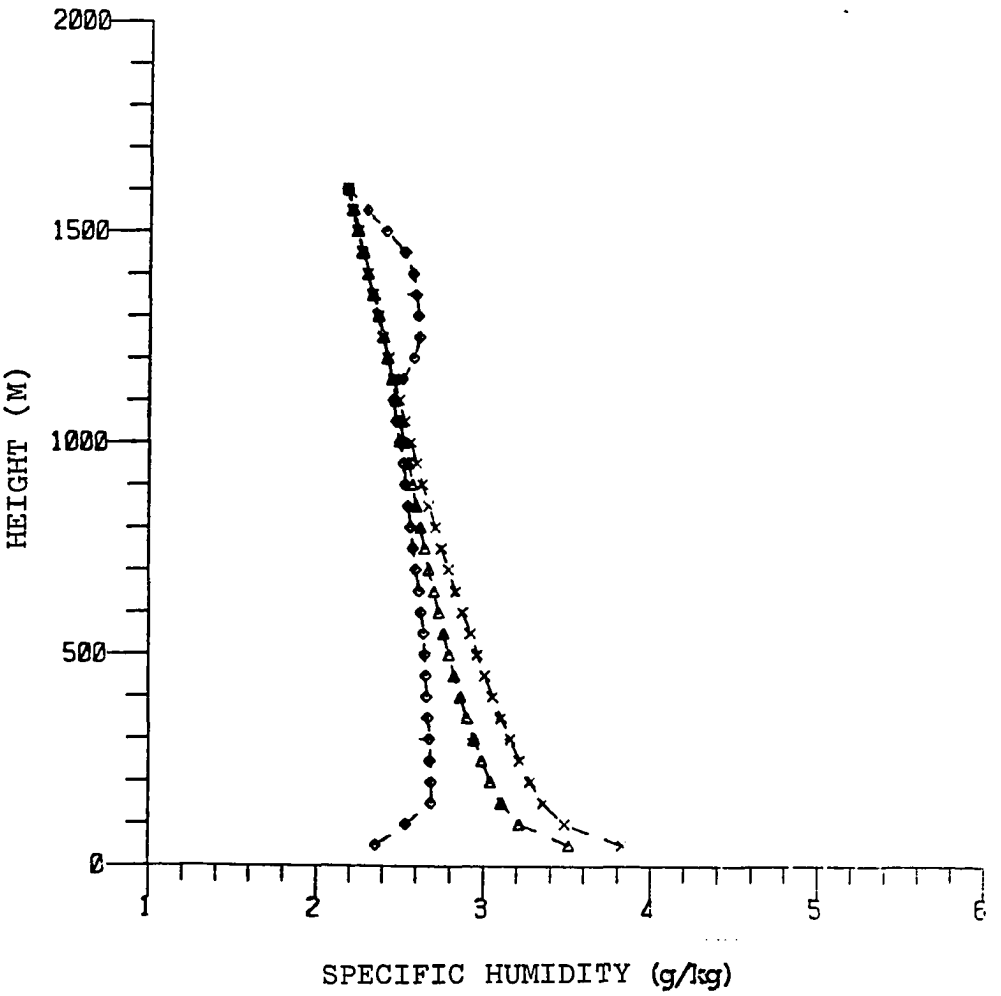

Figure 23. Specific humidity profiles of Simulation III-B for November 16, 1972. Dx = 250 m, S = 0.1, ◇ = initial profile, Δ = mid-distance profile, x = offshore station profile.

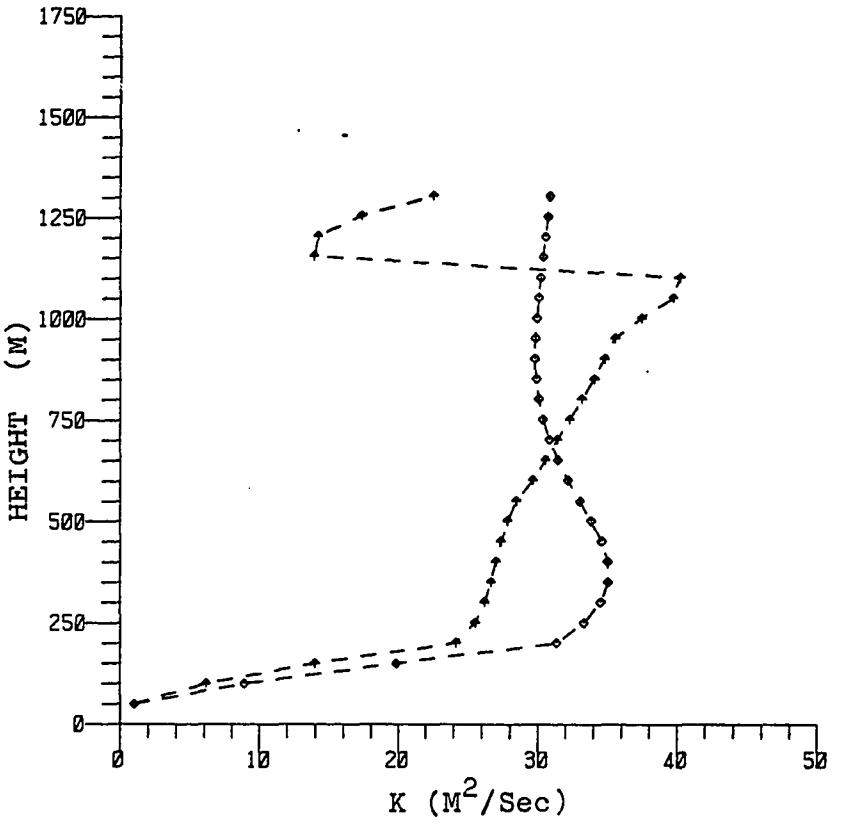

Figure 24. Estoque and Bhumralkar's (1970) eddy viscosity profile generated by Simulation III-B for case 1. ♦ = initial profile, ◇ = offshore station profile.

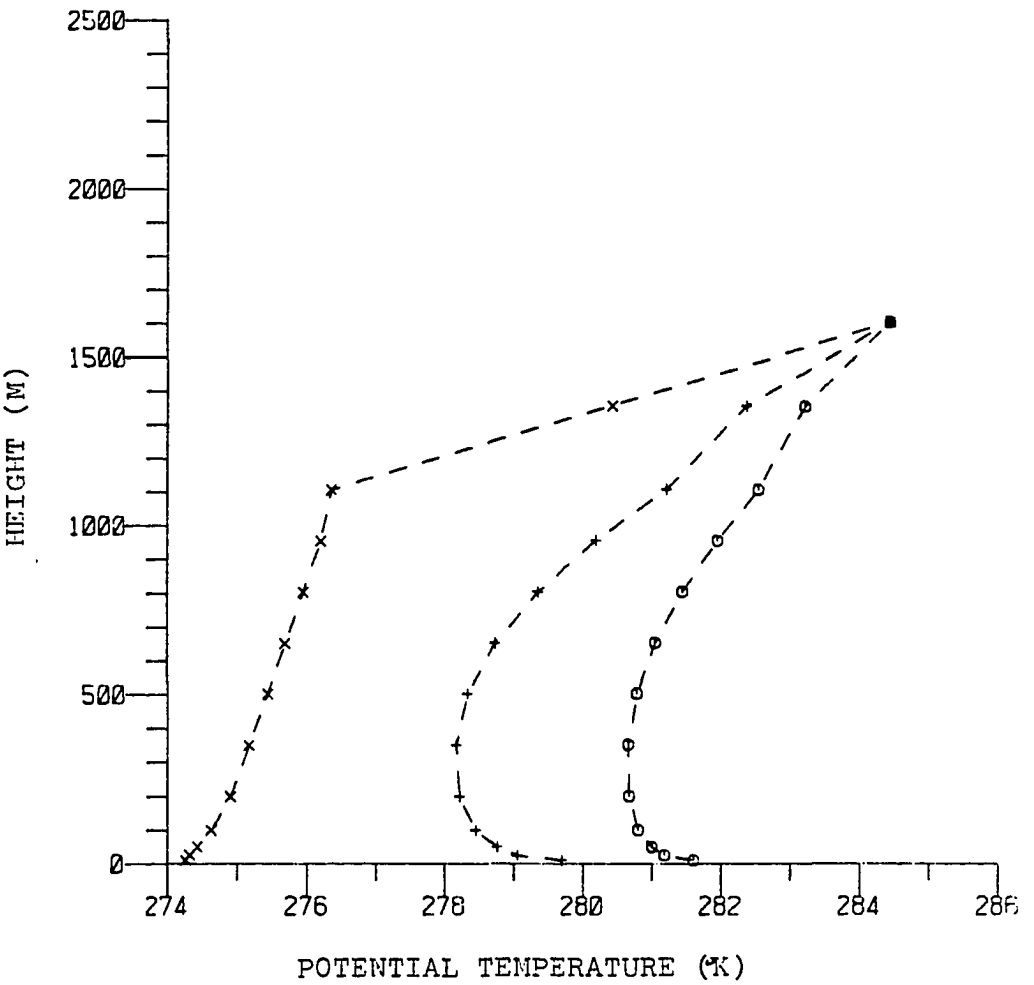

Figure 25. Potential temperature profiles of Simulation IV-A for November 16, 1972. Dx = 250 m, S = 0.1, x = initial profile, + = mid-distance profile, o = offshore station profile.

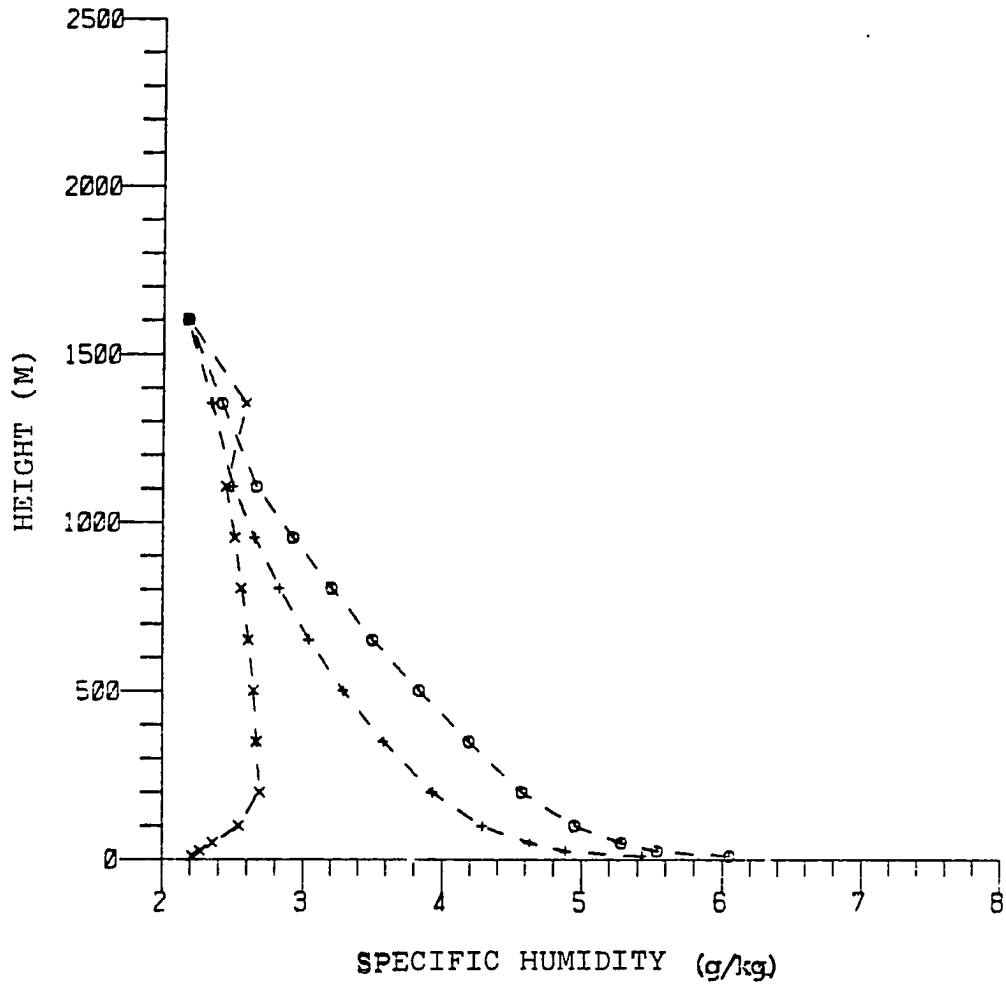

Figure 26. Specific humidity profiles of Simulation IV-A for November 16, 1972. Dx = 250 m, S = 0.1, x = initial profile, + = mid-distance profile, o = offshore profile.

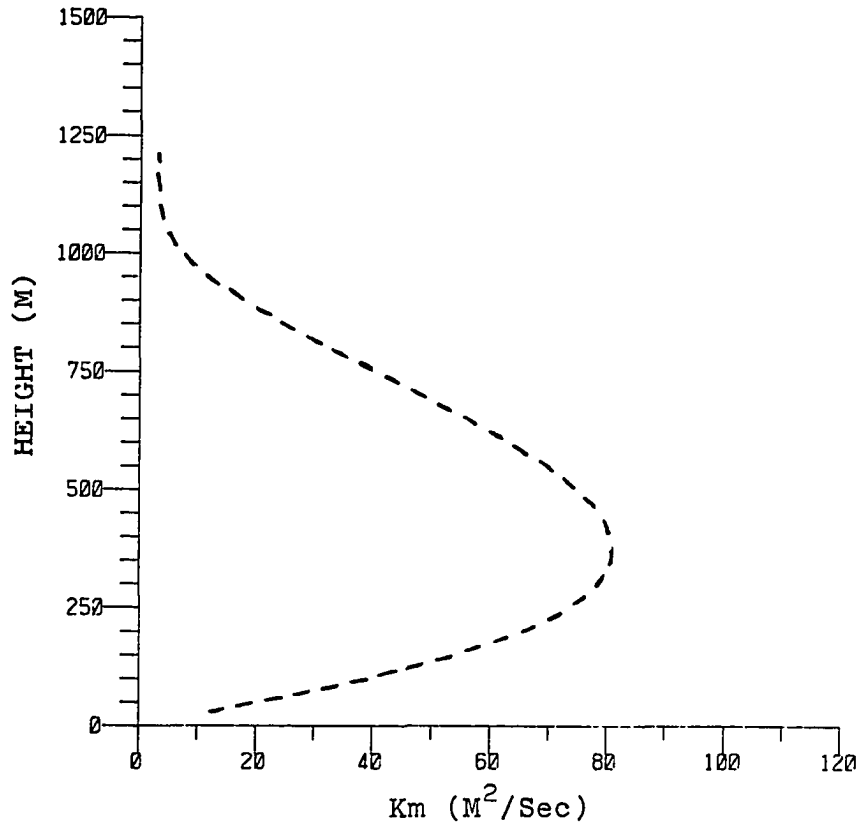

Figure 27. O'Brien's (1970) eddy viscosity profile generated by Simulation V-A for case 1.

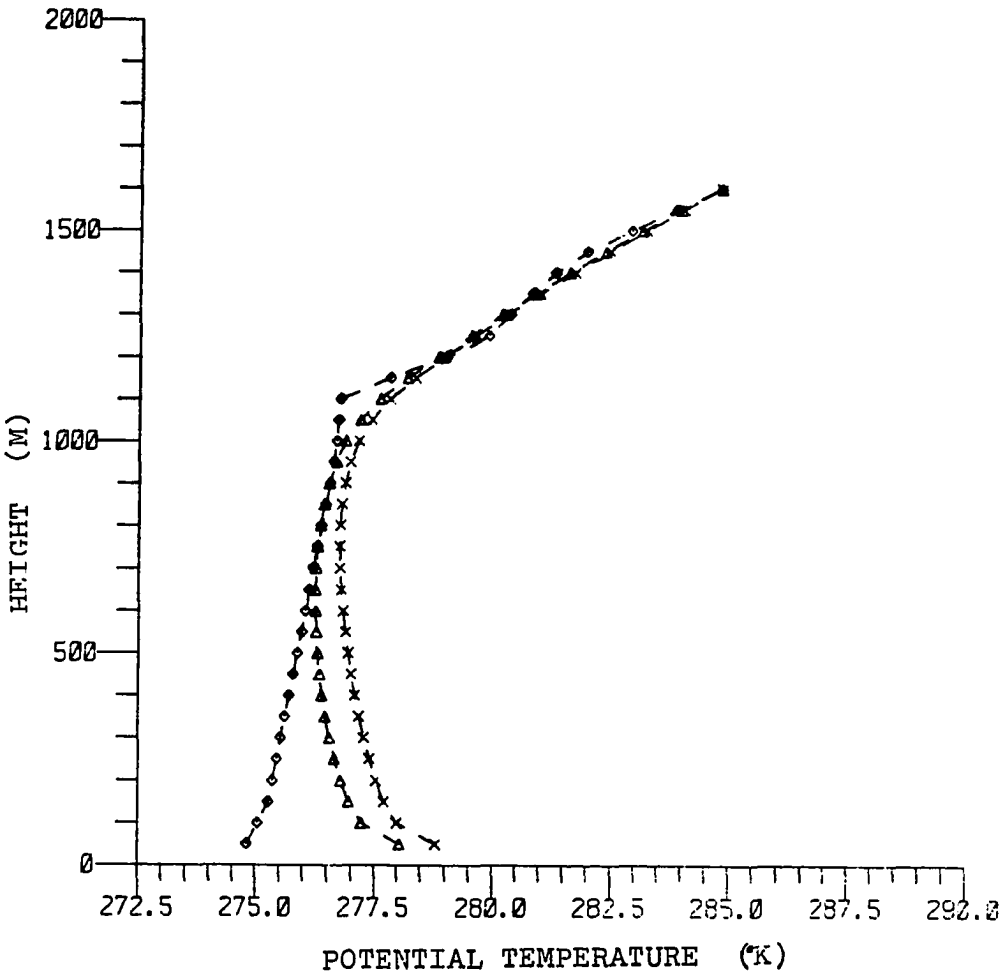

Figure 28. Potential temperature profiles of Simulation V-A for November 16, 1972. Dx = 1000 m, S = 0.1, ◇ = initial profile, Δ = mid-distance profile, ✕ = offshore station profile.

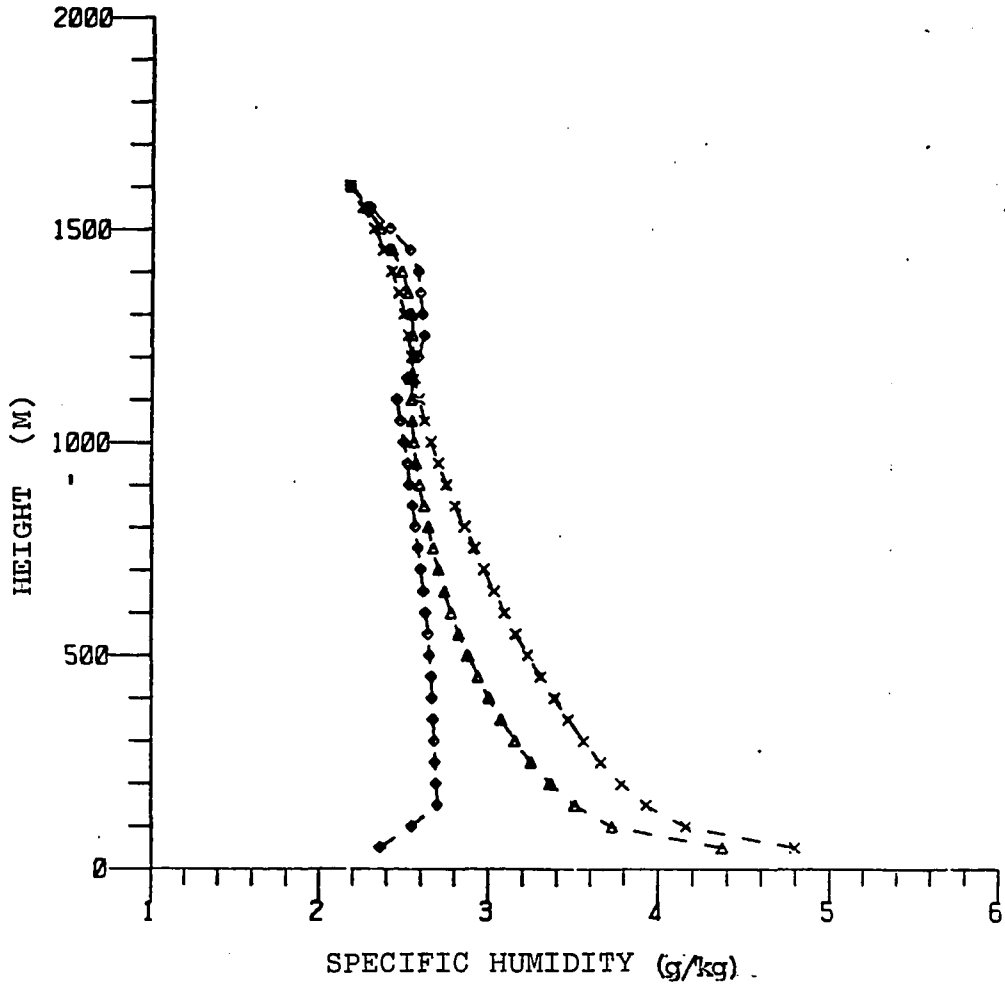

Figure 29. Specific humidity profiles of Simulation V-A for November 16, 1972. Dx = 1000 m, S = 0.1, ◇ = initial profile, Δ = mid-distance profile, x = offshore station profile.

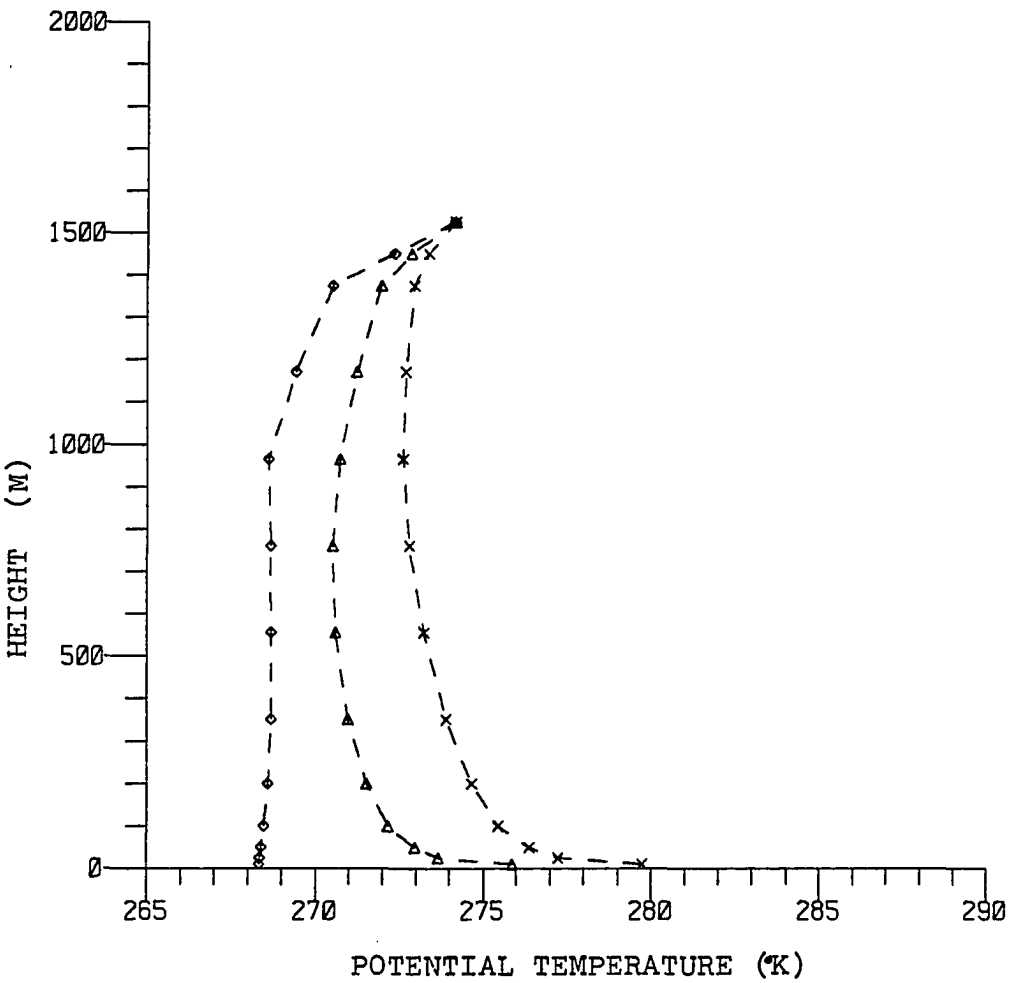

Figure 30. Potential temperature profiles of Simulation V-B for December 18, 1972. Dx = 2000 m, S = 0.2, ◇ = initial profile, Δ = mid-distance profile, x = offshore station profile.

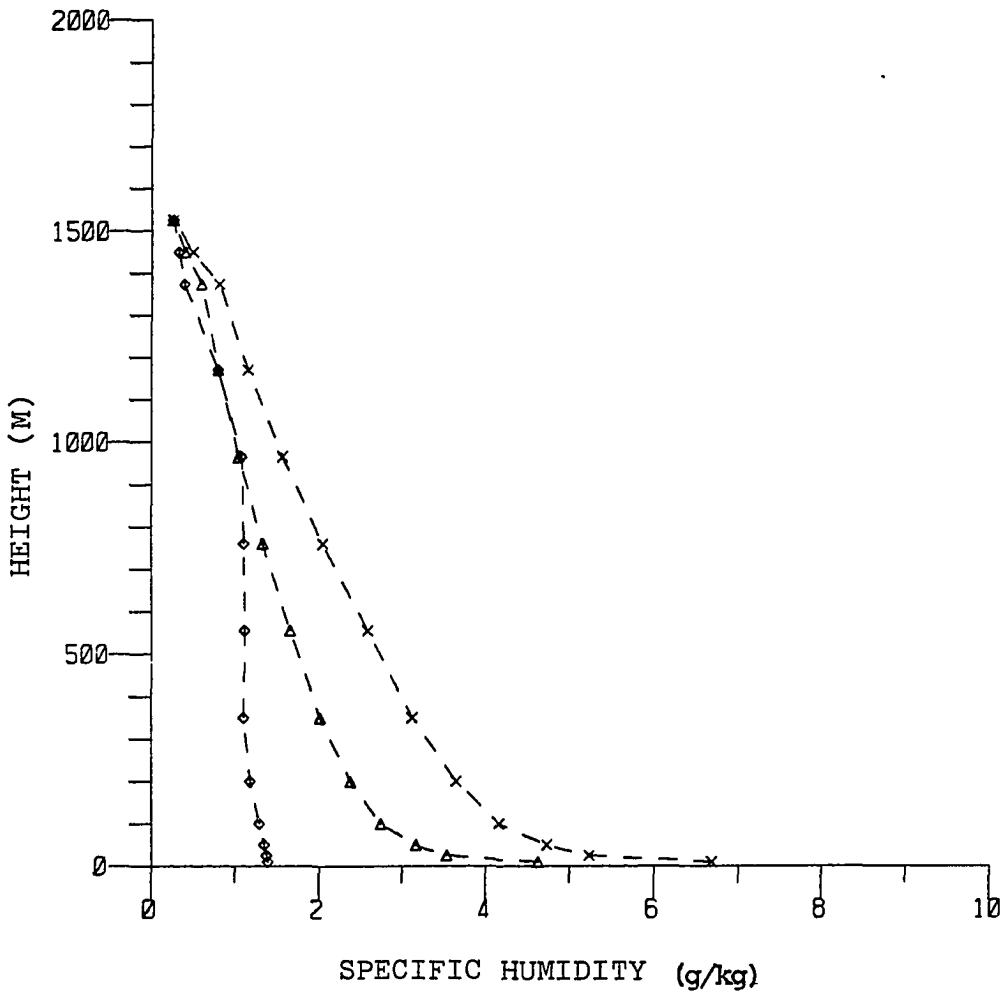

Figure 31. Specific humidity profiles of Simulation V-B for December 18, 1972. Dx = 2000 m, S = 0.2, ◇ = initial profile, △ = mid-distance profile, X = offshore station profile.

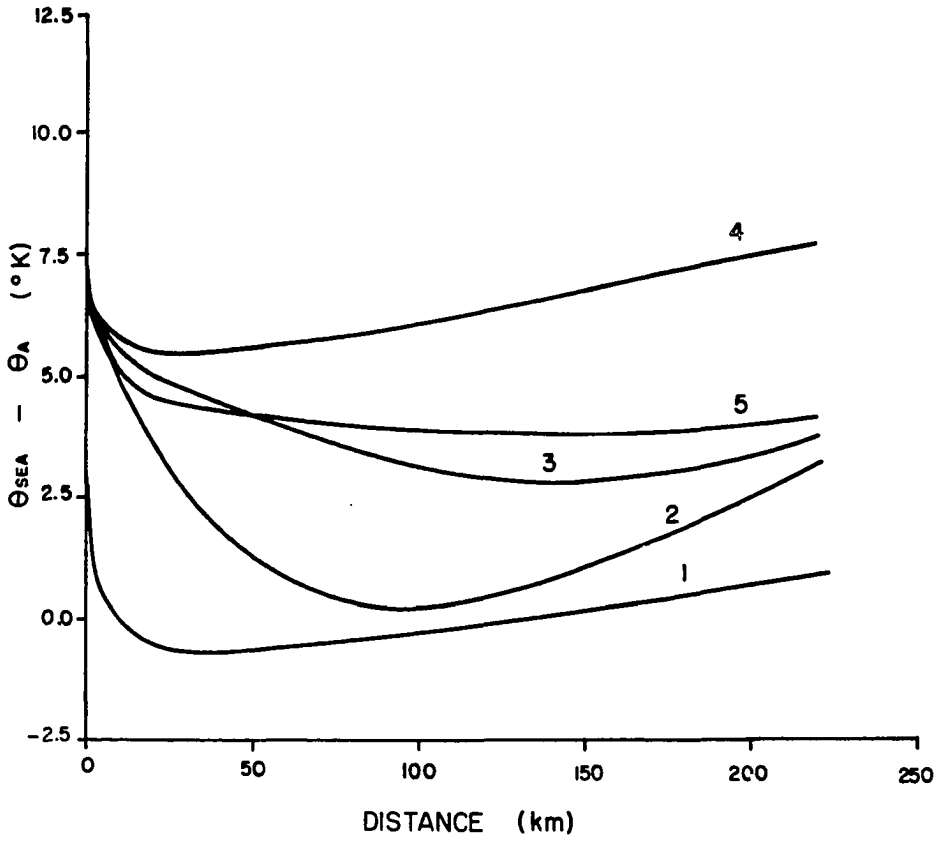

Figure 32. Distance evolution of the sea surface-air potential temperature differences for selected simulations.

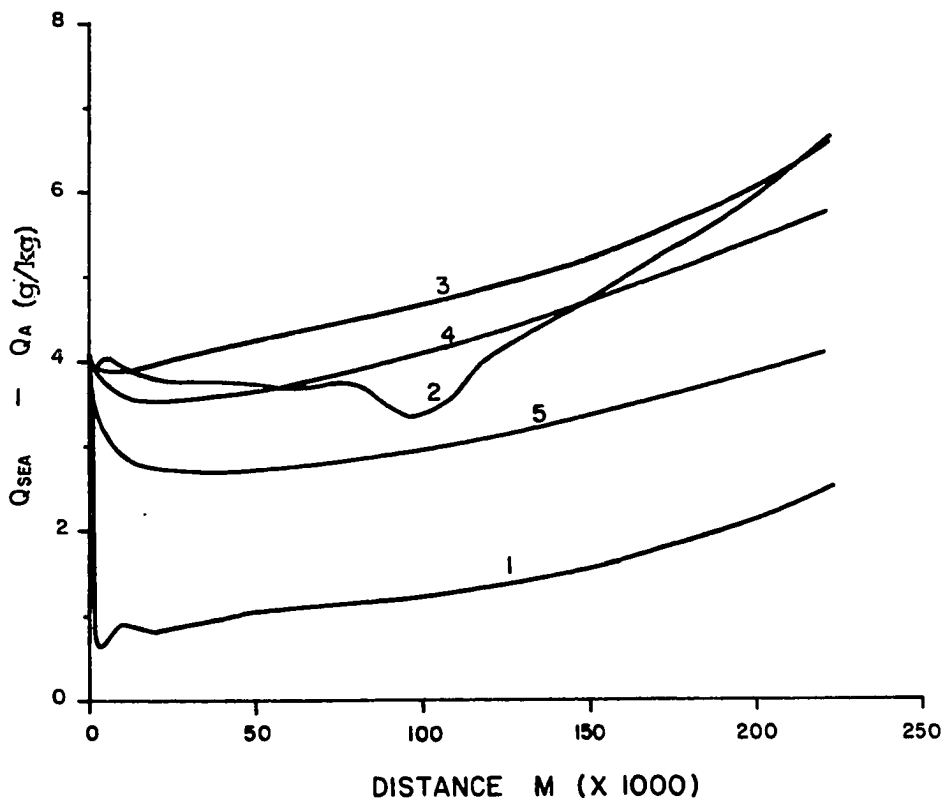

Figure 33. Distance evolution of the sea surface-air specific humidity differences for selected simulations.

REFERENCES

Bean, B. R. 1975. The spatial and temporal variations of the turbulent fluxes of heat, momentum and water vapor over Lake Ontario. J. Phys. Oceanogr. 5:532-540.

Blackadar, A. K. 1962. The vertical distribution of wind and turbulent exchange in a neutral atmosphere. J. Geophys. Res. 67:3095-3102.

Blackadar, A. K. 1969. High-resolution models of the planetary boundary layer. Advances in Environmental Science and Engineering. Vol. I. Gordon and Breach, New York. 276 pp.

Bodin, S. 1980. Atmospheric planetary boundary layer physics. Elsevier, Amsterdam. 424 pp.

Brook, R. R. 1978. The influence of water vapor fluctuations on turbulent fluxes. Bound.-Layer Meteor. 15:481-488.

Brown, P. S., and Pandolfo, J. P. 1979. Numerical stability of the combined advection-diffusion equation with nonuniform spatial grid. Mon. Wea. Rev. 107: 959-962.

Bunker, A. F. 1960. Heat and water-vapor fluxes in air flowing southward over the western North Atlantic Ocean. J. Meteor. 17-52:63.

Burbidge, F. E. 1951. The modification of Continental Polar air over Hudson Bay. Quart. J. Roy. Meteor. Soc. 77:365-374.

Burke, C. J. 1945. Transformation of polar continental air to polar maritime air. J. Meteor. 2:94-109.

Charnock. H. 1955. Wind stress on a water surface. Quart. J. Roy. Meteor. Soc. 81:639-640.

Clarke, R. H. 1970. Recommended methods for the treatment of the boundary layer in numerical models. Australian Meteor. Soc. Mag. 18:51-71.

Craddock, J. M. 1951. The warming of artic air masses over the eastern North Atlantic. Quart. J. Roy. Meteor. Soc. 77:355-364.

Deardorff, J. W. 1968. Dependence of air-sea transfer coefficients on bulk stability. J. Geophys. Sci. 73:2549-2557.

Deardorff, J. W. 1972. Numerical investigation of neutral and unstable planetary boundary layers. J. Atmos. Sci. 29:91-115.

Deardorff, J. W. 1974. Three dimensional numerical study of the height and mean structure of a heated planetary boundary layer. Bound.-Layer Meteor. 7:81-106.

Estoque, M. A. 1963. A numerical model of the atmospheric boundary layer. J. Geophys. Res. 68:1103-1113.

Estoque, M. A., and Bhumralkar, C. M. 1970. A method for solving the planetary boundary layer equations. Bound.-Layer Meteor. 1:169-194.

Grosch, C. E., and Orszag, S. A. 1977. Numerical solution of problems in unbounded regions: Corodinate transforms. J. Computational Phys. 25:273-295.

Haltiner, G. J., and Williams, R. T. 1980. Numerical prediction and dynamic meteorology. John Wiley & Sons, New York. 477 pp.

Hanna, S. R. 1969. Characteristics of wind and turbulence in the planetary boundary layer. ESSA Res. Lab. Tech. Mem-ARL8. 61 pp.

Jarvis, E. C. 1964. An adaptation of Burke's graphs of air mass modication for operational use. J. Appl. Meteor. 3:744-749.

Kindle, E. C.; Bhumralkar, C.; and Smith, J. E. 1976. Results of numerical model analysis of strong offshore winter winds. Conference on Coastal Meteorology, September 1976, American Meteorological Society, 75-78.

Krauss, E. B. 1972. Atmosphere-ocean interaction. Clarendon Press, London. 275 pp.

Lavoie, R. L. 1972. A mesoscale numerical model of lake-effect storms. J. Atmos. Sci. 29:1025-1040.

Lenschow, D. H. Airborne measurements of atmospheric boundary later structure. Annual Report, 1965.

University of Wisconsin, Dept. of Meteorology. 257 pp.

Lenschow, D. H. 1972. The air mass transformation experiment (AMTEX). Bull. Amer. Meteor. Soc. 53:353-357.

Lenschow, D. M. 1973. Two examples of planetary boundary layer modification over the Great Lakes. J. Atmos. Sci. 30:568-581.

Lumley, J. L. 1969. Simulating turbulent transport in urban air-pollution models. Advances in Environmental Science and Engineering. Vol. I. Gordon and Breach, New York. 276 pp.

Lumley, J. L., and Panofsky, H. A. 1964. The structure of atmospheric turbulence. Wiley-Interscience, New York. 239 pp.

Maddukuri, C. S.; Slawson, P. R.; and Danard, M. B. 1978. The application of a two-dimensional numerical model of the planetary boundary layer to the Nanticoke region on the north shore of Lake Erie. Bound.-Layer Meteor. 15:163-179.

Mahrt, L., and Lenschow, D. H. 1976. Growth dynamics of the convectively mixed layer. J. Atmos. Sci. 33:41-57.

Manabe, S. 1957. On the modification of an air mass over the Japan Sea when the outburst of cold air predominates. J. Meteor. Soc. Japan 35:1-16.

Manogo, C.; Harimaya, T.; and Adachi, S. 1974. An observation of a mesoscale cold air mass over a warm sea surface, utilizing the height and temperature of steam fog top. J. Meteor. Soc. Japan 52:491-497.

McBean, G. A. 1975. Turbulent fluxes over Lake Ontario during a cold frontal passage. Atmosphere 13:37-48.

O'Brien, J. J. 1970. A note on the vertical structure of the eddy exchange coefficient in the planetary boundary layer. J. Atmos. Sci. 27:1213-1215.

Pandolfo, J. P. 1971. Numerical experiments with alternative boundary layer formulations using Bomex data. Bound.-Layer Meteor. 1:277-289.

Pielke, R. A. 1974. A three-dimentional numerical model of the sea breezes over South Florida. Mon. Wea. Rev. 102:115-139.

Ralston, A. 1962. Runge-Kutta methods with a minimum error bounds. Math. Computation 16:431-437.

Reinking, R. F. 1980. The respective effects of water vapor and temperature on the turbulent fluxes of sensible and latent heat. Bound.-Layer Meteor. 19:373-385.

Shapiro, R. 1970. Smoothing, filtering, and boundary effects. Rev. Geophys. Space Phys. 8:359-387.

Smagorinsky, J. 1963. General circulation experiments with the primitive equations: 1. The basic experiment. Mon. Wea. Rev. 91:90-164.

Smith, S. D. 1980. Wind stress and heat flux over the ocean in gale force winds. J. Phys. Oceanogr. 10:709-726.

Taylor, P. A. 1971. Airflow above changes in surface heat flux, temperature and roughness; an extension to include the stable case. Bound.-Layer Meteor. 1:474-497.

Taylor, P. A., and Delage, Y. 1971. A note on finite difference schemes for the surface and planetary boundary layer. Bound.-Layer Meteor. 2:108-121.

Weisman, R. N. 1975. A developing boundary layer over an evaporating surface. Bound.-Layer Meteor. 8:437-445.

Wessels, H. R. 1979. Growth and disappearance of evaporating fog during the transformation of a cold air mass. Quart. J. Roy. Meteor. Soc. 105:963-977.

Yasuda, N. 1979. Paremeters of the Rossby similarity law for the sensible heat and vapor fluxes in the planetary boundary layer over the ocean. Papers in Meteor. Geophys. 30:123-132.

APPENDIXES

APPENDIX A

DERIVATIVES FOR A NONUNIFORM VERTICAL GRID THE FINITE DIFFERENCE EQUATIONS

The differential equation that described the processes was

$$u\,(\partial S/\partial x) = (\partial K/\partial z)(\partial S/\partial z) + K(\partial^2 S/\partial z^2) \qquad (A1)$$

where S stands for any parameter to be computed (i.e. θ, q). This is a second order differential equation. To obtain the first and second vertical derivatives for a nonuniform grid, the following procedure was used. By using a Taylor series expansion, any variable at levels $(\ell+1)$ and $(\ell-1)$ was written as

$$S_{\ell+1} = S_\ell + \partial S/\partial z)_\ell\,(z(\ell+1) - z(\ell))$$

$$+ \partial^2 S/\partial z^2)_\ell\,\frac{(z(\ell+1) - z(\ell))}{2} \qquad (A2)$$

$$S_{\ell-1} = S_\ell + \partial S/\partial z)_\ell\,(z(\ell-1) - z(\ell))$$

$$+ \partial^2 S/\partial z^2)_\ell\,\frac{(z(\ell-1) - z(\ell))^2}{2} \qquad (A3)$$

Solving equations (A2) and (A3) for $(\partial S/\partial z)$ and $(\partial^2 S/\partial z^2)$, one obtained

$$\partial S/\partial z = C(1,\ell)\ S_{\ell+1} + C(2,\ell)\ S_{\ell} + C(3,\ell)\ S_{\ell-1} \qquad (A4)$$

where

$$C(1,\ell) = 0.5\ (Z(\ell-1) - Z(\ell))^2/Den$$

$$C(2,\ell) = 0.5\ ((Z(\ell+1) - Z(\ell))^2 - (Z(\ell-1) - Z(\ell))^2)/Den$$

$$C(3,\ell) = -\ 0.5\ (Z(\ell+1) - Z(\ell))^2/Den$$

$$Den = ((Z(\ell+1) - Z(\ell))\ (Z(\ell-1) - Z(\ell))^2$$

$$- (Z(\ell-1) - Z(\ell))\ (Z(\ell+1) - Z(\ell))^2/2$$

and

$$\partial^2 S/\partial z^2) = Cp(1,\ell)\ S_{\ell+1} + Cp(2,\ell)\ S_{\ell} + Cp(3,\ell)\ S_{\ell-1} \qquad (A5)$$

where

$$Cp(1,\ell) = (Z(\ell) - Z(\ell-1)/Den$$

$$Cp(2,\ell) = (Z(\ell-1) - Z(\ell+1))/Den$$

$$Cp(3,\ell) = (Z(\ell+1) - Z(\ell))/Den$$

The coefficient C and Cp depended on Z alone for each level. Therefore, they were calculated at the beginning of the program.

Equation (A1) must then be written in finite difference form:

$$S_{\ell}^{n+1} = S_{\ell}^{n-1} + (2\ Dx/u_{\ell}^{n})\ (\partial K/\partial z)_{\ell}^{n}\ (\partial S/\partial z)_{\ell}^{n}$$

$$+ (2\ Dx/u_{\ell}^{n})\ K(\partial^2 S/\partial z^2) \qquad (A6)$$

The first and second derivatives of equation (A6) were calculated by equations (A4) and (A5). A Dufort-Frankel scheme was used. This technique replaced the center node point value, in the diffusion term of equation (A6) by its average at times (n-1) and (n+1). The finite difference forms of the governing equations for the potential temperature and specific humidity can then be written as

$$\theta_{\ell}^{n+1} = \left[\frac{2 + \sigma\ C(2,1) + \beta\ Cp(2,1)}{2 - \sigma\ C(2,1) + \beta\ Cp(2,1)}\right]\ \theta_{\ell}^{n-1}$$

$$+ \left[\frac{2(\sigma\ C(1,\ell) + \beta\ Cp(1,\ell))}{2-\sigma\ C(2,\ell) - \beta\ Cp(2,\ell)}\right]\ \theta_{\ell+1}^{n}$$

$$+ \left[\frac{2(\sigma\ C(3,\ell) + \beta\ Cp(3,\ell))}{2-\sigma\ C(2,\ell) - \beta\ Cp(2,\ell)}\right]\ \theta_{\ell-1}^{n}$$

and

$$q_{\ell}^{n+1} = \left[\frac{2 + \sigma\ C(2,\ell) + \beta\ Cp(2,\ell)}{2 - \sigma\ C(2,\ell) + \beta\ Cp(2,\ell)}\right]\ q_{\ell}^{n-1}$$

$$+ \left[\frac{2(\sigma\ C(1,\ell) + \beta\ Cp(1,\ell))}{2 -\sigma\ C(2,\ell) - \beta\ Cp(2,\ell)}\right]\ q_{\ell+1}^{n}$$

$$+ \left[\frac{2(\sigma\ C(3,\ell) + \beta\ Cp(3,\ell))}{2-\sigma\ C(2,\ell) - \beta\ Cp(2,\ell)}\right]\ q_{\ell-1}^{n}$$

where

$$\sigma = (2\ Dx\ K'^{n}_{\ell})\ /U^{n}_{\ell}$$

$$\beta = 2\ Dx\ K^{n}_{\ell}\ /U^{n}_{\ell}$$

K'^{n}_{ℓ} was obtained by solving equation (A4) for the eddy coefficient formulation.

APPENDIX B

METHOD OF SOLUTION

These steps were followed to solve the complete set of equations for each case:

I. Set up of the initial conditions.

a. Calculation of the vertical levels and interpolation of the different parameters for each level.

b. Computation of the variables that define the lower boundary conditions (i.e. sea surface temperature, specific humidity at the sea surface temperature, etc.).

c. Calculation of the geostrophic wind.

d. Computation of the coefficients C and Cp.

II. Computations for each increment, Dx, that the air mass moved along the x direction.

a. Second order model.

(1) Calculation of the eddy coefficient for the vertical grid points and integration of the wind with height.

(2) Computation of the air potential temperature and specific humidity profiles for the next step (Dx).

b. First order model.

(1) Calculation of the eddy coefficient for the vertical grid points and integration of the wind with height.

(2) Computation of the sensible heat and latent heat for each layer.

(3) Computation of the air potential temperature and specific humidity profiles for the next step (Dx).

APPENDIX C

SIMPLIFIED SOLUTION OF THE DIFFERENTIAL EQUATION

One of the main difficulties with all these simulations has been that the model could not properly handle the large DT and the continuous increase in the sea surface temperature at the very first layer. To study this problem, a simple two layer system was considered (Figure 19). Several simplifications were made in order to solve the partial differential equation.

The potential temperature at the top (θ_3) and the eddy coefficients for the two layers ($K_{1.5}$, K_2, $K_{2.5}$) were considered constant in time. The temperature at the bottom was given by a linear increase with time

$$\theta_1 = \theta_1^o + \dot{\theta}\, t \qquad \text{(C1)}$$

where θ_1^o is the sea surface temperature at the coast and is assumed to be several degrees greater than θ_3, which occurred in the unstable cases.

The nonlinear differential equation that describes the problem at the intersection of the two layers is

$$\frac{\partial \theta_2}{\partial t} = \frac{\partial K}{\partial z}\Big)_2 \frac{\partial \theta}{\partial z}\Big|_2 + K_2 \frac{\partial^2 \theta}{\partial z^2}\Big|_2 \qquad (C2)$$

Applying the differential equation to the two layer system, one obtains the following:

$$\frac{\partial \theta_2}{\partial t} = \frac{K_{2.5} - K_{1.5}}{Dz} \cdot \frac{(\theta_3 - \theta_1)}{2Dz} + \frac{K_2}{Dz^2} (\theta_1 + \theta_3 - 2\theta_2)$$

which may be rearranged:

$$\frac{\partial \theta_2}{\partial t} + \frac{2K_2}{Dz} \theta_2 = \frac{K'(\theta_3 - \theta_1)}{2\ Dz^2} + \frac{K_2}{Dz^2} (\theta_1 + \theta_3) \qquad (C3)$$

where $K' = K_{2.5} - K_{1.5}$. A parameter Gamma is defined:

$$\gamma = \frac{2K}{Dz^2} \qquad (C4)$$

Substitution of (C1) and (C4) into (C3) gives

$$\frac{\partial \theta_2}{\partial t} + \gamma \theta_2 = \frac{K'}{2Dz} (\theta_3 - \theta_1^o) + \frac{K_2}{Dz^2} (\theta_3 - \theta_1^o) - \frac{K'}{2Dz^2} \mathring{\theta} t + \frac{K_2}{Dz^2} \mathring{\theta} t \qquad (C5)$$

The following terms are defined

$$\theta_o' = \frac{\theta_3 - \theta_1^o}{2}$$

$$\bar{\theta}_o = \frac{\theta_3 + \mathring{\theta}_1}{2} \qquad (C6)$$

and incorporated into (C5) to obtain:

$$\frac{\partial \theta_2}{\partial t} + \gamma \theta_2 = \frac{K'}{2K_2}\, \theta_o' + \gamma\, \bar{\theta}_o + \frac{\gamma}{2}\, \dot{\theta}\, t\, (1 - \frac{K'}{2K_2}) \qquad (C7)$$

Since $\bar{\theta}_o$, θ_o', γ, etc. are constants under these particular conditions, two constants M and B are defined as

$$M = \frac{\gamma K'}{2K_2}\, \theta_o' + \gamma\, \bar{\theta}_o$$

$$B = \frac{\gamma}{2}\, \dot{\theta}\, (1 - \frac{K'}{2K_2})$$

Then, (C7) becomes

$$\frac{\partial \theta_2}{\partial t} + \gamma \theta_2 = M + B\, t\ , \qquad (C8)$$

(C8) is solved for the integration factor, and the solution becomes

$$\theta_2(t) - \theta_2^o = (\frac{M}{\gamma} - \theta_2^o)\, (1 - e^{-\gamma t}) + \frac{B}{\gamma^2}\, (e^{-\gamma t} - 1 + \gamma\, t) \qquad (C9)$$

however,

$$\frac{M}{\gamma} = \frac{K'}{2K_2}\, \theta_o' + \bar{\theta}_o \qquad (C10)$$

$$\frac{B}{\gamma^2} = \frac{\dot{\theta}}{2\gamma}\, (1 - \frac{K'}{2K}) \qquad (C11)$$

$$\Delta\theta = \theta_2 (t) - \theta_2^o \qquad (C12)$$

Substitution of (C10), (C11) and (C12) gives

$$\Delta\theta = (\bar{\theta}_o - \theta_2^o)(1 - e^{-\gamma t}) + (\frac{K'}{2K_2})(1 - e^{-\gamma t})\ \theta_o' - \frac{\mathring{\theta}}{2\gamma}(1 - \frac{K'}{2K_2})(1 - \gamma t - e^{-\gamma t}) \qquad (C13)$$

This equation yields interesting results when extreme conditions are applied. Assume a large t (τ) and the following:

$$K_{1.5} = 1.0\ m^2/sec$$

$$K_2 = 5.0\ m^2/sec$$

$$K_{2.5} = 20.0\ m^2/sec$$

$$Dz = 50\ m$$

$$\mathring{\theta}_1 = 280°K$$

$$\theta_2 = 270°K$$

$$\theta_3 = 268°K$$

$$t = 2.0\ 10^4\ sec$$

$$\gamma = 0.004\ sec^{-1}$$

$$\mathring{\theta} = 10^{-3}°K/sec$$

With these assumptions equation (C13) becomes

$$D\theta(\tau) = (\bar{\theta} - \theta_2) + (K'/2\,K_2)\,\theta' - (\mathring{\theta}/2\gamma)(1. - K'/2\,K))(1. - \gamma t)$$

$$D\theta(\tau) = (4.°K) + (-12.°K) - 1./8)(-1)(1. - 80.)\ °K$$

$$D\theta(\tau) = -\ 17.8°K\ .$$

This simple calculation shows that the analytical solution, when a large DT and a large $\partial K/\partial z$ are present, decreases the temperature at layer two even though the temperature at the bottom increased linearly with time. The last term in equation (C13) becomes important when the time is large. If (K'/2K) is greater than one, that term becomes negative and large in magnitude. The second term of the right hand side of equation (C13) is always negative, and in winter conditions, is always large. Therefore, even if the last term of (CL3) becomes negligible, because $\mathring{\theta}$ is small, the magnitude of K'/2K will determine the sign of the final results.

APPENDIX D

LINEAR COMPUTATIONAL STABILITY OF THE DUFORT-FRANKEL SCHEME

The finite different equation for the Dufort-Frankel numerical solution is

$$\theta_m^{n+2} = \theta_m^n \left(\frac{1 - \gamma}{1 + \gamma}\right) + \frac{\gamma}{1 + \gamma} \left[\theta_{m+1}^{n+1} + \theta_{m+1}^{n+1}\right] \qquad (D1)$$

where

$$\gamma = \frac{2\ K\ Dx}{U\ Dz^2}$$

Defining

$$\theta_m^n = \sum_{\mu=-\infty}^{\infty} A_{\mu,o}\ e^{-\mu^2 Km\,\delta t}\ e^{i\mu\, m\delta z} \qquad (D2)$$

Writing the amplification factor B_μ^* as

$$B_\mu^* = e^{-\mu^2 K\delta t}\ ; \quad \mu\delta x = \frac{2\pi\,\delta z}{L}$$

quation (D2) becomes:

$$\theta_m^n = \sum_{\mu=-\infty}^{\infty} A_{\mu,o}\ B_\mu^n\ e^{i\mu\, m\,\delta z} \qquad (D3)$$

or

$$-1 \leq -\cos \mu\delta z$$

Equation (D5) is valid for all gammas, therefore, the real solutions will always be stable.

However, in this case a priori cannot be assumed that B is stable and/or real, since the finite approximation may introduce systematic errors.

Substituting (D3) into (D1) gives

$$B^2 - \frac{2\gamma}{1+\gamma} \cos(\mu \delta z)\, B - \frac{1-\gamma}{1+\gamma} = 0 \qquad \text{(D4)}$$

Solving equation (D4) the following expression is obtained for B:

$$B = \frac{\gamma}{1+\gamma} \cos \mu\delta z \pm \left[\left(\frac{\gamma}{1+\gamma}\right)^2 \cos^2 \mu\delta z + \frac{1-\gamma}{1+\gamma} \right]^{\frac{1}{2}}$$

Considering the case for the real solution, stable conditions requiring $|B|<|1|$, therefore

$$\left| \frac{\gamma}{1+\gamma} \cos \mu\delta z + \left[\left(\frac{\gamma}{1+\gamma}\right)^2 \cos^2 \mu\delta z + \frac{1-\gamma}{1+\gamma} \right]^{\frac{1}{2}} \right| \leq |1|$$

or

$$\left[\left(\frac{\gamma}{1+\gamma}\right)^2 \cos^2 \mu\delta z + \frac{1-\gamma}{1+\gamma} \right]^{\frac{1}{2}} \leq 1 - \frac{\gamma}{1+\gamma} \cos \mu\delta z$$

Since both are greater than zero, it is possible to retain the inequality while both sides of the equation are squared

$$\frac{1-\gamma}{1+\gamma} \leq 1 - \frac{2\gamma}{1+\gamma} \cos \mu\delta z$$

then

$$\frac{1-\gamma}{1+\gamma} - 1 \leq - \frac{2\gamma}{1+\gamma} \cos \mu\delta z$$

APPENDIX E

SUMMARY OF THE SIMULATIONS

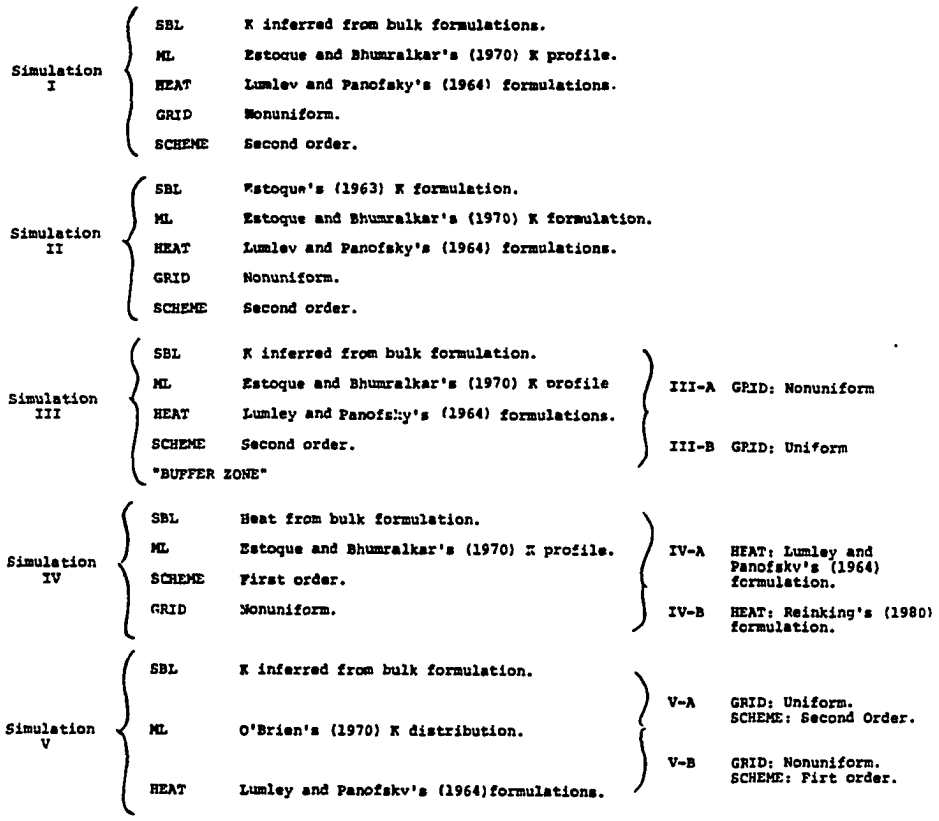

AUTOBIOGRAPHICAL STATEMENT

MARIA CINTIA PICCOLO

BORN

24 June 1951, Puerto Belgrano, Buenos Aires, Argentina

EDUCATION:

Maestra Normal Nacional, Colegio Nino Jesus de Praga, Buenos Aires, Argentina, 1969.

Licenciada en Ciencias Meteorologicas, Universidad de Buenos Aires, Argentina, 1975.

APPOINTMENTS AND POSITIONS:

RESEARCH ACTIVITIES

Assistant Investigator, Servicio de Hidrografia Naval, Armada Argentina, 1975.

Assistant Investigator, Servicio Meteorologico de la Argentina, since 1976.

TEACHING POSITIONS

Assistant Professor, Instituto Tecnologico Buenos Aires, 1st semester 1977.

Professor, Instituto Tecnologico Buenos Aires, 2nd semester 1977.

Teaching Assistant, Universidad de Buenos Aires, 1977-1978.

Teaching Assistant, Old Dominion University, 1980-1981.

Tecnical Secretary of Tercer Congreso de Meteorologia. Buenos Aires, Argentina, 1978.

PUBLICATIONS:

Piccolo, M. C., 1980. Climatologia sinoptica del area adyacente al cabo San Antonio y del Rio de

la Plata. Estudio de los principales parametros aplicados especialmente a la navegacio maritima. Zubillaga, J. V. (Ed.): Climatologia sinoptica de las regiones adyacentes al cabo San Antonio. Distintas aplicaciones de la Meteorologia. Cap. II:7-50. Servicio de Hidrografia Naval.

Piccolo, M. C., 1980. Climatologia costera y continental. Zubillaga, J. V. (Ed.): Climatologia sinoptica de las regiones adyacentes al cabo San Antonio. Distintas aplicasiones de la Meteorologia. Cap. III:51-113. Servicio de Hidrografia Naval.

Zubillaga, J. V., and Piccolo, M. C., 1980. Procesos atmosfericos locales. Mesocirculacion. Brisas de mar y tierra. Zubillaga, J. V. (Ed.): Climatologia sinoptica de las regiones adyacentes al cabo San Antonio. Distintas aplicaciones de la Meteorologia. Cap. IV:115-156. Servicio de Hidrografia Naval.

Piccolo, M. C., 1979. Analisis de maximos de precipitacion en base a la convergencia subtropical en el Oceano Atlantico Sur. Meteorologica.